

Tokyo Metropolitan University
Graduate School of System Design
Department of Aerospace Engineering

Efficient Global Optimization with Multi-Fidelity Approach for Aeronautical Applications

(マルチフィデリティ法による効率的な大域最適化法の
構築と航空機設計への応用)

Atthaphon Ariyarit
(13991572)

Abstract

Developing a highly efficient optimization methodology is critical for the design process in the aerospace arena because an aeronautical design is usually complicated and expensive. In addition, design problems often have several objectives for simultaneous consideration. To increase the performance of optimization methodology, the efficiency global optimization (EGO) has been developed. The EGO needs to be further improved via an exploratory method, such as genetic algorithm (GA) and surrogate methods.

This thesis begins with reviews and the development of GA using an exploratory method for real-world design problems. Focusing on the distribution of the population, GA with a multimodal crossover method (MMDX) was proposed to consider the skewness of the distribution of parent candidates. The proposed crossover method creates four segments from four selected parents, of which two segments are bounded by selected parents and two are bounded by one parent and another segment. After defining these segments, four offspring are generated. This study considered the application of a proposed optimization method for the real-world problem of creating a multi-objective airfoil design using a class-shape polynomial function transformation parameterization (CST), which is of aerodynamic shape, to investigate the effectiveness of the algorithm. The exploration results are compared with the results of blend crossover (BLX) and unimodal normal distribution crossover (UNDX) algorithms, which are widely used. According to the design results, the developed algorithm found solutions that were superior to those found by the BLX and UNDX algorithms with regard to maintaining diversity of solutions. This is a beneficial feature for real-world problems.

Next, a multi-fidelity optimization technique based on an efficient global optimization method using a multi-fidelity approach was investigated for solving real-world design problems. In the proposed approach, a multi-fidelity surrogate model was developed for evaluating local deviation using Kriging method and for constructing a global model using a radial basis function. The expected improvement (EI) was computed based on the uncertainty of the model, which was evaluated using the Kriging method, to determine additional samples to improve the model and EGO. The proposed multi-fidelity approach was investigated by solving mathematical test problems whose results were compared with those of ordinary Kriging-based EGO using a single-fidelity approach and the co-Kriging-method-based EGO. The proposed method obtained better solutions than the other two. It was applied to the aerodynamic design optimization of

helicopter blades for hovering to maximize blade efficiency. The shapes of the helicopter blades were designed by changing their twist angle distributions. The performance of the optimal shape obtained using the proposed method was almost equal to that obtained using high-fidelity evaluation based on single-fidelity optimization by an ordinary Kriging. The results of the proposed method were compared with that of a co-Kriging - based multi-fidelity approach. The accuracy of the proposed method was the highest, while the total number of high-fidelity evaluation runs required to obtain a converged solution was the lowest.

Finally, the method was expanded to solve multi-fidelity/multi-objective problems. An expected hypervolume improvement (EHVI) was used as an index to find additional samples for the optimization process. EHVI is computed based on the model's uncertainty to determine additional samples as well as EI. First, the proposed approach was applied to two-objective optimization test functions. Then, it was applied to airfoil design optimizations that have two- and three-objective functions, namely, minimization of aerodynamic drag and maximization of airfoil thickness at the trailing edge for the two-objective problem and minimization of aerodynamic drag at cruising speed, maximization of airfoil thickness at the trailing edge, and maximization of lift at low speed assuming a landing attitude for the three-objective problem. A panel method was used to apply the low-fidelity inviscid aerodynamic force and a Reynolds-averaged Navier-Stokes simulation was applied for high-fidelity aerodynamics in conjunction with a high-cost approach. For comparison, multi-objective optimization was applied using only a Kriging model with a high-fidelity solver (single fidelity). The design results indicate that the non-dominated solutions of the proposed method achieve greater data diversity than the optimal solutions of the Kriging method. Moreover, the proposed method has a smaller error than the Kriging method with the single-fidelity approach.

Acknowledgements

I would like to thank a number of people who directly and indirectly contributed to the completion of this thesis. First of all, I would like to express my sincerely thank to my supervisor, Assoc. Prof. Masahiro Kanazaki, for all of his patient guidance, understanding and continuous support throughout my whole study. I would also like to acknowledge Dr. Yasutada Tanabe and Dr. Masahiko Sugiura from Japan Aerospace Exploration Agency (JAXA) for the interesting times spent discussing and help about my research.

I would like to dedicate my special thanks to all of my friends in my department who made my life in the Japan enjoyable and memorable. Certainly special mention goes to Dr. Norazila Othman, Mr. Yuta Kurata and Mr. Yuki Kishi for their help and friendship throughout these many years.

I would like to thank all other friends, both in Thailand, Taiwan and Japan, whose names I am not able to write down here.

I would like to dedicate my grateful and deep appreciation to my parents and aunt for their unconditional love, support and encouragement for the whole of my life. I would like to thank my brother and sisters who take good care of our parents during my study here.

Finally, I would like to acknowledge the Asian Human Resources Fund (AHRF) from the Tokyo Metropolitan Government for their financial support throughout my PhD study.

Contents

Abstract	i
Acknowledgements	iii
1 Introduction	1
1.1 Current Situation of Aeronautical Design	1
1.2 Recent Researches on Optimization Techniques for Real World Problems	3
1.3 Objectives of this Thesis	6
1.4 Outline of this Thesis	6
2 Genetic Algorithm for Aeronautical Application	16
2.1 Introduction	16
2.2 Overview of Crossover Method	18
2.2.1 Blended Crossover (BLX)	18
2.2.2 Unimodal Normal Distribution Crossover (UNDX)	18
2.2.3 Proposed Crossover Method	20
2.3 Investigation of Proposed Method by Solving Test Functions	21

2.3.1	Formulation	22
2.3.2	Results of Test Functions	23
2.4	Design Methods	24
2.4.1	Class-Shape Function Transformation Parameterization	24
2.4.2	Aerodynamics Evaluation	25
2.4.3	Cover Rate	26
2.4.4	Parallel Coordinate Plot (PCP)	26
2.5	Formulation	27
2.6	Results and Discussion	28
2.7	Conclusion	32
3	Multi-fidelity Efficient Global Optimization using Hybrid Surrogate Model	36
3.1	Introduction	36
3.2	Surrogate Model Methods for Multi-fidelity Optimization	39
3.2.1	Kriging Method	39
3.2.2	Hybrid Surrogate Model for a Multi-fidelity Approach	40
3.3	Efficient Global Optimization	42
3.3.1	Efficiency Global Optimization for single-fidelity optimization	42
3.3.2	Efficiency Global Optimization for multi-fidelity optimization	43
3.4	Investigation of Proposed Method by Solving Test Functions	44
3.4.1	Formulation	44
3.4.2	Results of Test Functions	47

3.5	Application of Proposed Method to Helicopter Blade Design	50
3.5.1	Evaluation Methods	55
3.5.2	Definition of Blade Geometry and Design variables	60
3.5.3	Objective Function and Calculation Condition	63
3.5.4	Results	63
3.6	Conclusion	69
4	Multi-objective/multi-fidelity Efficient Global Optimization	74
4.1	Introduction	74
4.2	Efficient Global Optimization for Multi-objective Problem	76
4.3	Investigation of Proposed Method by Solving Test Functions	77
4.3.1	Formulation	77
4.3.2	Two-objective Test Function Results	80
4.3.3	Three-objective Test Function Results	83
4.4	Airfoil Design Problem	85
4.4.1	Formulation	85
4.4.2	Evaluation Methods	88
4.5	Results	89
4.6	Conclusions	97
5	Conclusion	103
5.1	Conclusions	103

List of Tables

- 3.1 Blade properties. 63
- 4.1 Design spaces for airfoil design problem. 89

List of Figures

2.1	Schematic illustration and possible crossover region of UNDX (a) Selection parents (b) Generate offsprings (c) The possible crossover regions of the UNDX. . .	19
2.2	Schematic illustration and possible crossover region of the MMDX (a) Selection parents (b) Generate offsprings (c) The possible crossover region of MMDX. . .	22
2.3	The comparison of distribution of individuals generated by the MMDX, UNDX and BLX crossover method with 2000 offspring.	23
2.4	Best solution of 20 dimensional Rastrigin function (a) History of best solution (b) Close up view near optimum value	24
2.5	Best solution of 20 dimensional Rosenblock function (a) History of best solution (b) Close up view near optimum value	24
2.6	Schematic illustration and possible crossover region of the MMDX (a) Selection parents (b) Generate offsprings (c) The possible crossover region of MMDX. . .	26
2.7	Resulting non-dominated solutions of the CST problem.	28
2.8	The history of non-dominated solutions after the 30 th , 60 th , 80 th , 90 th , and 100 th generation. (a) Solutions obtained by BLX, (b) Solutions obtained by UNDX, (c) Solutions obtained by the MMDX method.	29
2.9	Comparison of the history of metrics: (a) Hypervolume, (b) Maximum spread, (c) Variance of Cover rate during the search.	30

2.10	The PCP of the non-dominated solution at the 100 th generation. (a) BLX (b) UNDX (c) MMDX.	31
3.1	CFD example [9].	38
3.2	Schematic illustration of a single-fidelity and multi-fidelity surrogate model. (a) Ordinary Kriging model (b) Hybrid model.	41
3.3	Flowchart of efficient global optimization. (a) Efficient global optimization (b) Proposed EGO with multi-fidelity surrogate model.	45
3.4	Search history of EI value for the first sampling of helicopter blade design problem.	46
3.5	Additional sampling in each iteration. (a) SC problem (b) BR problem (c) HIM problem (d) ROS problem.	50
3.6	Cross validation of SC problem. (a) Hybrid surrogate-model-based EGO (b) Co-Kriging-based EGO (c) Ordinary Kriging-based EGO.	51
3.7	Cross validation of BR problem. (a) Hybrid surrogate-model-based EGO (b) Co-Kriging-based EGO (c) Ordinary Kriging-based EGO.	52
3.8	Cross validation of HIM problem. (a) Hybrid surrogate-model-based EGO (b) Co-Kriging-based EGO (c) Ordinary Kriging-based EGO.	53
3.9	Cross validation of ROS problem. (a) Hybrid surrogate-model-based EGO (b) Co-Kriging-based EGO (c) Ordinary Kriging-based EGO.	54
3.10	Helicopter computation grid. (a) Grid around blade (b) Grid in stationary domain (c) Example of flow-field around rotor blades generated using CFD.	57
3.11	Blade section aerodynamics.	60
3.12	Comparison of the high-fidelity data by CFD and the low-fidelity data by BEMT.	60
3.13	Definition of glade geometry: (a) control points, (b) controlled parameters.	62

3.14	Additional sampling in each iteration of the helicopter design problem.	64
3.15	The history of the additional samples discovery. (a) Θ_1 (b) Θ_2	65
3.16	The multi-fidelity relationship contour of the design parameters (Θ_1 and Θ_2) and FOM. (a) Hybrid surrogate-model-based EGO (b) Co-Kriging-based EGO (c) Ordinary Kriging-based EGO.	66
3.17	Cross validation of helicopter design problem. (a) Hybrid surrogate-model-based EGO (b) Co-Kriging-based EGO (c) Ordinary Kriging-based EGO.	67
3.18	Twist distribution of optimal designs. (a) Full length (b) $r/R = 0.7'1.0$	68
4.1	Flowchart of efficient global optimization. (a) Efficient global optimization (b) Proposed EGO with multi-fidelity surrogate model.	78
4.2	Initial sampling data and additional sampling data: (a) multi-fidelity approach, (b) single-fidelity approach.	80
4.3	Hypervolume comparison of multi-fidelity approach and single-fidelity approach.	81
4.4	Non-dominated solution of two-objective optimization test problem.	81
4.5	Cross-validation results: (a) result of f_1 , (b) result of f_2	82
4.6	Initial sampling data and additional sampling data: (a) multi-fidelity approach, (b) single-fidelity approach.	84
4.7	Comparison of non-dominated solutions of three-objective optimization test problem.	84
4.8	Hypervolume comparison of multi-fidelity approach and single-fidelity approach.	85
4.9	Cross-validation of f_3 : (a) multi-fidelity approach, (b) single-fidelity approach. .	86
4.10	Computation structured grid: (a) full length, (b) grid around airfoil.	88

4.11 Initial sampling data and additional sampling data: (a) multi-fidelity approach, (b) single-fidelity approach.	90
4.12 Non-dominated solution of two-objective airfoil shape optimization problem. . .	91
4.13 Hypervolume comparison of multi-fidelity approach and single-fidelity approach.	91
4.14 Cross validation of C_d	91
4.15 Parallel coordinated plots of non-dominated solutions: (a) multi-fidelity ap- proach, (b) single-fidelity approach.	92
4.16 Comparison of design geometries: (a) multi-fidelity approach, (b) single-fidelity approach.	92
4.17 Initial sampling data and additional sampling data: (a) multi-fidelity approach, (b) single-fidelity approach.	94
4.18 Hypervolume comparison of multi-fidelity approach and single-fidelity approach.	94
4.19 Comparison of non-dominated solutions of three-objective optimization test prob- lem.	95
4.20 Cross-validation results: (a) results of C_d , (b) results of C_l	95
4.21 Parallel coordinated plots of non-dominated solutions: (a) multi-fidelity ap- proach, (b) single-fidelity approach.	96
4.22 Comparison of design geometries: (a) multi-fidelity approach, (b) single-fidelity approach.	96

Chapter 1

Introduction

1.1 Current Situation of Aeronautical Design

In recent years, optimized aeronautical design has been increasingly popular in commercial aircraft design. Airbus designed the A380 while employing an optimization method to reduce the weight of the aircraft wing [1, 2]. The Japan Aerospace Exploration Agency (JAXA) used a shape optimization method to design the supersonic jet [3]. This method was used to increase aerodynamic performance and reduce sonic boom [4-6]. Thus, it has been required to use high-fidelity computation in aeronautical design. However aeronautical design commonly involves complicated problems and high-fidelity computation is expensive. In addition, designers should consider aeronautical design as a problem that involves several objectives. For example, it is necessary for a designer to simultaneously reduce the aircraft weight [7-11] and improve the aerodynamic performance at all operating speeds, including during take-off, landing, and cruising conditions [12-14]. For this reason, several researchers [9, 10] have created optimization methods that consider the reduction of computational costs for multi- or many-objective optimization problems. For example, Drozdik [15] has developed multi-objective differential evolution (DE) algorithms to reduce the computation cost of multi-objective optimization problems. This method has better performance than the original multi-objective DE [16] because it includes domination rank and crowding distance in its process. The hybrid optimization algorithm [17],

which combines a genetic algorithm (GA) and neural network, has been developed to enhance the performance of the optimization algorithm. However, these methods could not be used for expensive functions because they still require many computation evaluations.

In principle, optimization techniques find the best solution to a problem by searching for the minimum or maximum values in a function. Unfortunately, traditional optimization methods, such as gradient-based methods [18-20] or evolutionary algorithms [21, 22], require several computation evaluations. Therefore, researchers have been trying to improve the efficiency of these traditional optimization algorithms. However, the highly accurate evaluations are too expensive if optimization algorithms are employed [23]. Consequently, a combination of surrogate models, such as the radial basis (RBF) [24-26], response surface [27, 28], and Kriging model [29, 30], are used to predict expensive functions and to find optimal shapes for aeronautical designs.

Highly accurate surrogate models that result in an accurate optimal solution are required for surrogate model-based optimizations. The efficient global optimization (EGO), which is based on model uncertainty, has been proposed [31]. The EGO uses expected improvement (EI) [31, 32] or expected hypervolume improvement (EHVI) to find an additional optimum point in the optimization process [33-35]. The advantage of the EGO is that it could increase the probability of the optimization process locating the global optimum point because the EGO involves an additional sampling process, which is based on model uncertainty.

To solve aeronautical design problems, aeronautic evaluations require many computation levels (i.e., fidelities that are determined by governing equations). For example, aerodynamic forces for airfoil design could be defined with a panel method for low-level computations [36, 47], as well as with a Navier-Stokes computation for high-level computations [28, 39]. Because of this feature of aerodynamic evaluations, the multi-fidelity approach can be considered for further improvements in the efficiency of surrogate model-based optimization [40-42].

The goal of this thesis is to propose a multi-fidelity optimization, using a surrogate model-based EHVI, that can improve efficiency and accuracy when using a high-fidelity function to find the optimum point for a multi-objective design problem.

1.2 Recent Researches on Optimization Techniques for Real World Problems

Many optimization tools for engineering designs have been developed [8]. The traditional design methods that use the function gradient are known as the Newton method or sequential quadratic programming (SQP) [18-20]. While they have been widely used, the disadvantage of the gradient-based methods is the requirement of function gradients, which cannot be easily defined for real world problems. Consequently, the evolutionary computation methods have increased in popularity because they do not require gradients. Examples of the evolutionary computation [21, 22] method are genetic algorithms GAs [43, 44], particle swarm optimization (PSO) [45-47], DE [17, 48], simulated annealing (SA) [49, 50], among others [51-55]. GAs are a well-known method for aeronautical design because it has a high probability of locating the global optimum point. In addition, the concept of the GAs are easy to understand, and it is easily applied to various applications.

The GAs [43, 44] are a stochastic search method based upon the theory of natural selection. It was developed by Holland at the University of Michigan in the 1960s and 1970s, and Goldberg further extended its theoretical foundations and applications. The GAs are a popular algorithm because it is easy to apply to optimization problems, and it can be considered a black box method. The search procedure starts with an initial population whose individuals are randomly created. By weighting the probability of a gene used for breeding in terms of its fitness, the characteristics that give the best solutions are passed on from one generation to the next generation. The genetic operators such as selection, crossover, and mutation are applied to the parents to create the offspring. For example, the blend crossover method (BLX) [56] and the unimodal normal distribution crossover (UNDX) [57] have been proposed and yield good exploration performances. The GAs can be expanded to solve multi-objective optimization problems via the Pareto ranking theory. A non-dominated sorting method that is called the non-dominated sorting genetic algorithm (NSGA-II) [58] is widely used as a multi-objective genetic algorithm. The performance metrics that have been considered for these multi-objective

optimization problems are maximum spread [59, 60] and hypervolume [60, 61].

In aeronautical design, GAs are popular for finding the optimum design. For example, the panel method [35, 36], blade element momentum theory (BEMT) [62, 63], and the NASA chemical equilibrium with applications (NASA-CEA) code [64] are often used to design rocket engines. However, they do not always yield the true optimum shape because the evaluation is low-fidelity, which results in low accuracy. To include high-fidelity functions in the optimization process, the surrogate model is widely used. This method was first studied by Schmit in 1974 [65] with respect to wing structural optimization. This research demonstrated the concept of finding the optimum size of the wing structure by approximation of the response variables via Taylor series expansions to reduce the computational time of the optimization process. Response surface [26 - 28] is another surrogate model that is often used, and the RBF [23-25] and the Kriging [29, 30] are more flexible methods for predicting complicated functions. The RBF method was originally developed by Broomhead et al. [21]. This approximation process can be interpreted as a simple kind of neural network. The Kriging method, which was originally developed by Matheron [29], constructs surrogate models based on Gaussian stochastic process models. These methods are popular for real world applications because aeronautical design always requires non-linear functions.

The design of experiments (DoEs) are an important technique for obtaining sampling designs while including input-output relationships. The DoEs were originally studied by Fisher [66]. Traditional DoE techniques [67, 68] include central composite design, Box-Behnken design, full-factorial designs, and the Taguchi method [69]. Because the number of samples is fixed, this method is not commonly used for the optimization process. For the optimization process, a popular DoE method is Latin hypercube sampling (LHS) [70], proposed by McKay; LHS can maintain the space filling quality of the sampling points. Because of limitations in the number of function calls, the EGO method was developed to find additional samples, increasing the efficiency of the surrogate model. EIs locate additional samplings by using evaluations based on the uncertainty of models, improving the accuracy of the models for single-objective functions. EHVI was developed from a concept similar to that of EI for multi-objective optimization problems. Note that iteration by EGO will locate the global optimum point with less additional

sampling if the surrogate model has higher accuracy.

The multi-fidelity approach is a promising way to increase the efficiency of the surrogate model-based optimization process, which requires time-consuming function evaluation to solve real-world design problems. Several multi-fidelity approaches and their applications have been studied using a co-Kriging model [41]. For example, Huang [71] used a co-Kriging method. A multi-fidelity optimization method based on the error estimation of response surfaces using low-fidelity and high-fidelity functions was used to design low-boom supersonic jets [72]. In this study, exact values of additional samples by high-fidelity evaluation were not acquired. Thus, the accuracy of high-fidelity functions could not be ensured, particularly around the optimum points for complicated functions. Another multi-fidelity approach with a parameter space reduction technique was proposed to reduce computational times for computational fluid dynamics (CFD) design of helicopter rotor blades [73]. This technique reduced the degree of the design parameter space (i.e., the number of design parameters) to define possible design ranges using a low-fidelity function. Then, a high-fidelity function was used to determine the optimum design in the primary defined design range. However, it is possible to obtain an optimal solution outside the parameter space because design ranges defined using low-fidelity functions are not always appropriate for high-fidelity functions. A multi-fidelity surrogate model was also applied to maximize annual energy production in wind turbine design [74]. An optimal point of a low-fidelity function was determined using GAs. Then, optimization was performed using a high-fidelity function and a gradient-based method, for which the optimum point obtained using the low-fidelity optimization, was used as the starting point. This method could not obtain the optimum for the high-fidelity function if the error between the low-fidelity and high-fidelity functions was large. Multi-fidelity optimization using the hybrid surrogate model based on the response surface method and the RBF method was developed by Sun [75]. This surrogate model could increase the efficiency when predicting a complex function. However, this multi-fidelity optimization procedure cannot find additional sampling based on uncertainty of data.

An alternative solution to the multi-fidelity multi-objective optimization problem is the model reduction technique [76, 77]. A multi-fidelity/multi-objective optimization approach with a

parameter space reduction technique was applied to the design of helicopter rotor blades and airfoils. This technique reduced the design parameter space to define possible design ranges with a low-fidelity function. Then, a high-fidelity function was used to find the optimum design in the primary defined design range. The sampling for the high-fidelity function was chosen by selecting interesting design points from non-dominated solutions in addition to the initial point that was generated from the primary defined design range. However, this method has the potential to obtain an unexpected optimal solution outside the parameter space because the design ranges of the low-fidelity function are not always appropriate for the high-fidelity function.

1.3 Objectives of this Thesis

The objective of this thesis is to develop the efficient optimization tool for engineering design problems. The final target of this research is increase the efficiency of the aeronautical performance optimization via mixed-fidelity approach of low-fidelity/ low-cost evaluations and high-fidelity/ high-cost evaluations. GA was employed to achieve the global design optimization by proposing the modification of the crossover method for improvement of the diversity and increase the convergence rate of the optimization process. The proposed multi-fidelity approach and GA were used in the enhanced EGO by means of the hybrid surrogate model for single-objective optimization problems. After the development of optimization method, it was tested by applying to real world problems, airfoil design and helicopter blade design. Then, the proposed multi-fidelity approach was expand to solve multi-objective design problems. The method was tested by applying to airfoil design problems which has two/three objective functions.

1.4 Outline of this Thesis

This dissertation is organized as follows: In Chapter 2, a new crossover method for GA, the multi-modal crossover, is developed to increase the diversity and the convergence rate of the

optimization algorithm for EI and EHVI maximization. The applicability of the proposed optimization to a real-world problem is considered by solving a multi-objective airfoil design problem. In Chapter 3, a multi-fidelity hybrid surrogate model for EGO is developed. The proposed multi-fidelity approach is investigated by solving mathematical test problems and is applied to an aerodynamic design optimization problem involving helicopter blades (hovering to obtain the maximum blade efficiency). In Chapter 4, the proposed multi-fidelity approach from the previous chapter is extended to solve a multi-objective optimization problem. The approach is investigated with multi-objective mathematical test problems and is applied to a multi-objective unmanned aerial vehicle (UAV) aerodynamic airfoil design problem. In Chapter 5, the conclusions are presented.

Bibliography

- [1] Krog, Lars, Alastair Tucker, and Gerrit Rollema. "Application of topology, sizing and shape optimization methods to optimal design of aircraft components." *Proc. 3rd Altair UK HyperWorks Users Conference*. 2002.
- [2] Krog, Lars, et al. "Topology optimisation of aircraft wing box ribs." *10th AIAA/ISSMO multidisciplinary analysis and optimization conference*. 2004.
- [3] Sato, Koma, et al. "Low-boom and low-drag optimization of the twin engine version of silent supersonic business jet." *Journal of Fluid Science and Technology* 3.4 (2008): 576-585.
- [4] Sakata, Kimio. "Japan's Supersonic Technology and Business Jet Perspectives." *51st AIAA Aerospace Sciences Meeting including the New Horizons Forum and Aerospace Exposition*. 2013.
- [5] Sun, Yicheng, and Howard Smith. "Review and prospect of supersonic business jet design." *Progress in Aerospace Sciences* (2016).
- [6] Kanazaki, M., H. Takagi, and Y. Makino. "Mixed-fidelity efficient global optimization applied to design of supersonic wing." *Procedia Engineering* 67 (2013): 85-99.
- [7] Hicks, Raymond M., and Preston A. Henne. "Wing design by numerical optimization." *Journal of Aircraft* 15.7 (1978):407-412.
- [8] Sobieszczanski-Sobieski, Jaroslaw, and Raphael T. Haftka. "Multidisciplinary aerospace design optimization: survey of recent developments." *Structural optimization* 14.1 (1997):1-23.

- [9] Miller, Gerald. "An active flexible wing multi-disciplinary design optimization method." *5th Symposium on Multidisciplinary Analysis and Optimization*. 1994.
- [10] RA Martins, Joaquim R., Juan J. Alonso, and James J. Reuther. "High-fidelity aerosturctural design optimization of a supersonic business jet." *Journal of Aircraft* 41.3 (2004): 523-530.
- [11] Chiba, Kazuhisa, et al. "High-fidelity multidisciplinary design optimization of wing shape for regional jet aircraft." *International Conference on Evolutionary Multi-Criterion Optimization*. Springer Berlin Heidelberg, 2005.
- [12] CWickramasinghe, Upali K., Robert Carrese, and Xiaodong Li. "Designing airfoils using a reference point based evolutionary many-objective particle swarm optimization algorithm." *IEEE Congress on Evolutionary Computation*. IEEE, 2010.
- [13] Nemec, Marian, David W. Zingg, and Thomas H. Pulliam. "Multipoint and multi-objective aerodynamic shape optimization." *AIAA journal* 42.6 (2004): 1057-1065.
- [14] Li, Wu, Luc Huyse, and Sharon Padula. "Robust airfoil optimization to achieve drag reduction over a range of mach numbers." *Structural and Multidisciplinary Optimization* 24.1 (2002): 38-50.
- [15] Drozdik, Martin, Hernan Aguirre, and Kiyoshi Tanaka. "Attempt to reduce the computational complexity in multi-objective differential evolution algorithms." *Proceedings of the 15th annual conference on Genetic and evolutionary computation*. ACM, 2013.
- [16] Babu, B. V., and M. Mathew Leenus Jehan. "Differential evolution for multi-objective optimization." *Evolutionary Computation, 2003. CEC'03. The 2003 Congress on*. Vol. 4. IEEE, 2003.
- [17] Poloni, Carlo, et al. "Hybridization of a multi-objective genetic algorithm, a neural network and a classical optimizer for a complex design problem in fluid dynamics." *Computer Methods in Applied Mechanics and Engineering* 186.2 (2000): 403-420.

- [18] Rao, Singiresu S., and Singiresu S. Rao. *Engineering optimization: theory and practice*. John Wiley & Sons, 2009.
- [19] Arora, Jasbir. *Introduction to optimum design*. Academic Press, 2004.
- [20] Vanderplaats, Garret N. *Numerical optimization techniques for engineering design: with applications*. McGraw-Hill College, 1984.
- [21] Back, Thomas. *Evolutionary algorithms in theory and practice: evolution strategies, evolutionary programming, genetic algorithms*. Oxford university press, 1996.
- [22] Eiben, Agoston E., and James E. Smith. *Introduction to evolutionary computing*. Springer Berlin Heidelberg: Imprint: Springer, 2015.
- [23] Samareh, Jamshid A. "Survey of shape parameterization techniques for high-fidelity multidisciplinary shape optimization." *AIAA journal* 39.5 (2001): 877-884.
- [24] Broomhead, David S., and David Lowe. *Radial basis functions, multi-variable functional interpolation and adaptive networks*. No. RSRE-MEMO-4148. ROYAL SIGNALS AND RADAR ESTABLISHMENT MALVERN (UNITED KINGDOM), 1988.
- [25] Park, Jooyoung, and Irwin W. Sandberg. "Universal approximation using radial-basis-function networks." *Neural computation* 3.2 (1991): 246-257.
- [26] Chen, Sheng, Colin FN Cowan, and Peter M. Grant. "Orthogonal least squares learning algorithm for radial basis function networks." *IEEE Transactions on neural networks* 2.2 (1991): 302-309.
- [27] Gunst, Richard F. "Response surface methodology: process and product optimization using designed experiments." (1996): 284-286.
- [28] BBezerra, Marcos Almeida, et al. "Response surface methodology (RSM) as a tool for optimization in analytical chemistry." *Talanta* 76.5 (2008): 965-977.
- [29] Matheron, Georges. "Principles of geostatistics." *Economic geology* 58.8 (1963): 1246-1266.

- [30] Oliver, Margaret A., and Richard Webster. "Kriging: a method of interpolation for geographical information systems." *International Journal of Geographical Information System* 4.3 (1990): 313-332.
- [31] Jones, Donald R., Matthias Schonlau, and William J. Welch. "Efficient global optimization of expensive black-box functions." *Journal of Global optimization* 13.4 (1998): 455-492.
- [32] Kleijnen, Jack PC, Wim van Beers, and Inneke Van Nieuwenhuysse. "Expected improvement in efficient global optimization through bootstrapped kriging." *Journal of global optimization* (2012): 1-15.
- [33] Emmerich, Michael TM, André H. Deutz, and Jan Willem Klinkenberg. "Hypervolume-based expected improvement: Monotonicity properties and exact computation." *Evolutionary Computation (CEC), 2011 IEEE Congress on*. IEEE, 2011.
- [34] Shimoyama, Koji, Shinkyu Jeong, and Shigeru Obayashi. "Kriging-surrogate-based optimization considering expected hypervolume improvement in non-constrained many-objective test problems." *Evolutionary Computation (CEC), 2013 IEEE Congress on*. IEEE, 2013.
- [35] Hupkens, Iris, Michael Emmerich, and André Deutz. "Faster computation of expected hypervolume improvement." *arXiv preprint arXiv:1408.7114* (2014).
- [36] Anderson Jr, John David. *Fundamentals of aerodynamics*. Tata McGraw-Hill Education, 2010.
- [37] Katz, Joseph, and Allen Plotkin. *Low-speed aerodynamics*. Vol. 13. Cambridge university press, 2001.
- [38] Nielsen, Eric J., and W. Kyle Anderson. "Aerodynamic design optimization on unstructured meshes using the Navier-Stokes equations." *AIAA journal* 37.11 (1999): 1411-1419.
- [39] Beam, Richard M., and RoF Warming. "An implicit factored scheme for the compressible Navier-Stokes equations." *AIAA journal* 16.4 (1978): 393-402.

- [40] Forrester, Alexander IJ, Andras Sobester, and Andy J. Keane. "Multi-fidelity optimization via surrogate modelling." *Proceedings of the royal society of london a: mathematical, physical and engineering sciences*. Vol. 463. No. 2088. The Royal Society, 2007.
- [41] A new cokriging method for variable-fidelity surrogate modeling of aerodynamic data." *Evolutionary Computation, 2003. CEC'03. The 2003 Congress on*. Vol. 4. IEEE, 2003.
- [42] Alexandrov, N., et al. "Optimization with variable-fidelity models applied to wing design." *38th Aerospace Sciences Meeting and Exhibit*. 2000.
- [43] Goldberg, David E., and John H. Holland. "Genetic algorithms and machine learning." *Machine learning* 3.2 (1988): 95-99.
- [44] Goldberg, David E. "Real-coded genetic algorithms, virtual alphabets, and blocking." *Complex systems* 5.2 (1991): 139-167.
- [45] Kennedy, James. "Particle swarm optimization." *Encyclopedia of machine learning*. Springer US, 2011. 760-766.
- [46] Eberhart, Russell, and James Kennedy. "A new optimizer using particle swarm theory." *Micro Machine and Human Science, 1995. MHS'95., Proceedings of the Sixth International Symposium on*. IEEE, 1995.
- [47] Reyes-Sierra, Margarita, and CA Coello Coello. "Multi-objective particle swarm optimizers: A survey of the state-of-the-art." *International journal of computational intelligence research* 2.3 (2006): 287-308.
- [48] Storn, Rainer, and Kenneth Price. "Differential evolution - a simple and efficient heuristic for global optimization over continuous spaces." *Journal of global optimization* 11.4 (1997): 341-359.
- [49] Van Laarhoven, Peter JM, and Emile HL Aarts. "Simulated annealing." *Simulated Annealing: Theory and Applications*. Springer Netherlands, 1987. 7-15.
- [50] Serafini, Paolo. "Simulated annealing for multi objective optimization problems." *Multiple criteria decision making*. Springer New York, 1994. 283-292.

- [51] Dorigo, Marco, Mauro Birattari, and Thomas Stutzle. "Ant colony optimization." *IEEE computational intelligence magazine* 1.4 (2006): 28-39.
- [52] Baluja, Shumeet. *Population-based incremental learning. a method for integrating genetic search based function optimization and competitive learning*. No. CMU-CS-94-163. Carnegie-Mellon Univ Pittsburgh Pa Dept Of Computer Science, 1994.
- [53] Yang, Xin-She, and Amir Hossein Gandomi. "Bat algorithm: a novel approach for global engineering optimization." *Engineering Computations* 29.5 (2012): 464-483.
- [54] Yang, Xin-She. "Firefly algorithm, stochastic test functions and design optimisation." *International Journal of Bio-Inspired Computation* 2.2 (2010): 78-84.
- [55] Passino, Kevin M. "Biomimicry of bacterial foraging for distributed optimization and control." *IEEE control systems* 22.3 (2002): 52-67.
- [56] Schaer, J. D., and L. Eshelman. "Real-Coded Genetic Algorithms and Interval Schemata. Foundations of Genetic Algorithms-2-, D. Whitley, ed." (1993).
- [57] Kita, Hajime, Isao Ono, and Shigenobu Kobayashi. "Theoretical analysis of the unimodal normal distribution crossover for real-coded genetic algorithms." *Transactions of the Society of Instrument and Control Engineers* 35.11 (1999): 1333-1339.
- [58] Deb, Kalyanmoy, et al. "A fast and elitist multiobjective genetic algorithm: NSGA-II." *IEEE transactions on evolutionary computation* 6.2 (2002): 182-197.
- [59] Okabe, Tatsuya, Yaochu Jin, and Bernhard Sendhoff. "A critical survey of performance indices for multi-objective optimisation." *Evolutionary Computation, 2003. CEC'03. The 2003 Congress on*. Vol. 2. IEEE, 2003.
- [60] Zitzler, Eckart. "Evolutionary algorithms for multiobjective optimization: Methods and applications." (1999).
- [61] Zitzler, Eckart, and Lothar Thiele. "Multiobjective evolutionary algorithms: a comparative case study and the strength Pareto approach." *IEEE transactions on Evolutionary Computation* 3.4 (1999): 257-271.

- [62] Johnson, Wayne. *Rotorcraft aeromechanics*. Vol. 36. Cambridge University Press, 2013.
- [63] Leishman, Gordon J. *Principles of helicopter aerodynamics with CD extra*. Cambridge university press, 2006.
- [64] Kuo, Kenneth K. "Principles of combustion." (1986).
- [65] Schmit, Lucien André , and B. Farshi. "Some approximation concepts for structural synthesis." *AIAA journal* 12.5 (1974): 692-699.
- [66] Fisher, Ronald Aylmer. "The design of experiments." *The design of experiments*. Ed. 5 (1949).
- [67] Montgomery, Douglas C. "Design and analysis of experiments." (1991).
- [68] Keane, Andy, and Prasanth Nair. *Computational approaches for aerospace design: the pursuit of excellence*. John Wiley & Sons, 2005.
- [69] Taguchi, Genichi. *System of experimental design: engineering methods to optimize quality and minimize costs*. UNIPUB/Kraus International Publications, 1987.
- [70] McKay, Michael D., Richard J. Beckman, and William J. Conover. "Comparison of three methods for selecting values of input variables in the analysis of output from a computer code." *Technometrics* 21.2 (1979): 239-245.
- [71] Huang, Likeng, Zhenghong Gao, and Dehu Zhang. "Research on multi-fidelity aerodynamic optimization methods." *Chinese Journal of Aeronautics* 26.2 (2013): 279-286.
- [72] Choi, Seongim, et al. "Multifidelity design optimization of low-boom supersonic jets." *Journal of Aircraft* 45.1 (2008): 106-118.
- [73] Leon, Enric Roca, et al. "Multi-Fidelity Concurrent Aerodynamic Optimization of Rotor Blades in Hover and Forward Flight." *40th European Rotorcraft Forum*. 2014.
- [74] Rethore, Pierre-Elouan, et al. "TopFarm: Multi-fidelity optimization of offshore wind farm." *The Twenty-first International Offshore and Polar Engineering Conference*. International Society of Offshore and Polar Engineers, 2011.

- [75] Sun, Guangyong, et al. "Multi-fidelity optimization for sheet metal forming process." *Structural and Multidisciplinary Optimization* 44.1 (2011): 111-124.
- [76] Leon, Enric Roca, et al. "Multi-Fidelity Concurrent Aerodynamic Optimization of Rotor Blades in Hover and Forward Flight." *40th European Rotorcraft Forum*. 2014.
- [77] Leusink, Debbie, David Alfano, and Paola Cinnella. "Multi-fidelity optimization strategy for the industrial aerodynamic design of helicopter rotor blades." *Aerospace Science and Technology* 42 (2015): 136-147.

Chapter 2

Genetic Algorithm for Aeronautical Application

2.1 Introduction

The meta-heuristic optimization method is widely used to improve aspects of aircraft performance, such as aerodynamics and structural dynamics. In particular, optimizing airfoil design is very effective in increasing the performance of aircraft. In this chapter, the design performance improvement of real-coded genetic algorithms (GA) is carried out through the modification of the crossover and investigated by optimizing an airfoil's performance. Generally, the main operators of GA are the selection, crossover, and mutation operators. In particular, the crossover operator is effective for increasing efficiency. Several well-known crossover operators for real-coded GA are the blend crossover (BLX) [1], the simplex crossover (SPX) [2], the unimodal normal distribution crossover (UNDX) [3] and the Parent-centric crossover method [4].

One advantage of the BLX crossover is its simplicity; however, it is often hard to solve a nonlinear/multimodal problem. On the other hand, while UNDX converges quickly, it often results only in a local optimum, due to the lower diversity of potential solutions checked by this algorithm.

The SPX crossover method is the multi-parents crossover based on a uniform probability to generate offspring. The advantage of SPX is it has simple scheme for multi-parent crossover method but it has show converge compared with other multi-parent crossover method because the crossover region of the SPX crossover method is too large [4]

The UNDX crossover is the multi-parents crossover which the offspring is close to the centroid of their parents. On advantage of UNDX is it has high efficiency for the low population size. However, it has slower convergence rate than the PCX method [4].

The PCX crossover method is the multi-parents crossover which the offspring is close to their parents. It has fast converge compared to other multi-parent crossover method. However, this method has low efficiency when the population size is low [4].

In this chapter, the multi-modal distribution crossover method (MMDX) is proposed. The proposed crossover method is the multi-parents crossover which the offspring is close to the centroid of their parents but the centroid of this crossover method is expanded by another one parents. From this effect, the proposed crossover method could be has skewedness of the data, which it can in crease the diversity of the offspring.

The Roulette Wheel selection method is used for operator selection operator and the uniform mutation method is used for selecting the mutation operator. The advantage of the uniform mutation method is it has a simple scheme, but it has slower convergence than the Gaussian Mutation Operator [5]. The mutation rate is defined as 0.5.

The effect of this crossover for real-coded GA is investigated by test function. Then it applied to an airfoil optimization problem to investigate the effectiveness of the proposed crossover method for real-world problems, and is compared to the BLX and the UNDX operators.

This chapter is organized as follows. In Section 2.2, we provide an overview of the BLX and UNDX operators, and the multi-modal distribution crossover (MMDX) operator in introduced. In Section 2.3, we investigated the effect of the MMDX crossover method by solving test function. In section 2.4, we discuss the theory of the CST airfoil model [6], the aerodynamic evaluation, the cover rate and the parallel coordinate plot (PCP). The airfoil optimization

problems are discussed in Section 2.5. The results of these optimization problems are discussed in Section 2.6.

2.2 Overview of Crossover Method

2.2.1 Blended Crossover (BLX)

The BLX operator is a popular crossover for real-coded GA. This operator creates two offsprings from two parents according to the following equations:

$$o_{c_1} = (1 - \gamma_i)o_1 + \gamma_i o_2, \quad (2.1a)$$

$$o_{c_2} = (1 - \gamma_i)o_1 - \gamma_i o_2, \quad (2.1b)$$

where o_{c_1} is offspring 1, o_{c_2} is offspring 2, o_1 is parent 1, and o_2 is parent 2. Moreover, $\gamma_i = (1 + 2\nu)h_i - \nu$, where h_i is a random number between 0 and 1, and ν is set to 0.5 in accordance with Eshelman and Schaffer [1].

2.2.2 Unimodal Normal Distribution Crossover (UNDX)

The UNDX operator is a multi-parent crossover operator for real-coded GA. The general UNDX operator uses three parents to create one offspring. The offspring of the UNDX operator is decided by the procedure shown in Fig.2.1.

The process begins by choosing parents o_1 , o_2 , and o_3 by the selection process. After the parents are selected, the midpoint o_p between parents o_1 and o_2 is located where

$$o_p = \frac{1}{2}(o_1 + o_2). \quad (2.2)$$

The differential vector is then calculated by

$$q = o_2 - o_1. \quad (2.3)$$

The distance, Q , between the third parent, o_3 , and the line connecting o_1 and o_2 is calculated using the following equation:

$$Q = |o_3 - o_1| \times \left(1 - \left(\frac{(o_3 - o_1)^T (o_2 - o_1)}{|o_3 - o_1| |o_2 - o_1|} \right) \right). \quad (2.4)$$

Finally, an offspring, o_c , is created by the following equation:

$$o_c = o_p + \xi d + \sum_{i=1}^{n-1} \eta_i e_i Q, \quad (2.5)$$

where ξ is a random number following the normal distribution $N(0, \sigma_\xi^2)$. η_i are $n - 1$ random number independently following a normal distribution $N(0, \sigma_\eta^2)$ and the vector $e_i, i = 1, \dots, n-1$ is a normalized orthogonal vector. Recall that q is the differential vector, o_p is the midpoint, and Q is given by (2.4). The recommend values [3] for the parameters of the UNDX operator are based on numerical experiments where the variance of each normal distribution is $\sigma_\xi^2 = \frac{1}{4}$ and $\sigma_\eta^2 = \frac{(0.35)^2}{n}$.

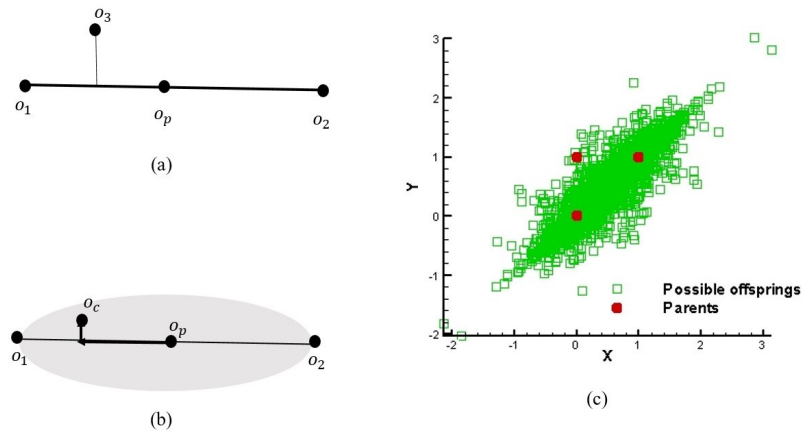


Figure 2.1: Schematic illustration and possible crossover region of UNDX (a) Selection parents (b) Generate offsprings (c) The possible crossover regions of the UNDX.

2.2.3 Proposed Crossover Method

Note that the number of offspring in the UNDX algorithm is less than the number of parents. To increase the efficiency of the crossover, a new crossover operator is proposed as discussed in following paragraphs.

The multi-modal distribution crossover (MMDX) algorithm starts by selecting four parents, o_1 , o_2 , o_3 , and o_4 . The midpoint between parents o_1 and o_2 , and the midpoint between o_3 and o_4 are calculated using the following equations:

$$o_{p_1} = \frac{1}{2}o_1 + o_2, \quad (2.6)$$

$$o_{p_2} = \frac{1}{2}o_3 + o_4, \quad (2.7)$$

where o_{p_1} is the midpoint between o_1 and o_2 , and o_{p_2} is the midpoint between o_3 and o_4 . The differential vectors, q_1 and q_2 , are given by:

$$q_1 = o_2 - o_1, \quad (2.8)$$

$$q_2 = o_4 - o_3, \quad (2.9)$$

After the set of parents is selected, The distance, Q_1 , between the third parent, o_3 , and line connecting o_1 and o_2 and The distance, Q_2 , between the fourth parent, o_4 , and line connecting o_1 and o_2 are calculated by

$$Q_1 = |o_3 - o_1| \times \left(1 - \left(\frac{(o_3 - o_1)^T(o_2 - o_1)}{|o_3 - o_1||o_2 - o_1|} \right) \right), \quad (2.10)$$

$$Q_2 = |o_4 - o_1| \times \left(1 - \left(\frac{(o_4 - o_1)^T(o_2 - o_1)}{|o_4 - o_1||o_2 - o_1|} \right) \right) \quad (2.11)$$

Likewise, The distance, Q_3 , between the first parent, o_1 , and the line connecting o_3 and o_4 and

The distance, Q_4 , between the second parent, o_2 , and line connecting o_3 and o_4 are calculated:

$$Q_3 = |o_1 - o_3| \times \left(1 - \left(\frac{(o_1 - o_3)^T(o_1 - o_3)}{|o_2 - o_1||o_4 - o_3|} \right) \right), \quad (2.12)$$

$$Q_4 = |o_2 - o_3| \times \left(1 - \left(\frac{(o_2 - o_3)^T(o_4 - o_3)}{|o_2 - o_1||o_4 - o_3|} \right) \right), \quad (2.13)$$

Finally, four offspring o_{c_i} where $i = 1, \dots, 4$ are generated by

$$o_{c_1} = o_{p_1} + \xi q_1 + \sum_{i=1}^{n-1} \eta_{1i} e_{1i} Q_1, \quad (2.14)$$

$$o_{c_2} = o_{p_1} - \xi q_1 + \sum_{i=1}^{n-1} \eta_{2i} e_{2i} Q_2, \quad (2.15)$$

$$o_{c_3} = o_{p_2} + \xi q_2 + \sum_{i=1}^{n-1} \eta_{3i} e_{3i} Q_3, \quad (2.16)$$

$$o_{c_4} = o_{p_2} - \xi q_2 + \sum_{i=1}^{n-1} \eta_{4i} e_{4i} Q_4, \quad (2.17)$$

where ξ is a random number following a normal distribution $N(0, \sigma_\xi^2)$. η_i are $n-1$ random numbers independently following a normal distribution $N(0, \sigma_\eta^2)$, and the vector $e_i, i = 1, \dots, n-1$, is a normalized orthogonal vector. The schematic illustration and possible crossover region of the MMDX is shown in Fig.2.2. The possible region of the proposed crossover method compared with the UNDX and the BLX with 2000 offspring is shown in Fig. 2.3. Figure 2.3 can show the proposed crossover method have larger crossover region than the UNDX and BLX.

2.3 Investigation of Proposed Method by Solving Test Functions

The efficiency of the GA with MMDX crossover is investigated by solving test function. The results are compared with the GA with BLX and the UNDX crossover method. For the test problem, the population number of GA is set to 300 and the generation is set to 500 with 20

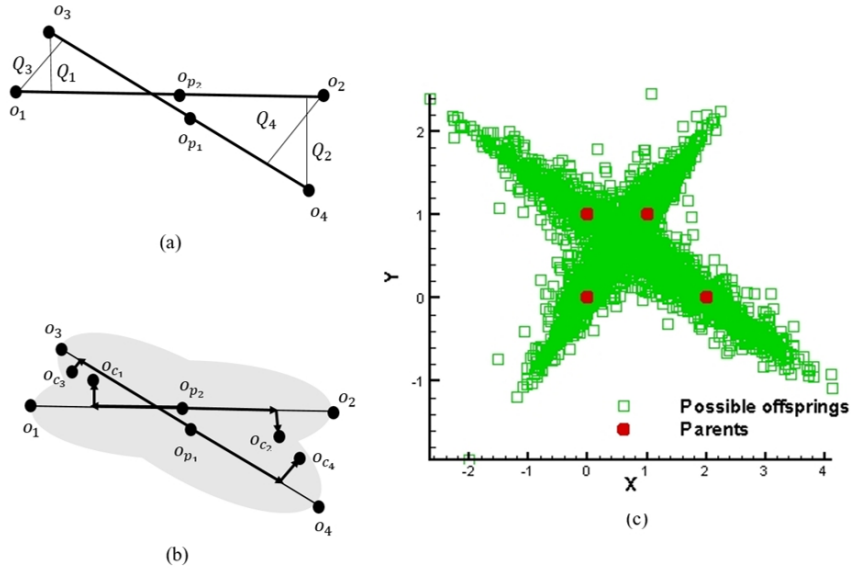


Figure 2.2: Schematic illustration and possible crossover region of the MMDX (a) Selection parents (b) Generate offsprings (c) The possible crossover region of MMDX.

trials.

2.3.1 Formulation

The first problem is Rastrigin problem [5]. The feature of this function is this function is multi-modal with low epistasis function. The definition of the Rastrigin problem is defined as follows:

$$f_{Rastrigin}(x) = 200.0 + \sum_{i=1}^{20.0} [x_i^2 - 10.0 \cos(2\pi x_i)] \quad (2.18)$$

$$- 5.12 \leq x_i \leq 5.12, 1 \leq i \leq 20$$

The second problem is Rosenblock problem [5]. The feature of this function is this function is multi-modal with high epistasis function. The definition of the Rosenblock problem is defined as follows:

$$f_{RosenbrockFunction}(x) = \sum_{i=2}^{20} [100(x_1 - x_i^2)^2 - (x_i - 1)^2] \quad (2.19)$$

$$- 2.048 \leq x_i \leq 2.048, 1 \leq i \leq 20$$

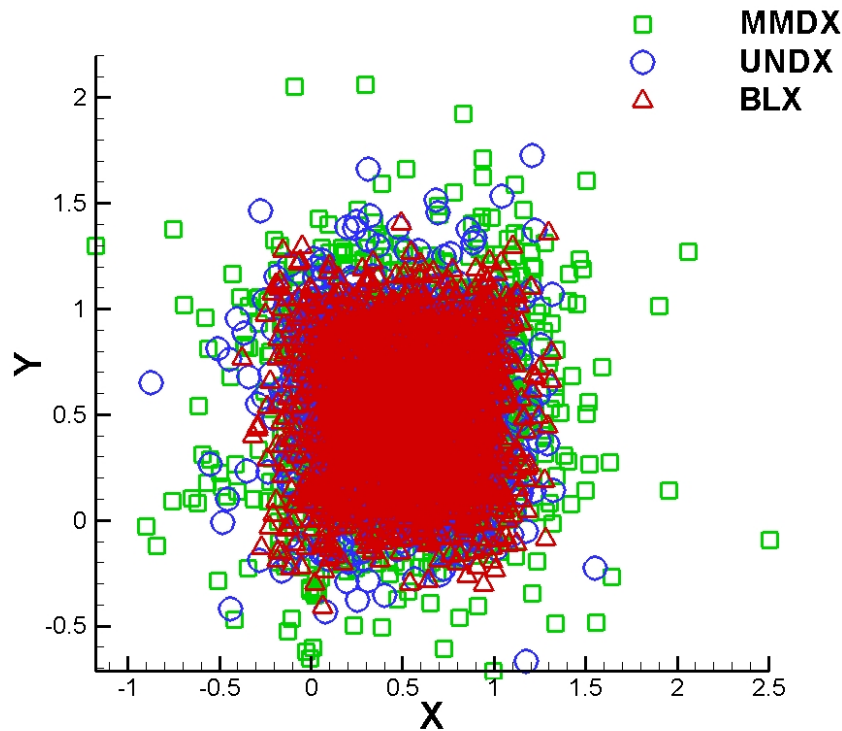


Figure 2.3: The comparison of distribution of individuals generated by the MMDX, UNDX and BLX crossover method with 2000 offspring.

2.3.2 Results of Test Functions

The results are calculated by the average best of solution of these 20 trials. For the 20-dimensional Rastrigin function, the proposed crossover method obtained the best average optimal solution of 0.051938 among all three crossover methods. The history of the best solution for the 20-dimensional Rastrigin function is shown in Fig.2.4. The results could be show the proposed crossover method could be used well for the multi-modal with low epistasis function.

The results of the 20-dimensional Rosenbrock function reveal that the proposed crossover method obtains a best average optimal solution of 11.38014. The history of the best solution of the 20-dimensional Rosenbrock function is shown in Fig.2.5. However, the proposed crossover method has slower converge than the UNDX. The results could be show the proposed crossover method could be used well, but it has slow converge for the multi-modal with high epistasis function.

The results from the test functions could be show the proposed crossover method could be used

well for multi-modal function, but it has slow converge for strong epistasis function.

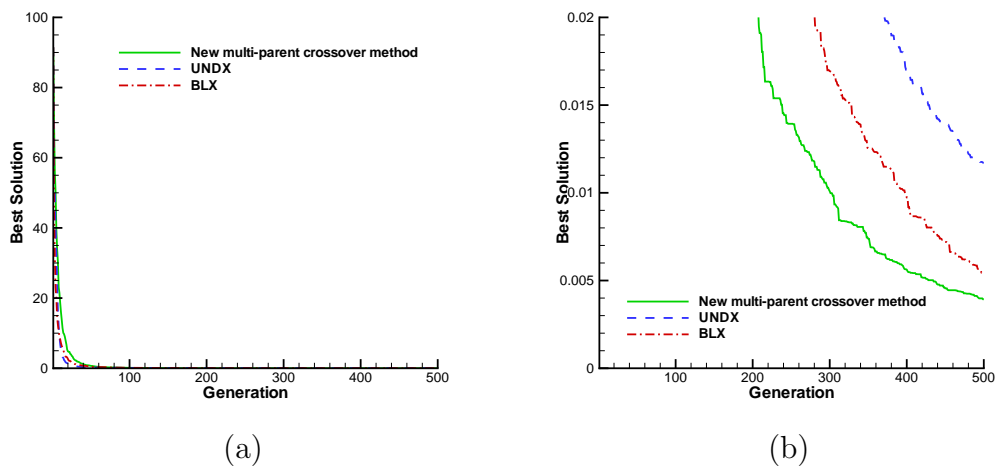


Figure 2.4: Best solution of 20 dimensional Rastrigin function (a) History of best solution (b) Close up view near optimum value

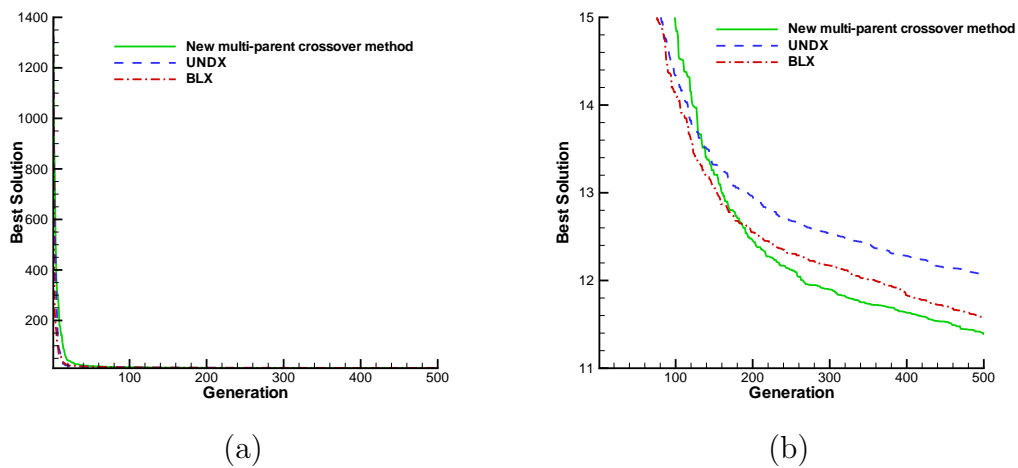


Figure 2.5: Best solution of 20 dimensional Rosenblock function (a) History of best solution (b) Close up view near optimum value

2.4 Design Methods

2.4.1 Class-Shape Function Transformation Parameterization

The CST proposed by Kulfan and Bussolletti [7] represents a two-dimensional geometry consisting of the product of a class function $C(v/c)$, and a shape function, $S(v/c)$, plus a term

that characterizes the trailing edge thickness:

$$\frac{w}{c} = C\left(\frac{v}{c}\right)S\left(\frac{v}{c}\right) + \frac{v}{c} \frac{\Delta z_{te}}{c}, \quad (2.20)$$

where Δz_{te} is the trailing edge thickness, $C(v/c)$ is given in generic form by

$$C\left(\frac{v}{c}\right) \equiv \left(\frac{v}{c}\right)^{N_1} \left[1 - \frac{v}{c}\right]^{N_2} \text{ for } 0 \leq \frac{v}{c} \leq 1, \quad (2.21)$$

and the shape function, $S(v/c)$ is defined on the basis of the Bernstein binomials, by the introduction of weight factor b_i as follows:

$$S\left(\frac{v}{c}\right) = \sum_{i=0}^p \left[b_i \cdot K_{i,p} \cdot \left(\frac{v}{c}\right)^i \cdot \left(1 - \frac{v}{c}\right)^{p-i} \right], \quad (2.22)$$

where p is degree of the Bernstein binomials. And $K_{i,n}$ is given as

$$K_{i,p} = \frac{p!}{i!(p-i)!}. \quad (2.23)$$

Fig.2.6 shows the example of a CST airfoil using a second order polynomial, $N_1 = \frac{1}{2}$, $N_2 = 1$ with weight factors for the upper side of airfoil of .2 and 0.2, and for the lower side of airfoil of -0.3 and -0.1.

2.4.2 Aerodynamics Evaluation

XFOIL [8, 9] was employed as the computational flow solver. In XFOIL, the inviscid pressure distribution is modeled using a linear vortex strength distribution, while the viscous effects and the development of the laminar-turbulent boundary layer are modeled using integral boundary layer theory.

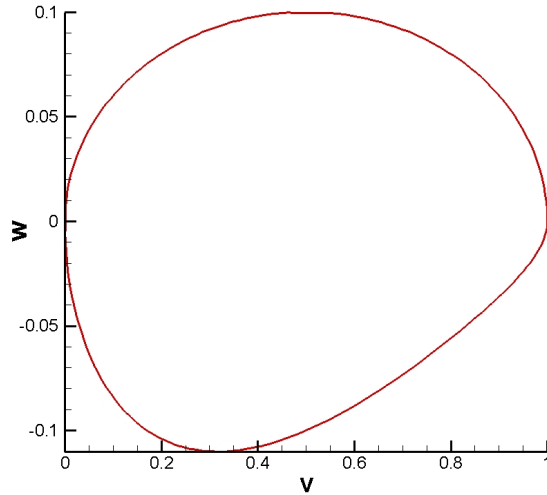


Figure 2.6: Schematic illustration and possible crossover region of the MMDX (a) Selection parents (b) Generate offsprings (c) The possible crossover region of MMDX.

2.4.3 Cover Rate

The cover rate (CR) [10] is the method to evaluate the distribution of the solutions in the objective space. The value of CR is calculated by the following procedures. First, the width of a set of non-dominated solutions of the archive is divided into K parts. Next, the number k_i of dominated domains that solutions exist in are counted. Finally, the CR is calculated by iteration for all M objectives by following equation:

$$CR = \frac{1}{M} \sum_{i=1}^M \frac{k_i}{K}. \quad (2.24)$$

CR can be used to estimate the spread and diversity of a Pareto set in objective space and it has valued between 0 and 1. When the valued of CR closed to 1, it means the Pareto set has the highest diversity.

2.4.4 Parallel Coordinate Plot (PCP)

The parallel coordinate plot (PCP) is one of the statistical visualization techniques for displaying high-dimensional data at a glance in a two-dimensional graph. To create the PCP, the

attribute values in the design problem must be normalized to allow comparison in the same axis. After the normalization, the axes are arranged in a parallel line. Generally, the distances between one line and the next are equivalent. In this study, the normalization value p_i from the design variable dv is given below.

$$p_i = \frac{dv_i - dv_{\min_i}}{dv_{\max_i} - dv_{\min_i}}, \quad (2.25)$$

where dv_{\min_i} represents the lower bound of the i^{th} design variable and dv_{\max_i} denotes the upper bound of the i^{th} design variable.

2.5 Formulation

The design problem considered in this study is the simultaneous minimization of drag (C_d) and maximization of lift (C_l), with a search boundary of C_l from 0.6 to 1.8. The optimization problem can be written as follows:

$$\begin{aligned} & \text{Maximize: } C_l \\ & \text{Minimize: } C_d \\ & \text{Subject to: } 0.6 \leq C_l \leq 1.8 \end{aligned} \quad (2.26)$$

NSGA-II [11] was used to solve this multi-objective optimization problem. The BLX, the UNDX, and the MMDX method are used to investigate the optimal design.

In this study, the Reynolds number is set to 10^6 . The population number is set to 100 and the generation number is set to 100 for NSGA-II execution.

The fifth order polynomial of the CST airfoil is used to generate the upper side and lower side of the airfoil for this optimization problem. Thus, this case has ten parameters to define the CST airfoil, and uses $N_1 = \frac{1}{2}$ and $N_2 = 1$. The design space is defined by the weight factors (b_i) for the lower surface of the airfoil ($dv1 - dv5$), and each factor is set from -0.3 to -0.1. For the upper surface of the airfoil, b_i ($dv6 - dv10$) are also set from 0.1 to 0.3.

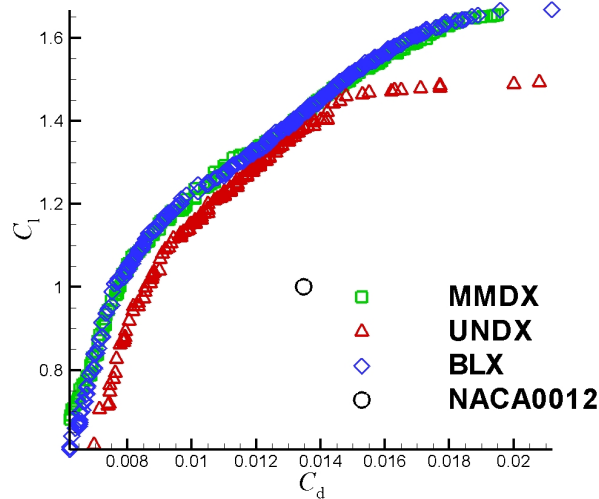
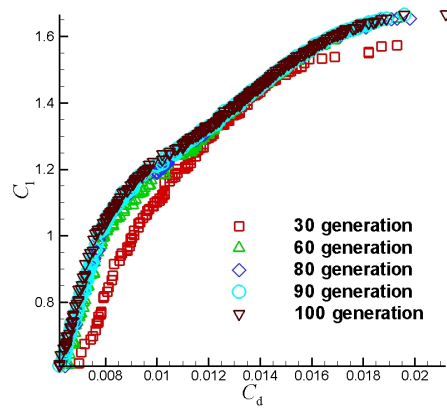


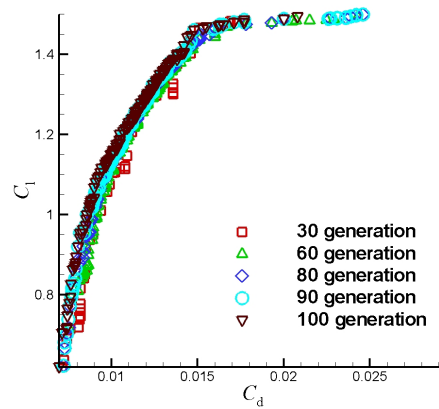
Figure 2.7: Resulting non-dominated solutions of the CST problem.

2.6 Results and Discussion

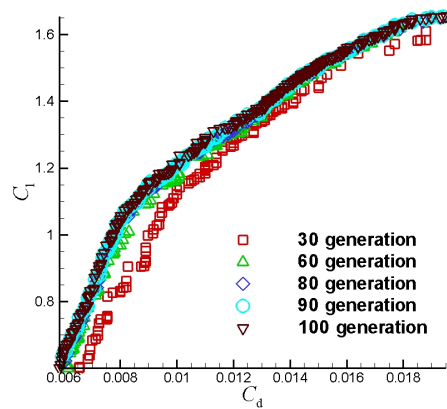
Non-dominated solutions are compared with the initial design. This study chose NACA0012 for BLX, UNDX, and MMDX after the 100th generation, as shown in Fig. 2.7. The initial design (NACA0012) obtained $C_d = 0.0137$ at $C_l = 1.0$. The solution showed that C_d was reduced by 0.013 for MMDX and BLX, and 0.047 for UNDX compared with NACA0012. Moreover, C_l improved by 0.433 for MMDX and BLX and 0.387 for UNDX compared with NACA0012. This result suggested that MMDX can obtain solutions similar to the BLX method and superior to that of the UNDX method, and all these solutions can obtain better solutions than the initial point, which indicates that the algorithm can be used to design a high-efficiency airfoil. The convergence of the MMDX method was faster than that of BLX, with crossover occurring at approximately $C_l = 1.6$, as shown in Fig. 2.7. However, UNDX did not show good non-dominated solution. Figs. 2.8(a)-(c) compare the history of the non-dominated solutions obtained by BLX, UNDX, and MMDX. According to these figures, the solution that was obtained by using the BLX and MMDX methods converged after the 80th generation. By contrast, the solution obtained by using the UNDX method converged after the 40th generation, and the non-dominated solutions did not advance. In addition, the solutions obtained by using the BLX and MMDX methods showed better non-dominated solution than UNDX after the



(a)

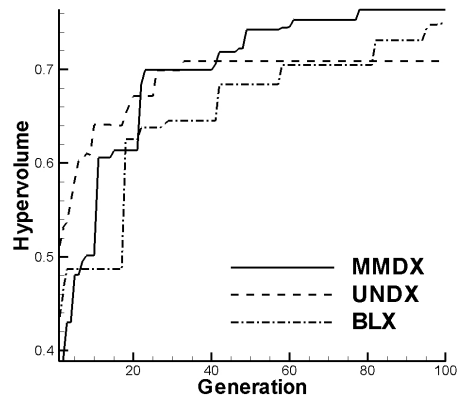


(b)

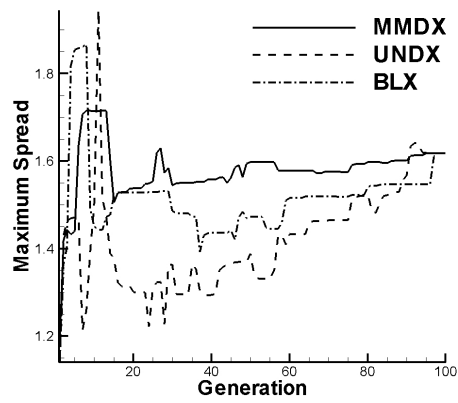


(c)

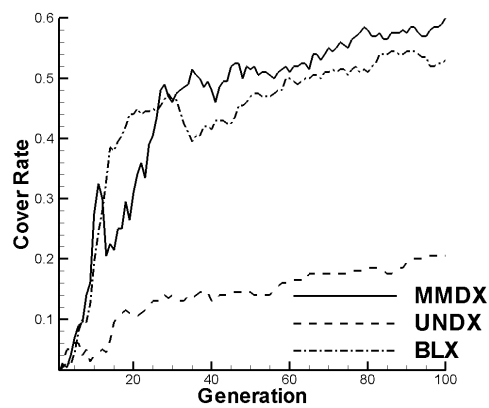
Figure 2.8: The history of non-dominated solutions after the 30th, 60th, 80th, 90th, and 100th generation. (a) Solutions obtained by BLX, (b) Solutions obtained by UNDX, (c) Solutions obtained by the MMDX method.



(a)

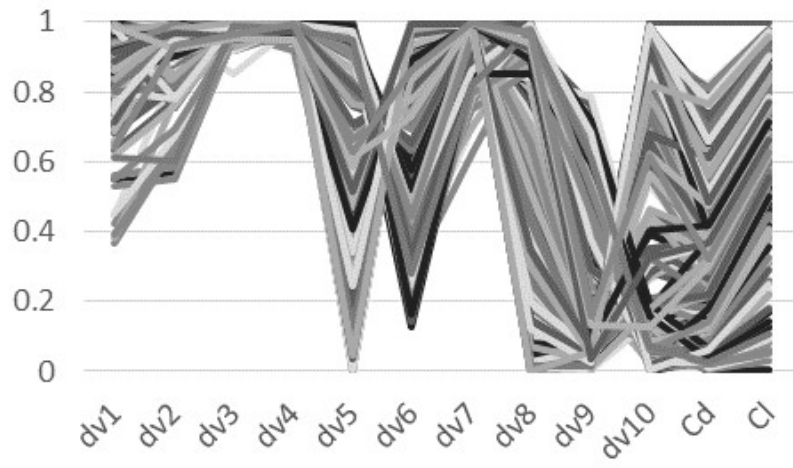


(b)

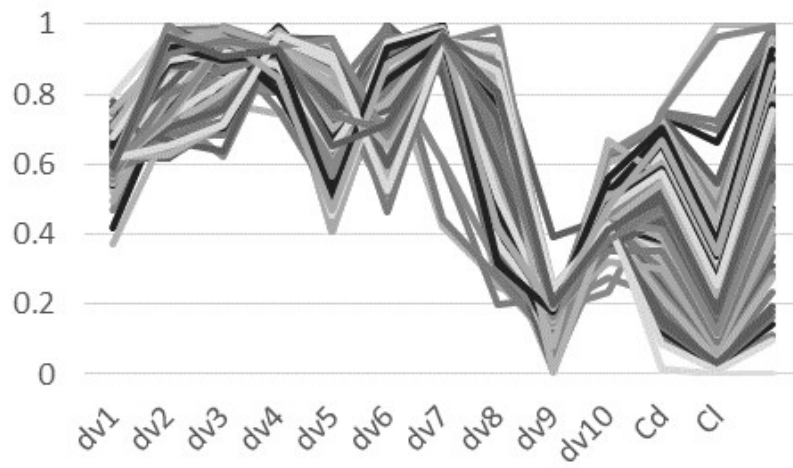


(c)

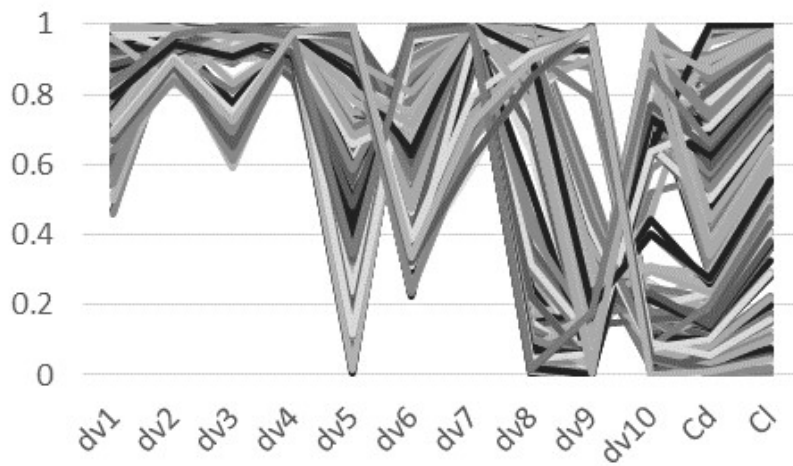
Figure 2.9: Comparison of the history of metrics: (a) Hypervolume, (b) Maximum spread, (c) Variance of Cover rate during the search.



(a)



(b)



(c)

Figure 2.10: The PCP of the non-dominated solution at the 100th generation. (a) BLX (b) UNDX (c) MMDX.

30th generation. This result suggested that GA with BLX and MMDX could achieve better exploration for the present airfoil design than UNDX. The history of metrics is shown in Figs. 2.9(a)-(c). Fig. 2.9(a) shows the hypervolume, and Fig. 2.9(b) shows the maximum spread [11]. Fig. 2.9(c) shows the variance of CR during the search. According to Fig. 2.9(a), the solutions that were obtained by using the MMDX and BLX methods converged after the 80th generation, and the solutions obtained by using UNDX converged after the 40th generation. The maximum spread also suggested that the MMDX method can maintain higher diversity than the BLX and UNDX methods, as shown in Fig. 2.9(b). The variance of CR during the search also suggested that the MMDX method can maintain higher diversity than others as shown in Fig. 2.9(c). The figure also indicates that the MMDX method can obtain a higher maximum CR value than the others. Most CR values that were obtained by using the MMDX method were higher than those obtained by using the other methods, which indicates that the MMDX method can obtain solutions with higher diversity than the UNDX and BLX methods. Thus, the MMDX method, which demonstrates fast convergence while maintaining diversity, is more suitable for real-world problems than the existing techniques, such as BLX and UNDX methods. PCPs for the Pareto solution using the BLX, UNDX, and MMDX methods are shown in Figs. 2.10(a)-(c). The design space of the MMDX method was widely spread, as shown in Fig. 2.10. Fig. 2.10 also suggests that the MMDX crossover can maintain higher diversity than the other crossover methods, as shown in Figs. 2.9. Consequently, the MMDX method can maintain a larger search space without early convergence, which allows a superior non-dominated solution to be obtained.

2.7 Conclusion

This chapter investigated the effectiveness of the MMDX crossover method to solve a real-world airfoil design problem. The fifth-order polynomial of CST airfoil representation was employed. The MMDX method was developed for use with NSGA-II and combined with the interactive program XFOIL. Results suggested that the MMDX method provided superior solutions compared with the BLX and UNDX crossovers because the MMDX method can

maintain higher diversity because of its larger search space. These results imply the possibility of obtaining better solutions to real-world problems using the MMDX crossover method.

Bibliography

- [1] Eshelman, Larry J. "Chapter real-coded genetic algorithms and interval-schemata." *Foundations of genetic algorithms 2* (1993): 187-202.
- [2] Tsutsui, Shigeyoshi, Masayuki Yamamura, and Takahide Higuchi. "Multi-parent recombination with simplex crossover in real coded genetic algorithms." *Proceedings of the 1st Annual Conference on Genetic and Evolutionary Computation-Volume 1*. Morgan Kaufmann Publishers Inc., 1999.
- [3] Kita, Hajime, Isao Ono, and Shigenobu Kobayashi. "Theoretical analysis of the unimodal normal distribution crossover for real-coded genetic algorithms." *Transactions of the Society of Instrument and Control Engineers* 35.11 (1999): 1333-1339.
- [4] Deb, Kalyanmoy, Dhiraj Joshi, and Ashish Anand. "Real-coded evolutionary algorithms with parent-centric recombination." *Evolutionary Computation, 2002. CEC'02. Proceedings of the 2002 Congress on*. Vol. 1. IEEE, 2002.
- [5] Cazacu, Razvan. "Comparative Study between the Improved Implementation of 3 Classic Mutation Operators for Genetic Algorithms." *Procedia Engineering* (2017): 634-640.
- [6] Molga, Marcin, and Czesław Smutnicki. "Test functions for optimization needs." *Test functions for optimization needs* (2005): 101.
- [7] Kulfan, Brenda, and John Bussolletti. "Fundamental" Parametric Geometry Representations for Aircraft Component Shapes." *11th AIAA/ISSMO multidisciplinary analysis and optimization conference*. 2006.

-
- [8] Drela, Mark, and Harold Youngren. "Xfoil 6.9 user primer." *Department of Aeronautics and Astronautics, Massachusetts Institute of Technology, Cambridge, MA* (2001).
- [9] Drela, Mark, and Michael B. Giles. "Viscous-inviscid analysis of transonic and low Reynolds number airfoils." *AIAA journal* 25.10 (1987): 1347-1355.
- [10] Kobayashi, Kenji, Tomoyuki Hiroyasu, and Mitsunori Miki. "Discussion of Clustering and Network Inversion for Multi-Objective Genetic Algorithms." *Frontiers Science Series* 49 (2007): 401.
- [11] Deb, Kalyanmoy, et al. "A fast and elitist multiobjective genetic algorithm: NSGA-II." *IEEE transactions on evolutionary computation* 6.2 (2002): 182-197.
- [12] Zitzler, Eckart. "Evolutionary algorithms for multiobjective optimization: Methods and applications." (1999).

Chapter 3

Multi-fidelity Efficient Global Optimization using Hybrid Surrogate Model

3.1 Introduction

In real-world design problems, computational costs such as those involved in high-fidelity computational fluid dynamics (CFD) are high. The design of a helicopter rotor blade, shown in Figure 1, is a complicated CFD problem that is computationally expensive. Dumont [1] used a Reynolds-averaged Navier - Stokes simulation to design a helicopter blade for hovering, using a gradient-based method. An optimum point was obtained; however, it was difficult to acquire global design knowledge using metaheuristic approaches owing to their high computational cost. Surrogate model-based optimization methods can overcome such problems in engineering design. Efficient global optimization (EGO), which is a kriging model-based method, was proposed by Jones, Schonlau, and Welch [2]. EGO consists of an additional sampling-based expected improvement (EI) that considers the uncertainty in models to improve their accuracy. EIs evaluated based on kriging models were proposed as index values to obtain additional samples that could improve the accuracy of a surrogate model. However, the functions used to

model real-world problems are often multi-modal. It is difficult to approximate these functions accurately using a limited number of sample designs in cases of high-cost computation.

To construct accurate models for real-world design problems with computationally time consuming functions, multi-fidelity optimization [3-8] was investigated for improving their efficiency. A multi-fidelity approach that combines high- and low-fidelity data can further improve efficiency by significantly reducing the number of functions for high-fidelity evaluations, such as those in CFD. Several multi-fidelity approaches and their applications were developed using a co-kriging model [3, 4]. A co-kriging model was employed to develop optimal airfoil designs [3]. Huang [4] used a co-kriging surrogate model, which could reduce the amount of high-fidelity data used in the optimization process. In other words, it is difficult to approximate complex and expensive functions with few evaluations using a co-kriging method. A multi-fidelity optimization method based on error estimation of the response surfaces using low- and high-fidelity functions was used to design low-boom supersonic jets [5]. However, additional samples of high-fidelity evaluations were not acquired. Thus, the global accuracy of high-fidelity functions could not be ensured, particularly around the optimum points for complicated functions. A multi-fidelity approach with a parameter-space reduction technique was applied for reducing the required computational time for the CFD design of helicopter rotor blades [6]. This technique could reduce the design parameter space to define possible design ranges using a low-fidelity function. Then, a high-fidelity function was used to determine the optimum design in the primary defined design range. However, it is possible to obtain an optimal solution outside the parameter space because the design ranges defined using the low-fidelity functions are not always appropriate for high-fidelity functions. A multi-fidelity surrogate model was used to maximize the annual energy production in a wind turbine design [7]. An optimal point for the low-fidelity function was determined using a genetic algorithm (GA). Then, the optimization was performed using a high-fidelity function and a gradient-based method, for which the optimum point obtained from the low-fidelity optimization was used as the starting point. This method cannot obtain the optimum for the high-fidelity function if the error between the low- and high-fidelity functions is large. Multi-fidelity optimization, using the hybrid surrogate model-based response surface method and the radial basis function (RBF) method, was developed by Sun in 2011 [8]. The

authors successfully showed that this hybrid surrogate model improves the efficiency of the surrogate model for the predicted complex function. However, this multi-fidelity optimization procedure cannot perform additional sampling based on the uncertainty of data.

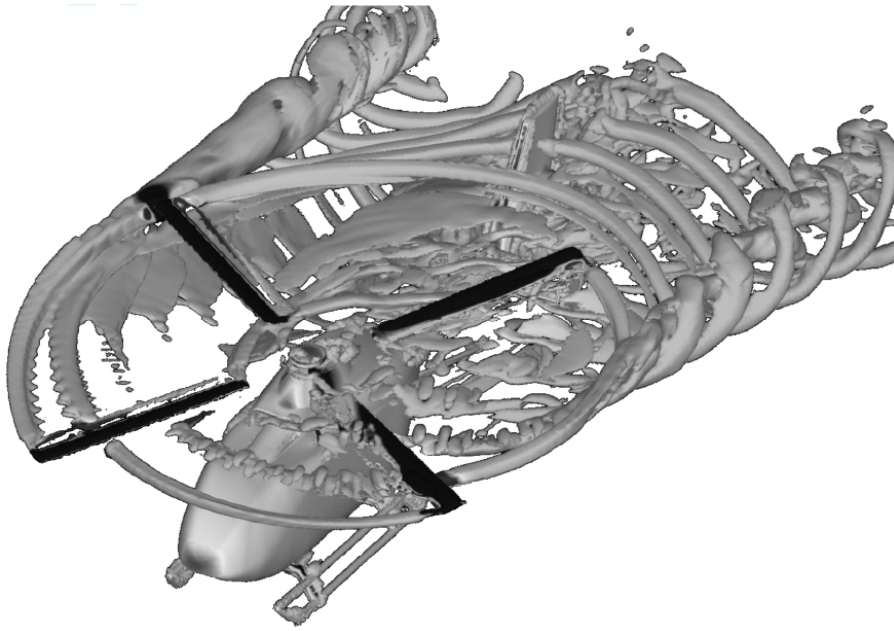


Figure 3.1: CFD example [9].

In this study, a hybrid surrogate model-based EGO, which could improve the efficiency and accuracy in determining an optimum point using a high-fidelity function, is proposed and investigated by applying it to a real-world problem. The proposed EGO uses a low-fidelity function to construct a global model that can obtain the global landscape of a high-fidelity function to evaluate local deviation. The global model is approximated by an RBF [10, 11] based on a database of low-fidelity evaluations that can predict the multi-modal function. The RBF can carry out highly accurate and smooth approximations to observe the landscape of a function with large data sets. Because of this advantage, the RBF is used as the global model of the hybrid surrogate model using local deviation evaluations by the kriging method. Local variances are predicted using a correlation term obtained through the kriging method. The proposed EGO is investigated by solving mathematical test problems and comparing the results with those of the co-kriging-based and ordinary kriging-based EGOs. In addition, the proposed EGO is applied to determine the optimal design of a primary helicopter rotor blade for hovering. The optimization results are compared with those of the co-kriging-based and ordinary kriging-based

EGOs.

3.2 Surrogate Model Methods for Multi-fidelity Optimization

3.2.1 Kriging Method

An ordinary kriging model [12] can predict the unknown function $\hat{y}(\mathbf{x})$ as

$$\hat{y}(\mathbf{x}) = \mu(\mathbf{x}) + \varepsilon(\mathbf{x}), \quad (3.1)$$

where $\mu(\mathbf{x})$ is global model, and $\varepsilon(\mathbf{x})$ denotes a local model. Sample points, \mathbf{x} , are interpolated using a Gaussian random function. The correlation between $Z(\mathbf{x}_i)$ and $Z(\mathbf{x}_j)$ is related to the distance between the two corresponding points, \mathbf{x}_i and \mathbf{x}_j . The distance function between points \mathbf{x}_i and \mathbf{x}_j is expressed as

$$d(\mathbf{x}_i, \mathbf{x}_j) = \sum_{k=1}^n \theta^k |\mathbf{x}_i^k - \mathbf{x}_j^k|^2, \quad (3.2)$$

where $\theta^k (0 \leq \theta^k \leq \infty)$ is the k^{th} element of the correlation vector parameter, n is the number of high-fidelity samples. The correlation between the points \mathbf{x}_i and \mathbf{x}_j is defined as

$$Corr[Z(\mathbf{x}_i), Z(\mathbf{x}_j)] = \exp[-d(\mathbf{x}_i, \mathbf{x}_j)]. \quad (3.3)$$

Kriging prediction can be expressed as

$$\hat{y}(\mathbf{x}) = \mu + \mathbf{r}^T \mathbf{R}^{-1} (\mathbf{F} - \hat{\mu}), \quad (3.4)$$

where $Z(\mathbf{x}_i)$ represents a local deviation from the global model [13], $\mathbf{F} = [f(\mathbf{x}_1), f(\mathbf{x}_2), f(\mathbf{x}_3), \dots, f(\mathbf{x}_n)]^T$ is the value of the evaluated high-fidelity function at $X = \{\mathbf{x}_1, \mathbf{x}_2, \mathbf{x}_3, \dots, \mathbf{x}_n\}$, \mathbf{R} denotes the

$n \times n$ matrix whose (i, j) entry is $\text{Corr}[Z(\mathbf{x}_i), Z(\mathbf{x}_j)]$, and \mathbf{r} is the vector i^{th} element is

$$r_i(\mathbf{x}) = \text{Corr}[Z(\mathbf{x}), Z(\mathbf{x}_i)]. \quad (3.5)$$

The unknown parameter, θ , for the kriging model can be estimated via maximum likelihood estimation (MLE):

$$Ln(\mu, \sigma^2, \theta) = -\frac{n}{2} \ln(\sigma^2) - \frac{1}{2} \ln(|\mathbf{R}|). \quad (3.6)$$

MLE is an m -dimensional unconstrained nonlinear optimization problem. In this article, a GA [14] is used to solve this problem. For a given θ , σ^2 can be defined as

$$\sigma^2 = \frac{(\mathbf{F} - \hat{\boldsymbol{\mu}})^T \mathbf{R}^{-1} (\mathbf{F} - \hat{\boldsymbol{\mu}})}{n}. \quad (3.7)$$

$\mu(\mathbf{x})$ is assumed to be constant in the original Kriging model, and $\hat{\boldsymbol{\mu}}$ is given by (3.8):

$$\hat{\boldsymbol{\mu}} = [\mu(\mathbf{x}), \mu(\mathbf{x}), \mu(\mathbf{x}), \dots, \mu(\mathbf{x})]^T, \quad (3.8)$$

$\mu(\mathbf{x})$ is defined as

$$\mu(\mathbf{x}) = \frac{\mathbf{1}^T \mathbf{R}^{-1} \mathbf{F}}{\mathbf{1}^T \mathbf{R}^{-1} \mathbf{1}}. \quad (3.9)$$

The mean square error $s^2(\mathbf{x})$ at a point \mathbf{x} of this function can be calculated using the following equation:

$$s^2(\mathbf{x}) = \sigma \left[1 - \mathbf{r}^T \mathbf{R}^{-1} \mathbf{r} + \frac{1 - \mathbf{1}^T \mathbf{R}^{-1} \mathbf{F}}{\mathbf{1}^T \mathbf{R}^{-1} \mathbf{1}} \right], \quad (3.10)$$

where $\mathbf{1}$ denotes an n -dimensional unit vector. Schematic illustration of the ordinary Kriging model is shown in Fig. 3.2(a).

3.2.2 Hybrid Surrogate Model for a Multi-fidelity Approach

The proposed hybrid surrogate-model-based EGO for the multi-fidelity approach employs an RBF to represent the global model, $\mu(\mathbf{x}) + fr(\mathbf{x})$, based on a data set obtained from low-fidelity

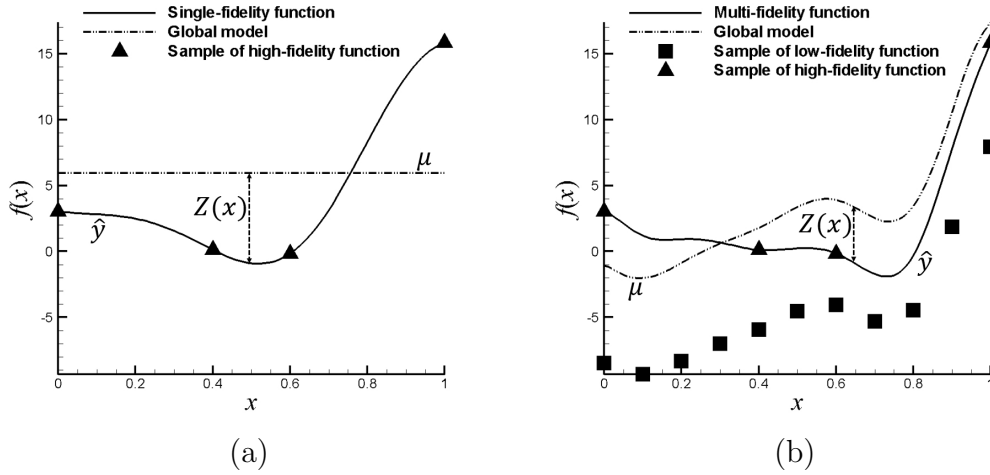


Figure 3.2: Schematic illustration of a single-fidelity and multi-fidelity surrogate model. (a) Ordinary Kriging model (b) Hybrid model.

evaluation. The hybrid surrogate model considered in this study can be expressed as

$$\hat{y}(\mathbf{x}) = [\mu(\mathbf{x}) + fr(\mathbf{x})] + \mathbf{r}^T \mathbf{R}^{-1} (\mathbf{F} - \hat{\mu} - \mathbf{F}_{\mathbf{R}}). \quad (3.11)$$

The local deviations $\mathbf{r}^T \mathbf{R}^{-1} (\mathbf{F} - \hat{\mu} - \mathbf{F}_{\mathbf{R}})$ are evaluated on the basis of a high-fidelity data set using the kriging method, where $\mathbf{F} = [f(\mathbf{x}_1), f(\mathbf{x}_2), f(\mathbf{x}_3), \dots, f(\mathbf{x}_n)]^T$ is the value of the high-fidelity function at $\mathbf{X} = \{\mathbf{x}_1, \mathbf{x}_2, \mathbf{x}_3, \dots, \mathbf{x}_n\}$; $\mathbf{F}_{\mathbf{R}} = [fr(\mathbf{x}_1), fr(\mathbf{x}_2), fr(\mathbf{x}_3), \dots, fr(\mathbf{x}_n)]^T$. Note that $\mu(x)$ is a mean value of the Gaussian process of the high-fidelity data, assumed to be a constant value expressed by Equation (3.9), and the definition of $\hat{\mu}$ is given by Equation (3.8). The RBF term of low-fidelity ($fr(\mathbf{x})$), predicted from the low-fidelity data, and can be expressed as

$$fr(\mathbf{x}) = a_0 + a_1 f_l(\mathbf{x}), \quad (3.12)$$

where $f_l(\mathbf{x})$ is a function predicted by an RBF using low-fidelity data, a_0 and a_1 are correlation terms between the low-fidelity data and the high-fidelity data. Further, σ^2 can be defined as

$$\sigma^2 = \frac{(\mathbf{F} - \hat{\mu} - \mathbf{F}_{\mathbf{R}})^T \mathbf{R}^{-1} (\mathbf{F} - \hat{\mu} - \mathbf{F}_{\mathbf{R}})}{n}. \quad (3.13)$$

The unknown parameters (θ , a_0 , and a_1) for the hybrid surrogate multi-fidelity model can be estimated by MLE, as expressed by (3.6).

Approximation of global model using RBF

An RBF [10, 11] can be used to approximate a function as follows:

$$f_l(\mathbf{x}) = \sum_{m=1}^N w_m \Phi(\mathbf{x} - \mathbf{x}_m) \quad (3.14)$$

where $\Phi(\mathbf{x})$ is a radial basis function, N is the number of low-fidelity sample points, and $\mathbf{w}_m (m = 1, 2, 3, \dots, N)$ is a weighting function. A multi-quadratic function is applied as an RBF in this study. The weighting function $\mathbf{w} = [w_1, w_2, w_3, \dots, w_N]^T$ is determined from the interpolation conditions

$$\mathbf{A}\mathbf{W} = \mathbf{F}_L \quad (3.15)$$

where $A = \begin{pmatrix} a_{1,1} & a_{1,2} & \cdots & a_{1,k} \\ a_{2,1} & a_{2,2} & \cdots & a_{2,k} \\ \vdots & \vdots & \ddots & \vdots \\ a_{m,1} & a_{m,2} & \cdots & a_{m,k} \end{pmatrix}$, $a_{m,k} = \Phi(\mathbf{x}_m - \mathbf{x}_k)$, $k = 1, 2, 3, \dots, N$, $m = 1, 2, 3, \dots, N$

Here, $F_L = [f(\mathbf{x}_1), f(\mathbf{x}_2), f(\mathbf{x}_3), \dots, f(\mathbf{x}_N)]^T$ is the value of the low-fidelity function at $X = \{\mathbf{x}_1, \mathbf{x}_2, \mathbf{x}_3, \dots, \mathbf{x}_N\}$.

3.3 Efficient Global Optimization

3.3.1 Efficiency Global Optimization for single-fidelity optimization

The procedure of EGO [2] based on the ordinary Kriging method is illustrated in Figure 3.3(a) that explained in the following paragraph.

- First, EGO is started with generated initial samples. In this study, Latin hypercube sampling (LHS) [15] is employed.
- Second, sample data are evaluated and the model is predicted using the Kriging method.

- Third, an arbitrary optimization method is used to find an additional point, \mathbf{x} , by maximizing EI. The EI at point \mathbf{x} can be expressed as

$$I(\mathbf{x}) = \max[f_{ref} - y(\mathbf{x}), 0], \quad (3.16)$$

$$E[I(\mathbf{x})] = \int_{-\infty}^{f_{ref}} (f_{ref} - y(\mathbf{x}))\phi(y(\mathbf{x}))dy, \quad (3.17)$$

where ϕ is the probability density function that represents uncertainty about $y(\mathbf{x})$.

- Fourth, additional sampling based on EI, referred to as EGO, is repeated the optimization process to second process until an objective function converges.

3.3.2 Efficiency Global Optimization for multi-fidelity optimization

Original EGO can be applied to the hybrid surrogate model given by Equation (11), because local deviations are estimated using the Kriging method. The proposed EGO based on the hybrid surrogate model is summarized in Figure 3.3(b) that explained in the following paragraph.

- First, the proposed EGO is started by acquiring initial samples for low-fidelity/inexpensive functions. Low-fidelity sample data are used to predict a global model.
- Second, another set of samples, obtained using a high-fidelity function, are obtained. This result is used to estimate local deviations using the Kriging method.
- Third, the multi-fidelity surrogate model, which can predict the value of an unknown point (an approximation of the high-fidelity function), is generated. A GA with the MMDX crossover method is used to find the maximum EI at point \mathbf{x} by Eq.(3.16) and (3.17).
- Fourth, additional sampling based on EI, referred to as EGO, is repeated the optimization process to second process until an objective function converges.

In this work, the GA with the MMDX crossover method was used to search the maximize of EI value because it design to find the optimum point of multi-modal function and the prediction

function by surrogate model always multi-modal function. The GA with MMDX crossover method has higher efficient than the GA with BLX and UNDX method. The search history of maximize of EI value to find the first sampling of helicopter blade design problem with the number of population is set to 100 and number of iteration is set to 100 is shown in Fig.3.4. It can shown the GA with MMDX crossover method have higher converge compared to the GA with BLX and UNDX method.

3.4 Investigation of Proposed Method by Solving Test Functions

The efficiency of the proposed hybrid surrogate model - based EGO is investigated by solving test functions. The results are compared with those of co-Kriging - based EGO and ordinary Kriging-based EGO.

3.4.1 Formulation

In this study, four test functions are used. y_h denotes a high-fidelity/expensive function and y_l denotes the low-fidelity/inexpensive function.

- Definition of the six-hump camel-back function (SC) is defined as follows:

$$\begin{aligned}
 &\text{minimize: } y_h(x_1, x_2) = sc(x_1, x_2) \\
 &y_l(x_1, x_2) = sc(0.7x_1, 0.7x_1) + x_1x_2 - 65 \\
 &sc(x_1, x_2) = 4x_1^2 - 2.1x_1^4 + \frac{x_1^6}{3} + x_1x_2 - 4x_2^2 + 4x_2^4 \\
 &x_1 \in [-2, 2], x_2 \in [-2, 2]
 \end{aligned} \tag{3.18}$$

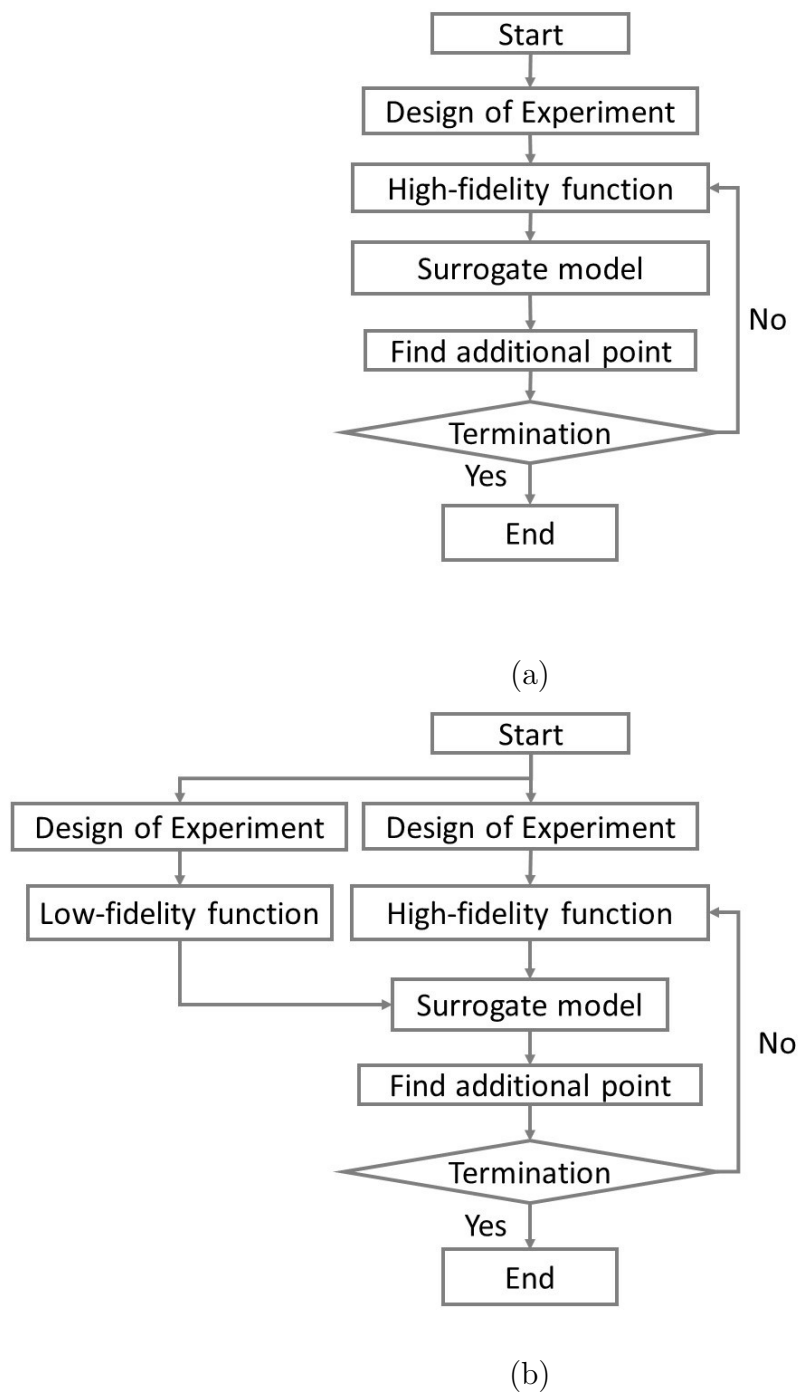


Figure 3.3: Flowchart of efficient global optimization. (a) Efficient global optimization (b) Proposed EGO with multi-fidelity surrogate model.

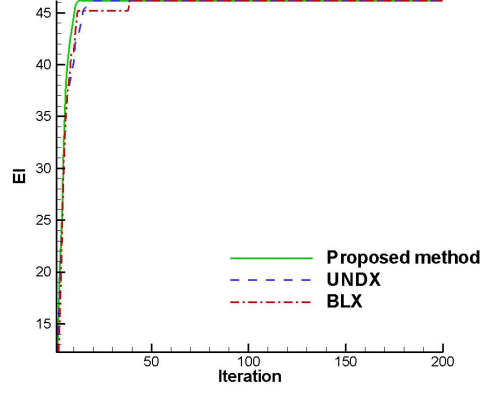


Figure 3.4: Search history of EI value for the first sampling of helicopter blade design problem.

- Definition of the Branin function (BR) is defined as follows:

$$\text{minimize: } y_h(x_1, x_2) = br(x_1, x_2) - 22.5x_2$$

$$y_l(x_1, x_2) = br(0.7x_1, 0.7x_2) - 15.75x_2 + 20(0.9 + x_1)^2 - 50$$

$$br(x_1, x_2) = 10 + \left[x_2 - \frac{5.1x_1^2}{4\pi^2} + \frac{5x_1}{\pi} \right] + 10\cos(x_1) \left[1 - \frac{1}{8\pi} \right] \quad (3.19)$$

$$x_1 \in [-5, 10], x_2 \in [0, 15]$$

- Definition of the Himmelblau function (HIM) is defined as follows:

$$\text{maximize: } y_h(x_1, x_2) = him(x_1, x_2)$$

$$y_l(x_1, x_2) = him(0.5x_1, 0.8x_2) + x_2^3 - (x_1 + 1)^2$$

$$him(x_1, x_2) = (x_1^2 + x_2 - 11)^2 + (x_2^2 + x_1 - 7)^2 \quad (3.20)$$

$$x_1 \in [-3, 3], x_2 \in [-3, 3]$$

- Definition of the Rosenbrock function (ROS) is defined as follows:

$$\begin{aligned}
\text{minimize: } y_h(x_1, x_2, x_3, x_4) &= \sum_{i=1}^3 [100(x_{i+1} - x_i^2)^2 - (x_i - 1)^2] \\
y_l(x_1, x_2, x_3, x_4) &= \sum_{i=1}^3 [100(0.5x_{i+1} - 0.6x_i^2)^2 - (0.6x_i - 0.5)^2] \quad (3.21) \\
x_1 \in [0, 2], x_2 \in [0, 2], x_3 \in [0, 2], x_4 \in [0, 2]
\end{aligned}$$

In each investigation, ten initial high-fidelity points, y_h , and 200 low-fidelity points, y_l , were acquired using LHS. The number of iterations was set as ten for every test function.

3.4.2 Results of Test Functions

Figure 3.5 shows the comparison of additional sampling across the four methods. The proposed hybrid surrogate-model-based EGO has the highest exploration performance; it obtained optimal values with the fewest iterations in each case. As shown in Figure 3.5(a), a minimum value of the SC minimization problem was obtained after the 7th iteration by the proposed hybrid surrogate-model-based EGO, while minimum values were obtained after the 9th iterations using the co-Kriging-based EGO, and the ordinary Kriging-based EGO could not obtain a minimum value by the 10th iteration. Because this is a multimodal problem, this result suggests that the proposed hybrid surrogate model-based EGO could increase diversity during the exploration process to find the global optimum point for multimodal optimization problems. It is shown that the proposed hybrid surrogate model could be more accurate than the surrogate model, based on the optimum results which show that the proposed surrogate model can find the global optimum point with the least number of iterations. Figure 3.5(b) shows that the proposed hybrid surrogate-model-based EGO obtained a minimum value for the BR minimization problem after the 3rd iteration; this was faster than the ordinary Kriging-based EGO and the co-Kriging-based EGO, which obtained minimum values after the 5th and 6th iteration, respectively. This problem has a smooth landscape and is single modal. This result suggests that the proposed hybrid surrogate model-based EGO could maintain the performance of such functions via uniform exploration. The result also shows that the co-Kriging method could converge later than other methods because it is not good for smooth landscape functions. The proposed surrogate model

could match the accuracy of the surrogate model for smooth landscape functions, unlike the co-Kriging surrogate model, which could not maintain the accuracy of surrogate model for this problem. According to Fig. 3.5(c), the proposed hybrid surrogate-model-based EGO obtained a maximum value after the 3rd iteration; this was better than the ordinary Kriging-based EGO, which could not obtain a maximum value after 10th iterations, and the co-Kriging-based EGO, which obtained a maximum value after the 7th iteration. Since this problem has a complicated landscape, the results of the proposed hybrid surrogate model-based EGO show that the algorithm could obtain the optimum value while maintaining higher diversity. Figure 3.5(d) shows that the proposed EGO found the minimum ROS value after the 4th iteration; this was faster than the co-Kriging-based EGO and Kriging-based EGO methods, which obtained the minimum value after the 5th and 6th iterations, respectively. Because this problem has a multi-variable function, this result suggests that the proposed EGO could obtain the optimum point with the least number of iterations for complicated shape function problems. It also shows that the proposed hybrid surrogate model could be as accurate as the surrogate model compared to other methods for multi-variable test functions. The hybrid surrogate model-based EGO obtained the optimum value with the least iterations, as shown in Fig. 3.5, because it had the highest accuracy among surrogate models for these test problems; the accuracy of surrogate model could have helped the EGO process obtain the optimum solution earlier.

Figures 3.6 - 3.9 show the cross-validation [16, 17] results of the SC, BR, and HIM problems. From Figure 3.6, the prediction by the proposed hybrid surrogate-model-based EGO is closest to the exact values. This result suggests that not only the optimum points but also the global trend could be represented more accurately by the proposed method than by the other methods.

According to Fig. 3.7, values predicted by the proposed hybrid surrogate model - based EGO and the ordinary Kriging-based EGO show a smaller error. On the other hand, the result obtained by the co-Kriging - based EGO shows the largest error. The function of the BR problem has a smoother landscape function than those of other problems; thus, a co-Kriging - based method cannot predict the simple landscape function well. The result suggests that the modelling with a co-Kriging method has possibility to achieve over-estimation, even if the exact function is not multi-modal and peaky. One reason for this is that it predicts the global model

and local deviations simultaneously by combining low-fidelity data and high-fidelity data. On the other hand, a hybrid model predicts the global model, which shows the landscape of the function with many low-fidelity samples, and local deviations, which show the detail variance of the function by high-fidelity function separately. Thus, a hybrid method could represent both multi-modal/complex functions and simple functions robustly. These results suggest that the hybrid model may represent the unknown function in real world problem well, because the global model is evaluated independently.

According to Fig. 3.8, the values predicted by the proposed hybrid surrogate model - based EGO show smaller error than those predicted by the co-Kriging - based EGO and the ordinary Kriging-based EGO globally. In particular, the results obtained by the ordinary Kriging-based EGO did not qualify as an accurate prediction in this problem. These results suggest the proposed hybrid surrogate model - based EGO is the most effective algorithm because it achieve the fastest convergence and the least prediction error.

According to Figure 3.9, the predicted value of the proposed hybrid surrogate model-based EGO show the fewest error than those of the co-Kriging based EGO and the ordinary Kriging-based EGO globally. Results from the co-Kriging based EGO and Kriging based EGO could not obtain an accurate prediction in this problem.

According to these results, the hybrid surrogate model-based EGO could be obtained the optimum value with the fewest iteration that shown in Fig. 3.5 because the hybrid surrogate model have highest accuracy of the surrogate model for these test problem and the accuracy of surrogate model could be help the EGO process to obtained the optimum solution earlier. These results suggest the proposed hybrid surrogate-model-based EGO is the most effective algorithm because it achieved the fastest convergence and the fewest prediction errors.

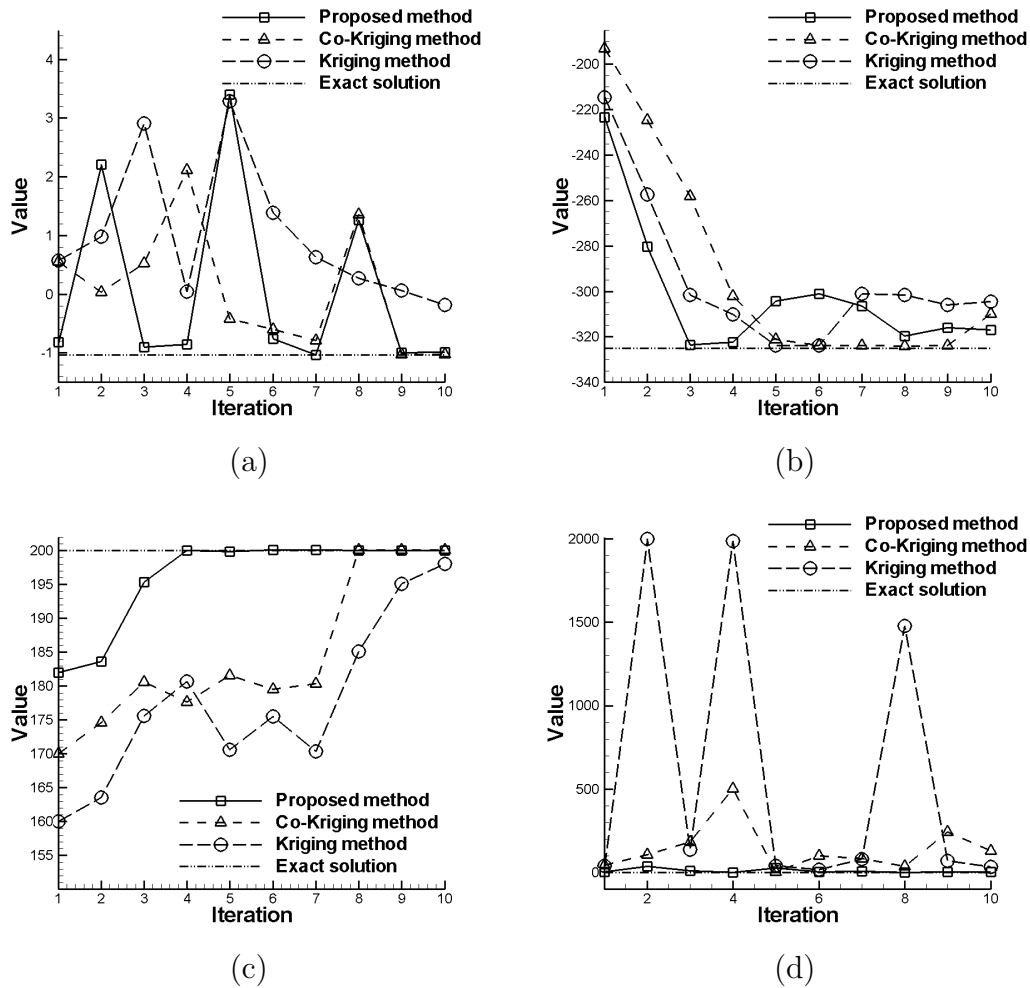
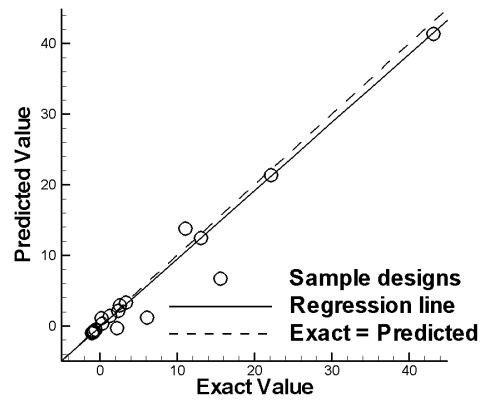


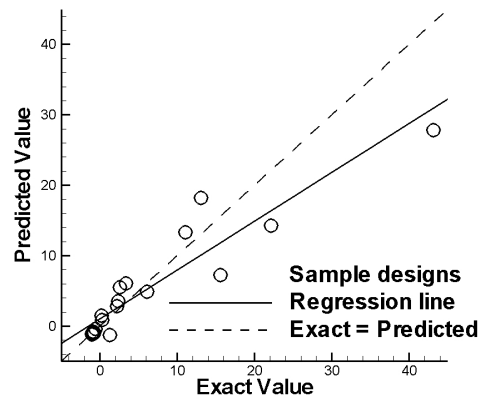
Figure 3.5: Additional sampling in each iteration. (a) SC problem (b) BR problem (c) HIM problem (d) ROS problem.

3.5 Application of Proposed Method to Helicopter Blade Design

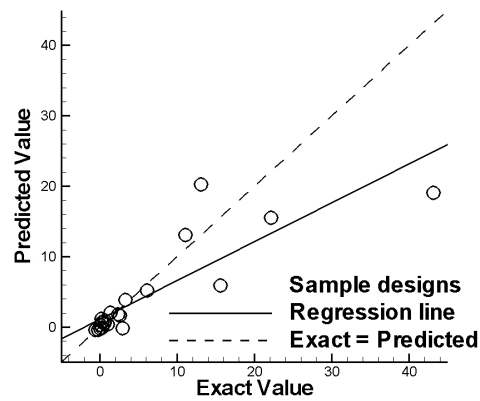
The proposed hybrid surrogate model - based EGO was also applied to a complex real world problem—helicopter rotor blade design. The co-Kriging - based EGO and the ordinary Kriging-based EGO are also applied, and results are compared with that obtained by the proposed hybrid surrogate model - based EGO. The aerodynamics of the helicopter blade is calculated by the low-fidelity and high-fidelity method. Then, the efficiency of the helicopter blade can



(a)

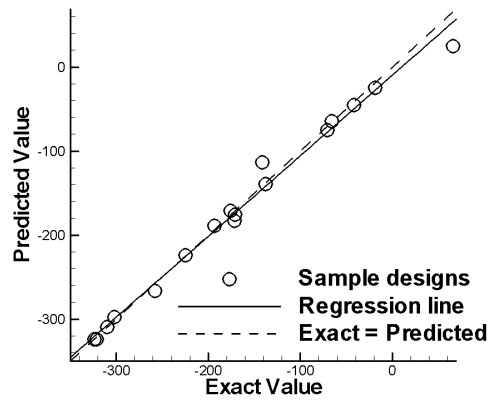


(b)

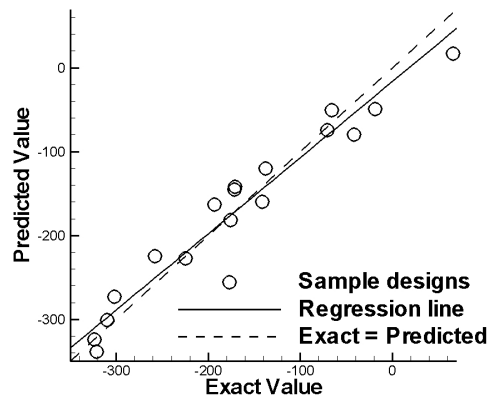


(c)

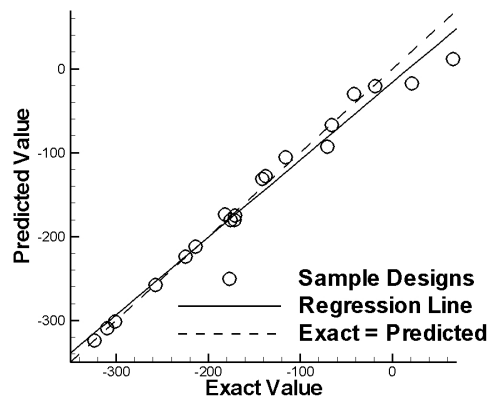
Figure 3.6: Cross validation of SC problem. (a) Hybrid surrogate-model-based EGO (b) Co-Kriging-based EGO (c) Ordinary Kriging-based EGO.



(a)

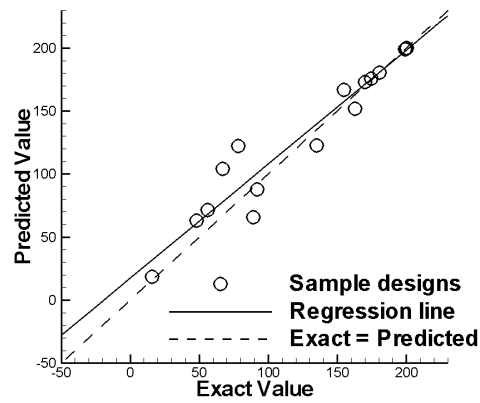


(b)

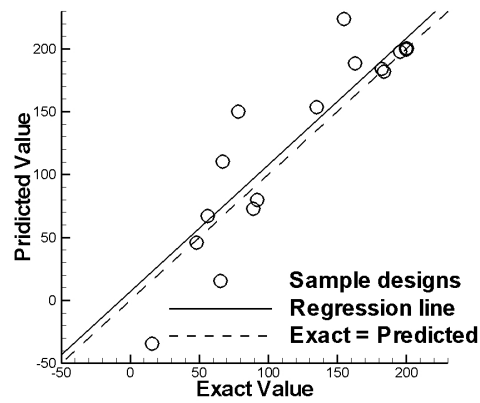


(c)

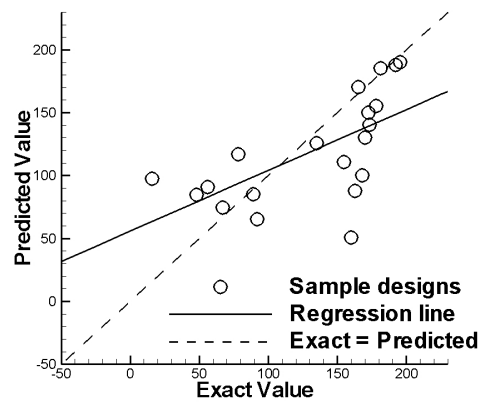
Figure 3.7: Cross validation of BR problem. (a) Hybrid surrogate-model-based EGO (b) Co-Kriging-based EGO (c) Ordinary Kriging-based EGO.



(a)

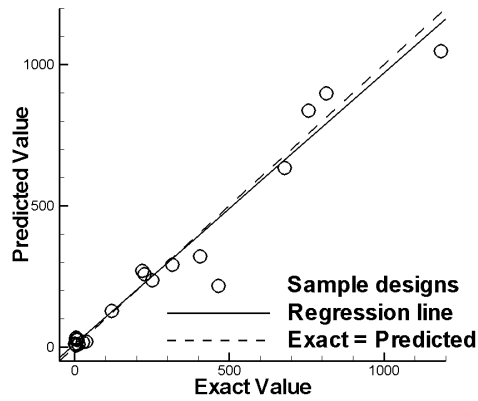


(b)

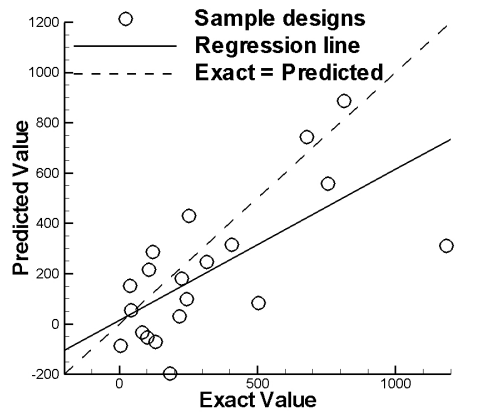


(c)

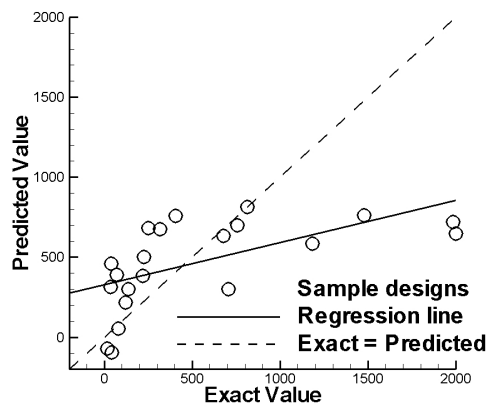
Figure 3.8: Cross validation of HIM problem. (a) Hybrid surrogate-model-based EGO (b) Co-Kriging-based EGO (c) Ordinary Kriging-based EGO.



(a)



(b)



(c)

Figure 3.9: Cross validation of ROS problem. (a) Hybrid surrogate-model-based EGO (b) Co-Kriging-based EGO (c) Ordinary Kriging-based EGO.

be evaluate by a metric called ‘figure of merit (*FOM*)’ expressed as,

$$FOM = \frac{C_T^{\frac{3}{2}}}{\sqrt{2}C_P} = \frac{T\sqrt{T/2\rho\pi R^2}}{P}, \quad (3.22)$$

where C_T is the thrust coefficient that given as $C_T = \frac{T}{\rho A \Omega^2 R^2}$, C_P is the power coefficient that given as $C_P = \frac{P}{\rho A \Omega^3 R^3}$, T is the thrust, ρ is the air density, R is the rotor radius, P is the actual power required to hover, A is the rotor disk area, and Ω is the angular velocity.

3.5.1 Evaluation Methods

To calculate low-fidelity aerodynamics, the blade element momentum theory (BEMT) [18, 19] is applied. To calculate high-fidelity aerodynamics, a Navier - Stokes solver is applied around the blades.

High-fidelity/expensive Evaluation using CFD

Reynolds-averaged Navier - Stokes (RANS) equations are used as the governing equations with the Spalart - Allmaras model [20] which is widely used as a turbulent model for CFD around aircraft. The governing equations are shown in following equation:

$$\frac{\partial}{\partial t} \int_{V(t)} \mathbf{W} dV + \oint_S \phi(t) (\mathbf{G}^i - \mathbf{G}^v) \cdot \mathbf{n} dS = 0 \quad (3.23)$$

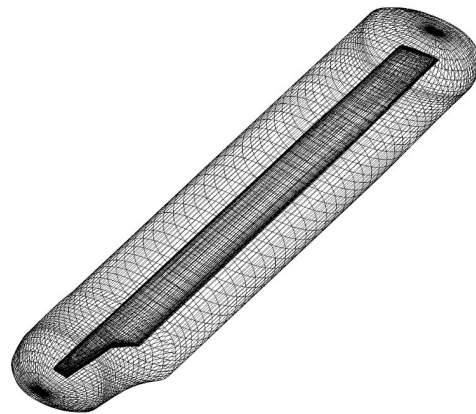
where $W = \begin{pmatrix} \rho \\ \rho \mathbf{v} \\ \rho e \end{pmatrix}$, $G^i = \begin{pmatrix} (\mathbf{v} - \dot{\mathbf{x}}) \cdot \mathbf{n} \rho \\ (\mathbf{v} - \dot{\mathbf{x}}) \cdot \mathbf{n} \rho \mathbf{v} + p \cdot \mathbf{n} \\ (\mathbf{v} - \dot{\mathbf{x}}) \cdot \mathbf{n} \rho e + p \mathbf{v} \cdot \mathbf{n} \end{pmatrix}$, $G^v = \begin{pmatrix} 0 \\ \boldsymbol{\tau} \cdot \mathbf{n} \\ (\boldsymbol{\tau} \cdot \mathbf{v} - \mathbf{q}) \cdot \mathbf{n} \end{pmatrix}$, ρ is the density,

\mathbf{v} is velocity vector, $\dot{\mathbf{x}}$ is velocity of moving particle, \mathbf{n} is unit vector, p is pressure, e is unit vector of summation of energy, q is average Reynold of heat flow velocity and $\boldsymbol{\tau}$ is deviatoric stress tensor. Overlapped grid method [21], in which grids around the blades automatically deform based on the shape design and their rotation, is employed. The computation grid for rotating domain (grid around blade) and the computation grid for all domains are separately generated

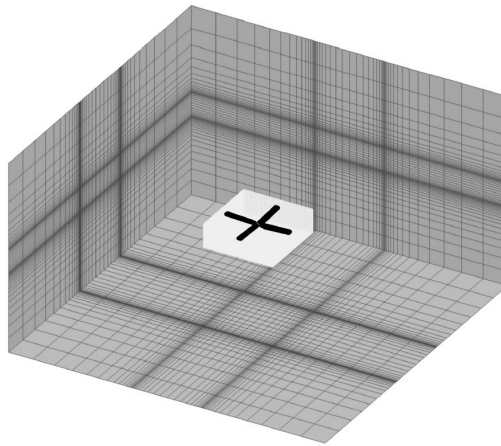
as shown in Fig. 3.10. In this study, ‘rFlow3D’ [22, 23] developed in Japan Aerospace Exploration Agency (JAXA) is employed. For time-accurate unsteady flow simulations, a dual-time stepping method is applied to time integration of the domain for a blade, and the lower-upper symmetric-Gauss-Seidel (LU-SGS) method [24] is selected for pseudo-time integration. The fourth-order Runge - Kutta method is adopted for time integration on the background mesh. For the numerical flux, the modified simple low-dissipation AUSM (mSLAU) scheme [21], which is based on the SLAU scheme [25] is employed for application to the rotary wings. The numerical flux for two-dimensional flow is given as:

$$\begin{aligned}
 \tilde{\mathbf{F}} &= \frac{\dot{m} + |m|}{2} \Phi^+ + \frac{\dot{m} - |m|}{2} \Phi^- + \tilde{p} \mathbf{N} \\
 \Phi &= (1, u, v, h)^T \\
 N &= (0, x_n, y_n, 0)^T \\
 h &= (e + p)/\rho
 \end{aligned} \tag{3.24}$$

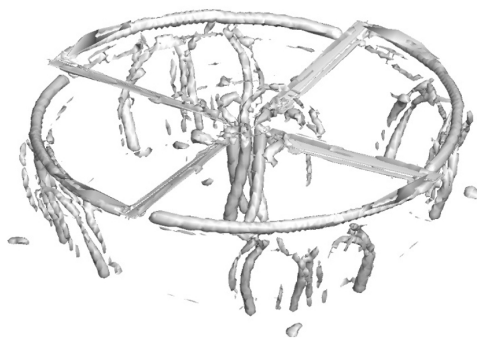
where x_n, y_n are Cartesian components of a normal vector from the left to the right, u and v are velocities in x, y directions, e is total energy of unit volume, and \dot{m} is mass flux. The SLAU is used because it can be used for wide speed range from low Mach number to high Mach number. In the helicopter blade simulation, the flow velocity at the tip blade is always high Mach number and the flow velocity at the root blade is always low Mach number. From the problem of the helicopter blade simulation, the SLAU is one of a good numerical flux for CFD simulation. The fourth-order compact monotonic upstream-centered scheme for conservation laws (MUSCL) total variation diminishing (TVD) scheme [26] is used to reconstruct flow field values to realize a fourth-order spatial accuracy. The example of the CFD flow-field is shown in Fig. 3.10(c). The computational time to evaluate the FOM for each design by present CFD is approximately 72 h.



(a)



(b)



(c)

Figure 3.10: Helicopter computation grid. (a) Grid around blade (b) Grid in stationary domain (c) Example of flow-field around rotor blades generated using CFD.

Evaluation using Blade Element Momentum Theory as a Low-fidelity/cheap Function

In a past study, the blade element momentum theory (BEMT) [18, 19] was developed to estimate the blade performance of a helicopter rotor blade in a short time. The blade is firstly divided into several sections. Sections are assumed as airfoil to calculate the forces on each cross section independently. To find the inflow distribution (λ) considering hovering, the momentum theory is first used through the following equation:

$$\lambda = \frac{sa}{16} \left[\sqrt{1 + \frac{32}{sa} \Theta r} - 1 \right] \quad (3.25)$$

where a is the two-dimensional lift-curve of the slope rotary wing section; Θ is the pitch angle; r is the blade radial coordinate; s is called solidity, which can be obtained from

$$s = \frac{Bc}{\pi r} \quad (3.26)$$

B is the number of rotary wings, c is chord length at each cross section; and R is the radius of rotary wing. Then, the inflow angle (Φ) is calculated for each section as

$$\Phi = \tan^{-1} \left(\frac{\lambda}{\Omega r} \right) \quad (3.27)$$

Figure 3.11 shows definitions of each parameter. Sectional forces, the lift, L , and drag, D , are calculated as

$$L = \frac{1}{2} \rho U^2 c C_l, \quad (3.28)$$

$$D = \frac{1}{2} \rho U^2 c C_d, \quad (3.29)$$

where ρ is the air density, U is the resultant velocity magnitude, C_l is lift coefficient, and C_d is drag coefficient. C_l and C_d could be defined by using the experiment data table of HART-II model, U is also shown in Figure 3.11; it can be computed from

$$U = \sqrt{u_p^2 + u_t^2} \quad (3.30)$$

where u_t is the air velocity of a blade section tangential to the disk plane and u_p is the air velocity of a blade section perpendicular to the disk plane. The normal force (F_z) and the longitudinal force (F_x) can be calculated as

$$F_z = L\cos\Phi - D\sin\Phi \quad (3.31)$$

$$F_x = L\sin\Phi + D\cos\Phi \quad (3.32)$$

The elemental thrust, torque, and power on the rotor are

$$dT = BF_z dr \quad (3.33)$$

$$dQ = BF_x r dr \quad (3.34)$$

$$dP = \omega dQ = BF_x r \omega dr \quad (3.35)$$

The FOM can be defined as in (3.22).

BEMT expressed by Eqs. (3.33) - (3.35) applied the lifting-line theory result, regardless of the approximation of fact that the theory breaks down near the blade tips. Therefore, the tip-loss effect is implemented using Prandtl's tip loading (F_{pl}), which is given by

$$F_{pl} = \frac{2}{\pi} \cos^{-1} e^{(r-1)N/2\lambda} \quad (3.36)$$

To combine this with BEMT, the induced velocity in hover from (3.23) becomes

$$\lambda = \frac{sa}{16F_{pl}} \left[\sqrt{1 + \frac{32F_{pl}}{sa} \Theta r} - 1 \right] \quad (3.37)$$

Prandtl's tip loading is effective to estimate the reduction effect of the FOM. This study uses Eq. (3.37) instead of Eq. (3.25).

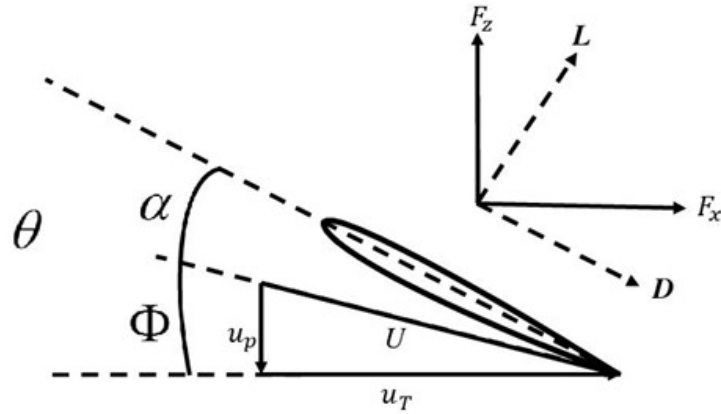


Figure 3.11: Blade section aerodynamics.

The Comparison of High-fidelity data and Low-fidelity Data

This chapter shows the relationship between the high-fidelity data by CFD and the low-fidelity data by BEMT. The relationship was compared by the *FOM* value of the ten initial samples by CFD and BEMT in Fig. 3.12. This relationship shows that the low-fidelity data and high-fidelity data have the same trend. From this relationship, it can be concluded that the low-fidelity data by BEMT is possible to predict the trend of the high-fidelity data by CFD.

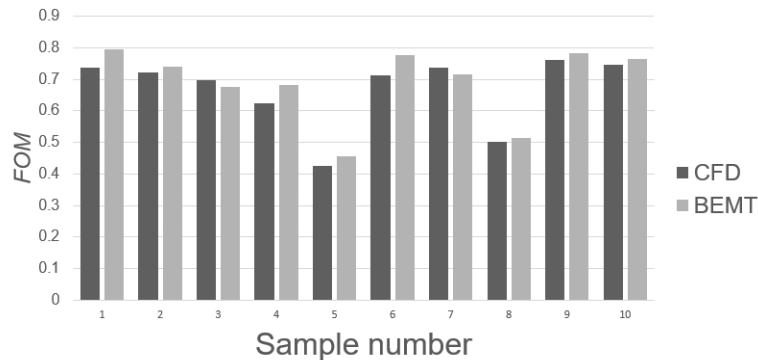


Figure 3.12: Comparison of the high-fidelity data by CFD and the low-fidelity data by BEMT.

3.5.2 Definition of Blade Geometry and Design variables

The standard helicopter model, HART-II [27, 28] is used in this investigation. The distribution of twist angles is designed as shown in Fig. 3.13(a). Three control points are allocated on the

1/4th chord line. The location in the spanwise direction and values of the control points are used as design parameters. Values of the design parameter between each control points are calculated with the cubic spline formulation [29] expressed as follows:

$$f(x) = b + cx + dx^2 + ex^3 \quad (3.38)$$

For $0 \leq h \leq 0.5$ (twist angle between 0.75 and 0.875 of chord length), the controlled parameter (b, c, d and e) can be defined by the following equation:

$$\begin{bmatrix} 1 & 0 & 0 & 0 \\ 1 & h_1 & h_1^2 & h_1^3 \\ 0 & 1 & 0 & 0 \\ 0 & 0 & 2 & 6h_1 \end{bmatrix} \begin{bmatrix} b \\ c \\ d \\ e \end{bmatrix} = \begin{bmatrix} \Theta_1 \\ \Theta_2 \\ 0 \\ 0 \end{bmatrix} \quad (3.39)$$

For $0.5 \leq h \leq 1.0$ (twist angle between 0.875 and 1.0 of chord length), the controlled parameter (b, c, d and e) can be defined by the following equation:

$$\begin{bmatrix} 1 & h_1 & h_1^2 & h_1^3 \\ 1 & 1 & 1 & 1 \\ 0 & 1 & 2h_1 & 3h_1^2 \\ 0 & 0 & 2 & 6 \end{bmatrix} \begin{bmatrix} b \\ c \\ d \\ e \end{bmatrix} = \begin{bmatrix} \Theta_1 \\ \Theta_2 \\ \frac{d\Theta_1}{dh} \\ 0 \end{bmatrix} \quad (3.40)$$

The cubic spline from Eq.(3.38) is used to control the twist distribution between the controlled point. This chapter deals with the two-parameter design problem to controlled the twist angles at the point that shown in Fig. 3.13(a), with Θ_1 defined at $0.875R$ and Θ_2 defined at $1.0R$, while Θ_0 , which is the twist 75% span, is fixed to zero. In addition h_1 is given as 0.5. The definitions of h_1 and h are shown in Fig. 3.13(b). Thus, two parameters, Θ_1 and Θ_2 , are controlled to define the geometry of the blade. The ranges of the design parameters are defined as

$$-10.0^\circ \leq \Theta_1 \leq 10.0^\circ,$$

$$-10.0^\circ \leq \Theta_2 \leq 10.0^\circ.$$

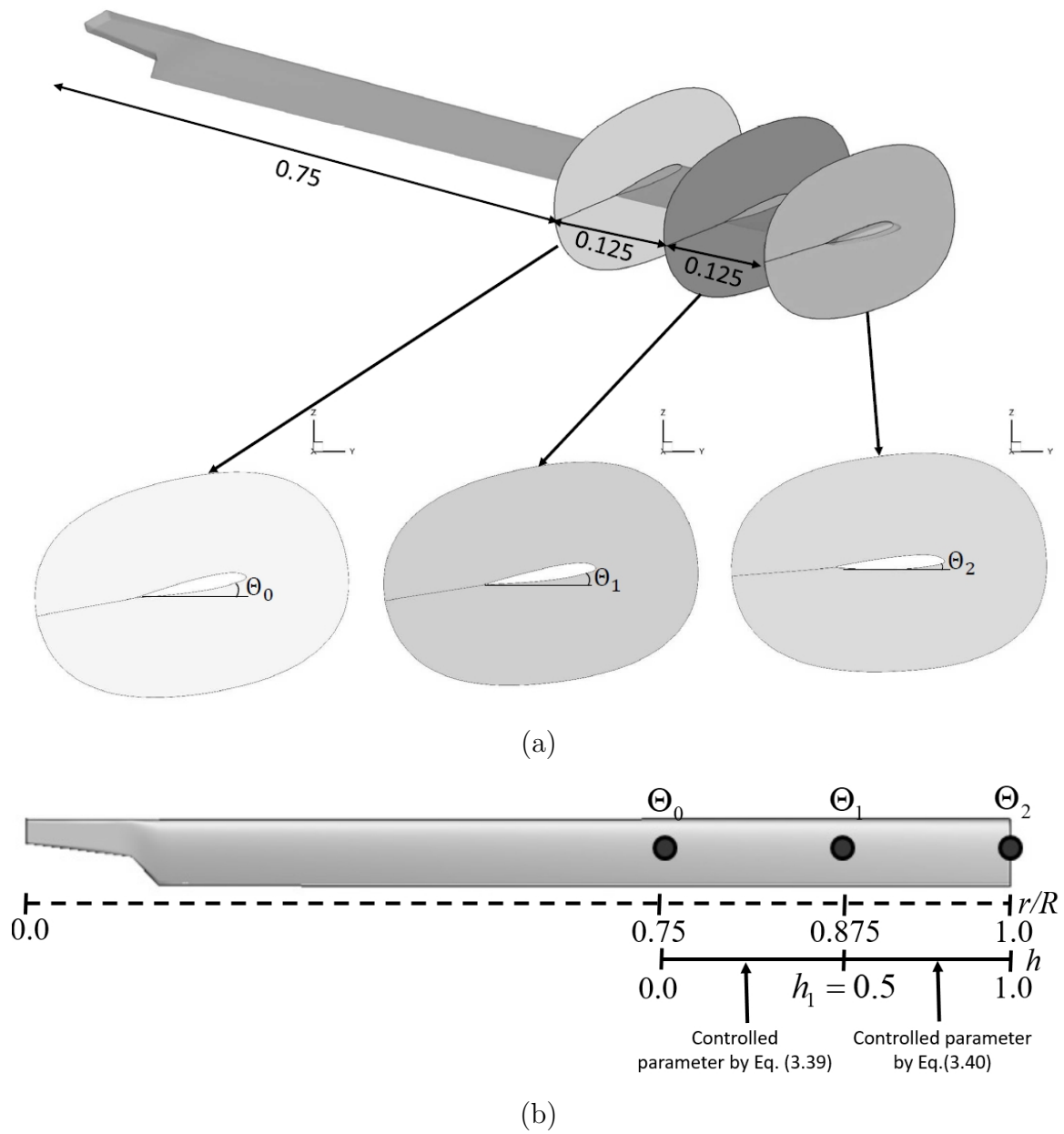


Figure 3.13: Definition of glade geometry: (a) control points, (b) controlled parameters.

Table 3.1: Blade properties.

Target thrust	$[N]$	5835.578
Rotation speed	$[rpm]$	1041.0
Number of blades	-	4
Rotor radius	$[m]$	2.0
Chord length	$[m]$	0.121
Airfoil	-	NACA23012

3.5.3 Objective Function and Calculation Condition

In this study, FOM maximization for hovering flight is considered.

Maximize: FOM

$$\begin{aligned} \text{Subject to: } & -10.0^\circ \leq \Theta_1 \leq 10.0^\circ \\ & -10.0^\circ \leq \Theta_2 \leq 10.0^\circ \end{aligned} \quad (3.41)$$

Blade properties are shown in Table 3.1. For a multi-fidelity design using the hybrid surrogate model and co-Kriging model, the number of initial samples for the high-fidelity/expensive function is set to 10, and the number of initial samples for the low-fidelity/cheap function is 200. The Reynolds number at the blade tip is 2×10^6 . For single-fidelity using ordinary Kriging-based EGO, the initial high-fidelity model is constructed with 10 samples. The additional sampling of this problem is set to 6.

3.5.4 Results

Additional samples from the methods are compared as shown in Figure 3.14. Fig. 3.14 shows that the proposed hybrid model - based EGO and the co-Kriging - based EGO can obtain designs which have a higher FOM than that obtained by the ordinary Kriging-based EGO. In particular, the proposed hybrid surrogate model - based EGO attained the design earlier than the co-Kriging - based EGO. As seen in Fig. 3.15, the hybrid method found an optimal point in the 4th iteration, with an FOM = 0.769, which is better than an optimal point found by the co-Kriging - based EGO (found in 6th generation, FOM = 0.767) and an optimal point found

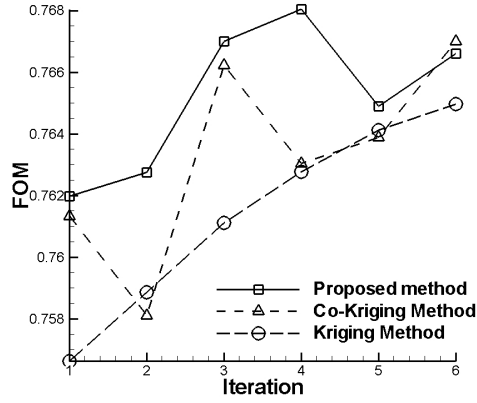
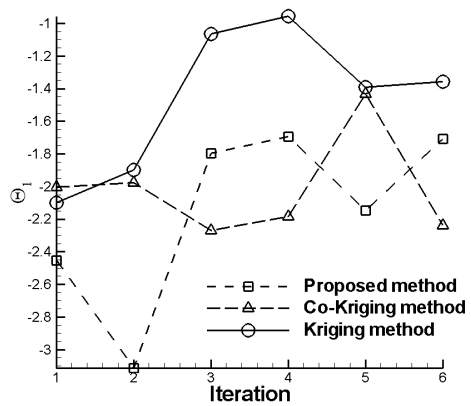


Figure 3.14: Additional sampling in each iteration of the helicopter design problem.

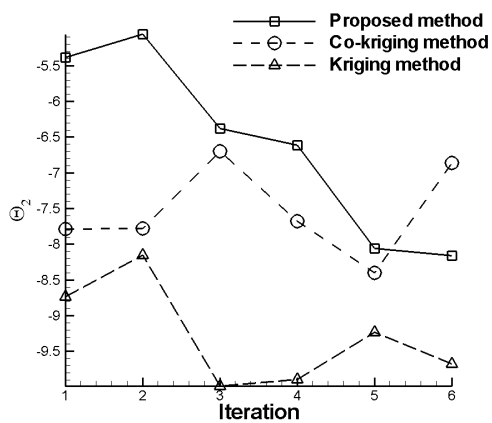
by the ordinary Kriging-based EGO (found in 6th generation, $FOM = 0.765$). Figure 3.15 shows the history of design variables of additional samples. According to Fig. 3.15, exploration by the proposed hybrid surrogate model - based EGO shows higher diversity than the others, especially for the design variable Θ_2 . The average value of additional samples of the proposed hybrid model-based EGO is obtained $FOM = 0.765$, better than the co-Kriging EGO that obtained $FOM = 0.763$ and the ordinary Kriging-based EGO that obtained $FOM = 0.763$. These results can show the proposed hybrid model-based EGO could be reduced the high-fidelity computation time.

Figure 3.16 shows comparisons of contour plots that show the relationship between FOM and the design parameters for the proposed hybrid surrogate-model-based EGO, the co-Kriging-based EGO, and the ordinary Kriging-based EGO. According to Figure 3.16, the optimal designs found by the proposed hybrid surrogate-model-based EGO, the co-Kriging-based EGO, and the ordinary Kriging-based EGO appeared in the same range: Θ_1 around -5.0° to 0.0° and Θ_2 around -5.0° to -10.0° .

Figure 3.17 shows the cross-validation results. It is found that a value predicted by the proposed hybrid surrogate model - based EGO could be obtained the lowest error not only in high density data due to the additional sampling. This result also shows that the cross-validation data by the proposed hybrid surrogate model - based EGO has smaller error at low data density than results by the co-Kriging - based EGO.

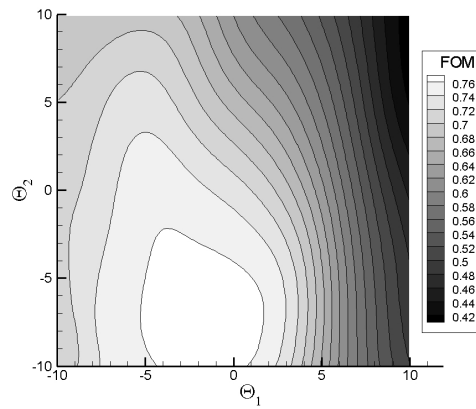


(a)

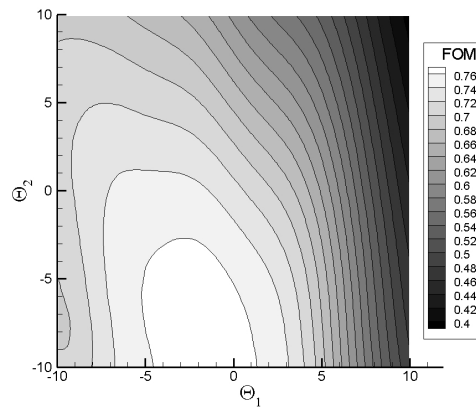


(b)

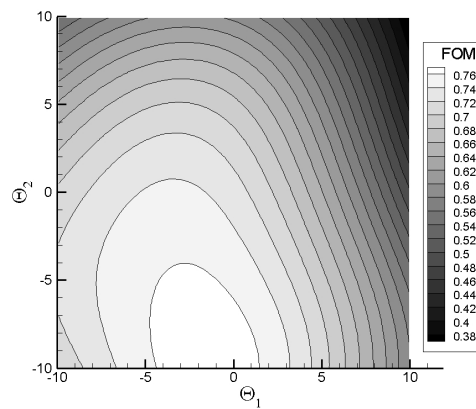
Figure 3.15: The history of the additional samples discovery. (a) Θ_1 (b) Θ_2 .



(a)

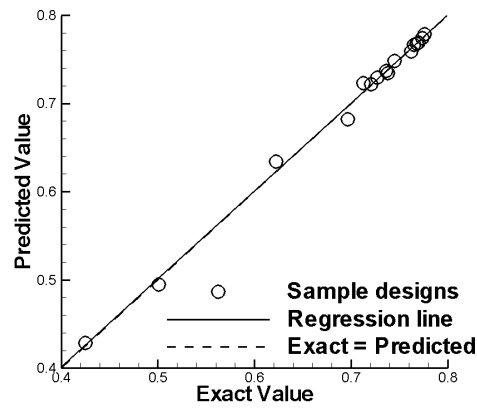


(b)

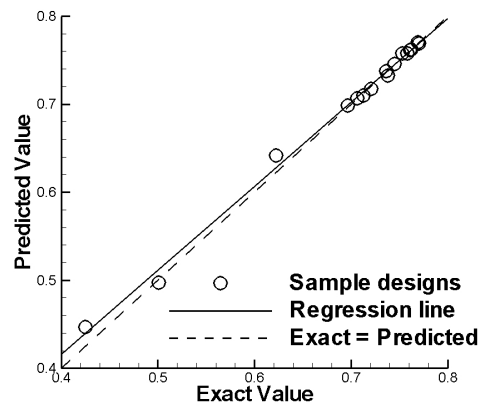


(c)

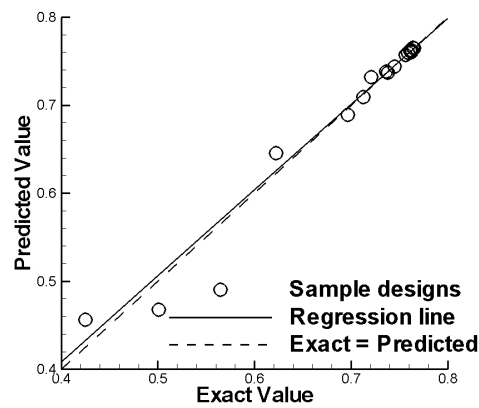
Figure 3.16: The multi-fidelity relationship contour of the design parameters (Θ_1 and Θ_2) and FOM. (a) Hybrid surrogate-model-based EGO (b) Co-Kriging-based EGO (c) Ordinary Kriging-based EGO.



(a)

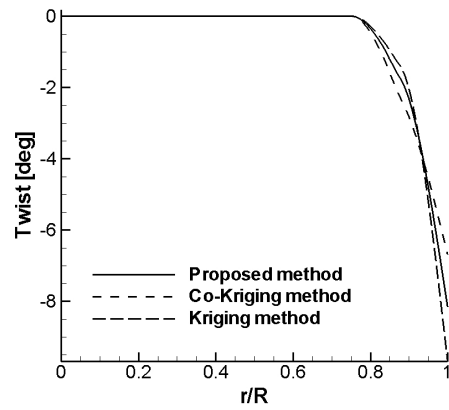


(b)

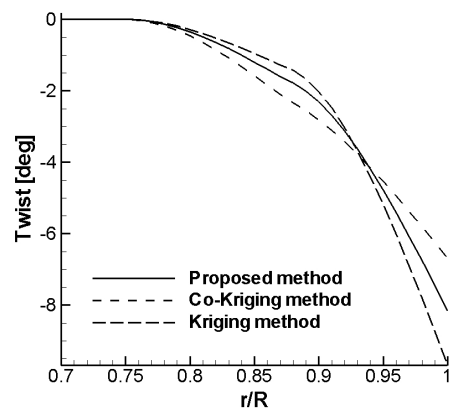


(c)

Figure 3.17: Cross validation of helicopter design problem. (a) Hybrid surrogate-model-based EGO (b) Co-Kriging-based EGO (c) Ordinary Kriging-based EGO.



(a)



(b)

Figure 3.18: Twist distribution of optimal designs. (a) Full length (b) $r/R = 0.7 \sim 1.0$.

Figure 3.18 shows the twist distribution of optimal shapes by the proposed hybrid surrogate model - based EGO, the co-Kriging - based EGO, and the ordinary Kriging-based EGO. The optimal result obtained by the proposed hybrid surrogate model - based EGO (FOM = 0.771 at $\Theta_1 = -1.70$ and $\Theta_2 = -8.16$) is better than the optimal result obtained by the ordinary Kriging-based EGO method (FOM = 0.770 at $\Theta_1 = -2.24$ and $\Theta_2 = -6.69$) and the optimal result obtained by the ordinary Kriging-based EGO (FOM = 0.768 at $\Theta_1 = -1.36$ and $\Theta_2 = -9.68$). Owing to this prediction accuracy, the optimal design can be obtained fastest by the proposed hybrid surrogate model - based EGO.

3.6 Conclusion

This study investigated a hybrid surrogate model based on a multi-fidelity efficient global optimization method. The proposed hybrid surrogate model - based EGO used a radial basis function to predict a global model, and an ordinary Kriging-based EGO was used to predict a local variance. For multi-fidelity optimization, a global model is constructed using a dataset evaluated using a low-fidelity/cheap function, and a local variance is estimated using a dataset evaluated using a high-fidelity expensive function.

To examine the proposed hybrid surrogate model - based EGO, four test functions are solved, and the results obtained by the proposed hybrid surrogate model - based EGO are compared with those obtained by the co-Kriging model - based EGO and ordinary Kriging-based EGO. The optimization results for the test functions show that the proposed hybrid surrogate model-based EGO achieved higher accuracy compared to the surrogate model, co-Kriging, and Kriging-based EGO methods for each test function. In addition, the results from the proposed EGO could obtain the optimum value with the least number of iterations for every test function. For this reason, the proposed EGO can reduce the number of high-fidelity functions in the optimization process. It is suggested that the proposed hybrid surrogate model - based EGO can achieve robust exploration.

The proposed hybrid surrogate model - based EGO is also applied to aerodynamic optimiza-

tion of a helicopter's blade shape. To evaluate aerodynamic performance, the blade element momentum theory is used to construct a low-fidelity/cheap dataset, and the Navier - Stokes solver is used to construct a high-fidelity dataset. Results by the proposed hybrid surrogate model - based EGO method are compared with those by the co-Kriging - based EGO and ordinary Kriging-based EGO. The results of the aerodynamic design problem also show that the proposed hybrid surrogate model - based EGO could design a better blade shape from the perspective of aerodynamic efficiency. The convergence of the proposed hybrid surrogate model - based EGO was the fastest compared with other methods. In addition, the error between the exact value and predicted value obtained by the hybrid surrogate model is smaller than those by other methods. These results suggest that the proposed hybrid surrogate model - based EGO is suitable for real-world design problems.

Bibliography

- [1] Dumont, A., et al. "Aerodynamic shape optimization of hovering rotors using a discrete adjoint of the Reynolds-Averaged Navier - Stokes Equations." *Journal of the American Helicopter Society* 56.3 (2011): 1-11.
- [2] Jones, Donald R., Matthias Schonlau, and William J. Welch. "Efficient global optimization of expensive black-box functions." *Journal of Global optimization* 13.4 (1998): 455-492.
- [3] Forrester, Alexander IJ, Andrés Óbester, and Andy J. Keane. "Multi-fidelity optimization via surrogate modelling." *Proceedings of the royal society of london a: mathematical, physical and engineering sciences*. Vol. 463. No. 2088. The Royal Society, 2007.
- [4] Huang, Likeng, Zhenghong Gao, and Dehu Zhang. "Research on multi-fidelity aerodynamic optimization methods." *Chinese Journal of Aeronautics* 26.2 (2013): 279-286.
- [5] Choi, Seongim, et al. "Multifidelity design optimization of low-boom supersonic jets." *Journal of Aircraft* 45.1 (2008): 106-118.
- [6] Leon, Enric Roca, et al. "Multi-Fidelity Concurrent Aerodynamic Optimization of Rotor Blades in Hover and Forward Flight." *40th European Rotorcraft Forum*. 2014.
- [7] Rethore, Pierre-Elouan, et al. "TopFarm: Multi-fidelity optimization of offshore wind farm." *The Twenty-first International Offshore and Polar Engineering Conference*. International Society of Offshore and Polar Engineers, 2011.
- [8] Sun, Guangyong, et al. "Multi-fidelity optimization for sheet metal forming process." *Structural and Multidisciplinary Optimization* 64.1 (2011): 111-124.

- [9] Tanabe, Yasutada, et al. "Numerical Simulations and Measurements of the Wake from a Helicopter Operating in Ground Effect." *AHS International's 71st Annual Forum & Technology Display, Virginia Beach, VA, USA*. 2015.
- [10] Orr, Mark JL. "Introduction to radial basis function networks." (1996).
- [11] Chandrashekarappa, Praveen, and Régis Duvigneau. *Radial basis functions and kriging metamodels for aerodynamic optimization*. Diss. INRIA, 2007.
- [12] Matheron, G. "Principles of geostatistics, economic geology." *Economic Geology* 58.8 (1963): 1246-1266.
- [13] Moore, R. "Geostatistics in hydrology: Kriging interpolation." *Mathematics Department, Macquarie University, Sydney., Tech. Rep* (1999).
- [14] Goldberg, David E., and John H. Holland. "Genetic algorithms and machine learning." *Machine learning* 3.2 (1988): 95-99.
- [15] Husslage, Bart GM, et al. "Space-filling Latin hypercube designs for computer experiments." *Optimization and Engineering* 12.4 (2011): 611-630.
- [16] Liem, Rhea P., Charles A. Mader, and Joaquim RRA Martins. "Surrogate models and mixtures of experts in aerodynamic performance prediction for aircraft mission analysis." *Aerospace Science and Technology* 43 (2015): 126-151.
- [17] Meckesheimer, Martin, et al. "Computationally inexpensive metamodel assessment strategies." *AIAA journal* 40.10 (2002): 2053-2060.
- [18] Johnson, Wayne. *Rotorcraft aeromechanics*. Vol. 36. Cambridge University Press, 2013.
- [19] Leishman, Gordon J. *Principles of helicopter aerodynamics with CD extra*. Cambridge university press, 2006.
- [20] Spalart, PRaA, and S1 Allmaras. "A one-equation turbulence model for aerodynamic flows." *30th aerospace sciences meeting and exhibit*. 1992.

- [21] Delfs, Jan. "An overlapped grid technique for high resolution CAA schemes for complex geometries." *7th AIAA/CEAS Aeroacoustics Conference and Exhibit*. 2001.
- [22] Tanabe, Yasutada. "Significance of All-Speed Scheme in Application to Rotorcraft CFD Simulations." *The 3rd International Basic Research Conference on Rotorcraft Technology, Nanjing, China*. 2009.
- [23] Sugiura, Masahiko, Yasutada Tanabe, and Hideaki Sugawara. "Development of a Hybrid Method of CFD and Prescribed Wake Model for Helicopter BVI Noise Prediction." *Transactions of the Japan Society for Aeronautical and Space Sciences* 56.6 (2013): 343-350.
- [24] Zhang, L. P., and Z. J. Wang. "A block LU-SGS implicit dual time-stepping algorithm for hybrid dynamic meshes." *Computers & fluids* 33.7 (2004): 891-916.
- [25] Shima, Eiji, and Keiichi Kitamura. "On new simple low-dissipation scheme of AUSM-family for all speeds." *47th AIAA Aerospace Sciences Meeting including the New Horizons Forum and Aerospace Exposition*. 2009.
- [26] Yamamoto, S., and H. Daiguji. "Higher-order-accurate upwind schemes for solving the compressible Euler and Navier-Stokes equations." *Computers & Fluids* 22.2-3 (1993): 259-270.
- [27] van der Wall, Berend G., et al. "The HART II test - measurement of helicopter rotor wakes." *Aerospace Science and Technology* 8.4 (2004): 273-284.
- [28] Goulos, I., V. Pachidis, and P. Pilidis. "Flexible rotor blade dynamics for helicopter aeromechanics including comparisons with experimental data." *The Aeronautical Journal* 119.1213 (2015): 301-342.
- [29] Takeda, Shigeru, et al. "Influence of Pre-twist Distribution at the Rotor Blade Tip on Performance during Hovering Flight." *Transactions of the Japan Society for Aeronautical and Space Sciences* 58.1 (2015): 39-44.

Chapter 4

Multi-objective/multi-fidelity Efficient Global Optimization

4.1 Introduction

To solve aerodynamic design problems is one of a very complicated problem because of it always has high-cost computation function and always has many objective targets for design condition [1, 2]. For example, when to design the aircraft, the computation cost is very expensive and the designer must be thinking about the performance of aircraft for every operation speed, such as the take-off condition, the cruising condition, or the landing condition. Due to these problems, most of the researcher try to reduce the computation cost and the optimization algorithm must be can find the optimum design for multi/many-objective optimization problem.

Fortunately for aerodynamic design problems, aerodynamic design problems have a lot of computation level to solve in one design [3]. For example, aerodynamic forces for airfoil design could be determined by a panel method for low level computation [4] or a Navier-Stokes computation for high level computation [5]. From this advantage, most of researcher try to combine the multi-fidelity to increase the efficiency of optimization process. A multi-fidelity approach with multi-fidelity surrogate model is one of popular way to combine the multi-fidelity function. Multi-fidelity optimization methods based on the error estimation of response surfaces

using low-fidelity and high-fidelity functions were successfully applied to design low-boom supersonic jets [6]. A co-Kriging model [7, 8] have been widely studied to combine multi-fidelity functions. A co-Kriging model was employed to solve optimal airfoil design. However, a co-Kriging method isn't good to predict the smooth landscape function. Another one technique of multi-fidelity optimization process is proposed by Rethore for wind turbine designs [9, 10]. This optimization process start with found an optimal point of a low-fidelity function using a genetic algorithm (GA). Then, they performed an optimization with a high-fidelity function using a gradient-based method, using the optimum point of the low-fidelity optimization result as a starting point. This method may fail to find the optimum high-fidelity function if the error between the low-fidelity and high-fidelity function is large.

One of alternative way to solve the multi-fidelity multi-objective optimization problem is using model reduction technique [11, 12]. A multi-fidelity multi-objective optimization approach with a parameter space reduction technique was applied to design the helicopter rotor blade and airfoil design. This technique reduced the design parameter space to define possible design ranges with a low-fidelity function. Then, a high-fidelity function was used to find the optimum design in the primary defined design range and the sampling of high-fidelity function was chose by selected the interested design points of non-dominated solutions plus the initial point that generated with primary defined design range. However, it has the potential to obtain an unexpected optimal solution outside the parameter space because the design ranges of the low-fidelity function are not always appropriate for the high-fidelity function.

The most popular way to solve the expensive function optimization problem are using efficiency global optimization (EGO) [13], which uses Kriging model based exploration. EGO has additional sampling-procedure-based expected improvement (EI) that consider the uncertainty of models to improve the accuracy of the models. However, the Kriging model based EGO with EI isn't a good alternative way to solved the multi/many-objective optimization problem, because the EI is design for single objective optimization. The expected hypervolume improvement (EHVI) [14, 15] were successfully developed from the basic idea of EI that consider the uncertainty of models to improvement the accuracy of the models for multi/many-objective optimization problem. However, there is no report for multi-fidelity many-objective optimization

technique.

In this chapter, a multi-fidelity optimization by a hybrid surrogate-model-based EHVI that can improve the efficiency and accuracy to finding the optimum point evaluated by a high-fidelity function is proposed, and its applied to airfoil design problems. The hybrid surrogate-model-based EHVI considered in this study uses a low-fidelity function to construct a global model that can show the global landscape of the function and a high-fidelity function to evaluate a local deviation. The global model is approximated by a radial basis function (RBF) [16, 17] based on a database of low-fidelity evaluations that can predict the multi-modal function. Local variances are predicted using a correlation term using a Kriging method [18]. The proposed hybrid-surrogate-model-based EHVI is applied to find the multi/many objective airfoil optimization problem. The objective of this studied is set to two to four objective airfoil design problems. Results of the optimization are compared with an ordinary Kriging-based EHVI.

4.2 Efficient Global Optimization for Multi-objective Problem

The procedure of EGO with the ordinary kriging model is illustrated in Fig. 4.1(a). The EGO process has been similar to the EGO for single-fidelity based single-objective problem that explained in Section 3.3.1. However, an arbitrary optimization method can be used to find an additional point by maximizing an EHVI [14, 15] instead of an EL.

The EHVI at a point can be expressed as

$$EHVI[f_1(\mathbf{x}), f_2(\mathbf{x}), \dots, f_M(\mathbf{x})] = \int_{-\infty}^{f_{ref1}} \int_{-\infty}^{f_{ref2}} \dots \int_{-\infty}^{f_{refM}} HVI[f_1(\mathbf{x}), f_2(\mathbf{x}), \dots, f_M(\mathbf{x})] \times \phi_1(F_1)\phi_2(F_2)\dots\phi_M(F_M)dF_1dF_2\dots dF_M, \quad (4.1)$$

where F_i denotes the Gaussian random variable $N[\hat{f}_i(\mathbf{x}), \hat{s}_i^2(\mathbf{x})]$. $\phi_i(F_i)$ is the probability density

function, and f_{ref_i} is the reference value used for calculating the hypervolume. The maximization of EHVI is considered as the updating criterion to determine the location of an additional sample point. In this study, the hypervolume is calculated on the basis of HypE, a hypervolume estimation algorithm for multi-objective optimization [19].

The basic idea of the original EGO, namely EHVI-based explanation, can also be applied to the hybrid surrogate model expressed in (4.1), because local deviations are estimated using the kriging method. The procedure of EGO with the hybrid surrogate model proposed in this study is shown in Fig. 4.1(b). The EGO process has been similar to the EGO for multi-fidelity based single-objective problem that explained in Section 3.3.2. A GA [20] is used to find the maximum EHVI point, x . In this study, the roulette wheel method was used in the selection process, blend crossover (BLX)-0.5 [21] was used in the crossover process, and uniform mutation [22] with a mutation rate of 0.1 was used in the mutation process.

4.3 Investigation of Proposed Method by Solving Test Functions

4.3.1 Formulation

The proposed multi-objective multi-fidelity EGO is investigated by solving two test functions; one has two objective functions and the other has three objective functions. The results are compared with those of a kriging-based multi-objective EGO. The high-fidelity function is denoted by f and the low-fidelity function is denoted by f_l .

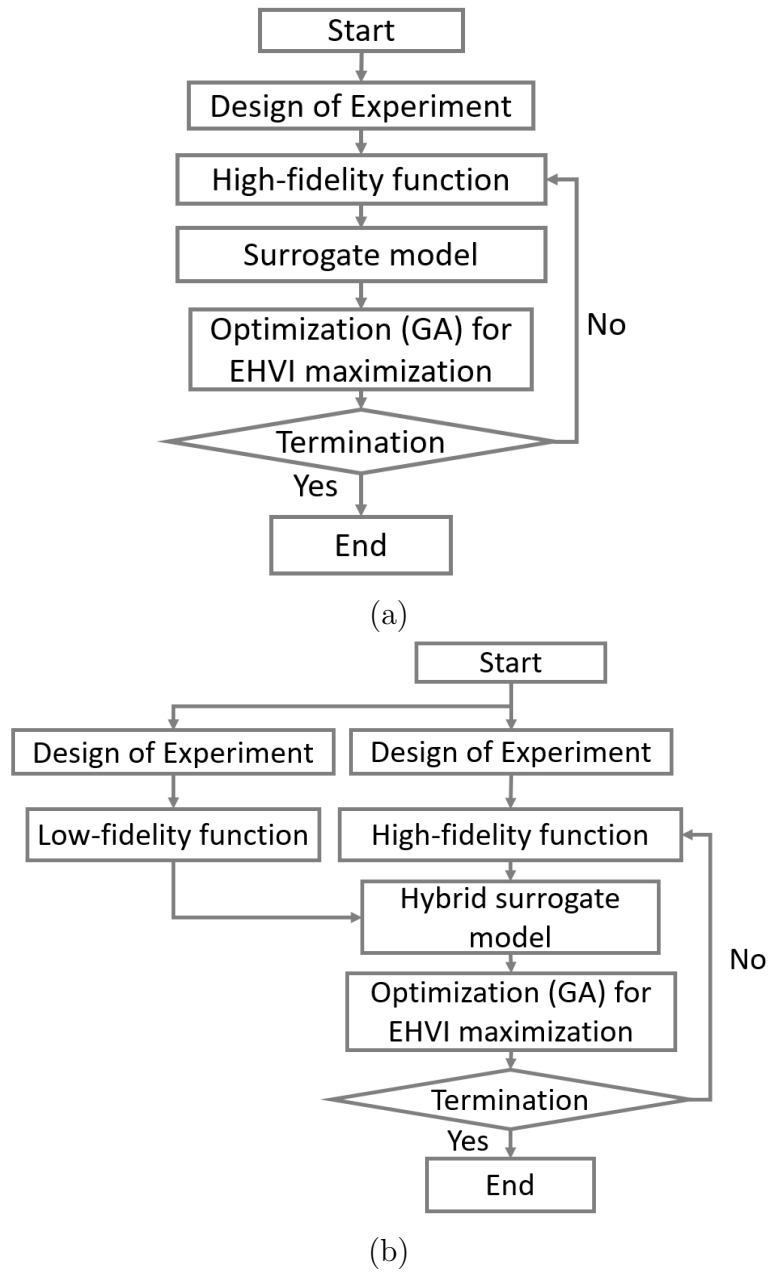


Figure 4.1: Flowchart of efficient global optimization. (a) Efficient global optimization (b) Proposed EGO with multi-fidelity surrogate model.

Definition of two-objective optimization problem from Van Valedhuizens test suite [23]:

$$\begin{aligned}
\text{Minimize: } f_1(x_1, x_2, \dots, x_5) &= 1 - \exp\left(-\sum_{i=1}^5 (x_i - 1/\sqrt{5})^2\right) \\
\text{Minimize: } f_2(x_1, x_2, \dots, x_5) &= 1 - \exp\left(-\sum_{i=1}^5 (x_i + 1/\sqrt{5})^2\right) \\
f_{l1}(x_1, x_2, \dots, x_5) &= 1 - \exp\left(-\sum_{i=1}^5 (0.5x_i - 0.05 - 1/\sqrt{5})^2\right) \\
f_{l2}(x_1, x_2, \dots, x_5) &= 1 - \exp\left(-\sum_{i=1}^5 (0.75x_i + 0.2 + 1/\sqrt{5})^2\right).
\end{aligned} \tag{4.2}$$

The design space of this problem is $x_1, x_2, \dots, x_5 \in [-2.5, 2.5]$.

Definition of the DTLZ2 three-objective optimization problem [25]:

$$\begin{aligned}
\text{Minimize: } f_1(x_1, x_2, \dots, x_5) &= (1 + g)\cos(0.5x_1\pi)\cos(0.5x_2\pi) \\
\text{Minimize: } f_2(x_1, x_2, \dots, x_5) &= (1 + g)\cos(0.5x_1\pi)\sin(0.5x_2\pi) \\
\text{Minimize: } f_3(x_1, x_2, \dots, x_5) &= (1 + g)\sin(0.5x_1\pi) \\
g &= \sum_{i=3}^5 (x_i - 0.5)^2 \\
f_{l1}(x_1, x_2, \dots, x_5) &= (0.5 + 1.5g_c)\cos(0.6x_1\pi)\cos(0.4x_2\pi) \\
f_{l2}(x_1, x_2, \dots, x_5) &= (0.3 + 1.2g_c)\cos(0.4x_1\pi)\sin(0.6x_2\pi) \\
f_{l3}(x_1, x_2, \dots, x_5) &= (0.4 + 1.3g_c)\sin(0.5x_1\pi) \\
g_c &= \sum_{i=3}^5 (0.8x_i - 0.3)^2.
\end{aligned} \tag{4.3}$$

The design space of this problem is $x_1, x_2, \dots, x_5 \in [0, 1]$.

In each investigation, 10 initial high-fidelity points, f , and 150 low-fidelity points, f_i , were acquired by LHS. The number of iterations was set to 30 for each test function.

4.3.2 Two-objective Test Function Results

The solution space acquired by the proposed multi-fidelity/multi-objective EGO is compared with that acquired by the single-fidelity/multi-objective EGO as shown in Fig. 4.2. Because the single-fidelity/multi-objective EGO finds local optimum points at the beginning of the optimization process, the solution for additional samples stalls earlier. On the other hands, the developed multi-fidelity/multi-objective EGO can find a solution close to the global optimum solution of this multi-objective optimization problem. The histories of the hypervolumes of the two methods are compared in Fig. 4.3. These results also indicate that the proposed multi-fidelity/multi-objective EGO provides better solutions which shows higher diversity because its hypervolume is larger than that of the single-fidelity/multi-objective EGO. In addition, comparisons of the hypervolumes show that the solution of additional samples by the single-fidelity/multi-objective EGO continues to stall at earlier.

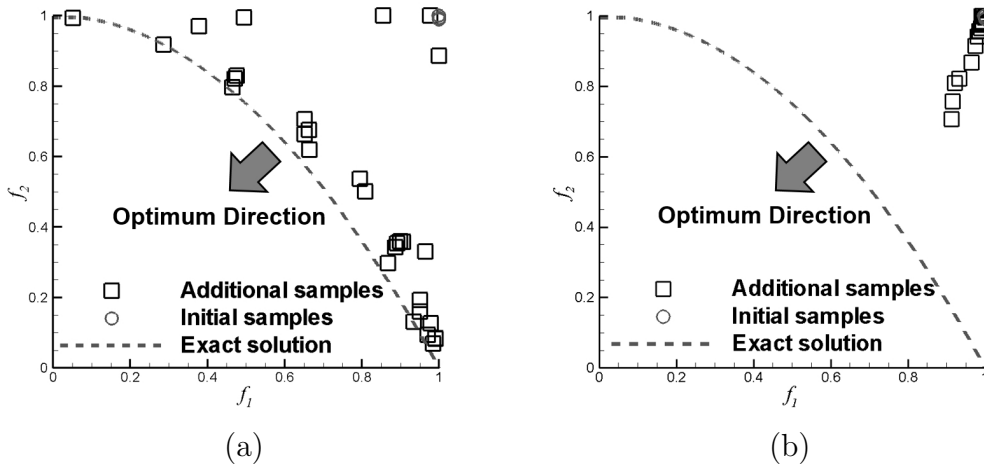


Figure 4.2: Initial sampling data and additional sampling data: (a) multi-fidelity approach, (b) single-fidelity approach.

Comparing non-dominated solutions of the proposed multi-fidelity/multi-objective EGO and the single-fidelity/multi-objective EGO as shown in Fig. 4.4. it suggests that the proposed multi-fidelity/multi-objective EGO obtains better solutions than the single-fidelity/multi-objective EGO, because the non-dominated solutions of the former can dominate all the non-dominated solutions of the latter.

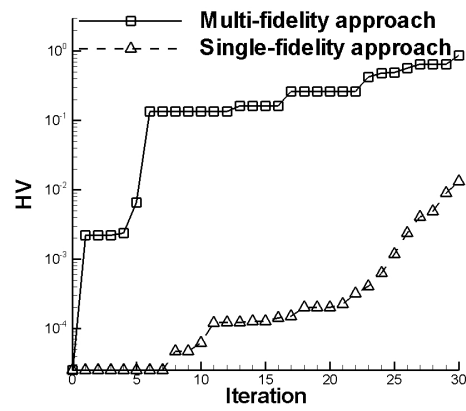


Figure 4.3: Hypervolume comparison of multi-fidelity approach and single-fidelity approach.

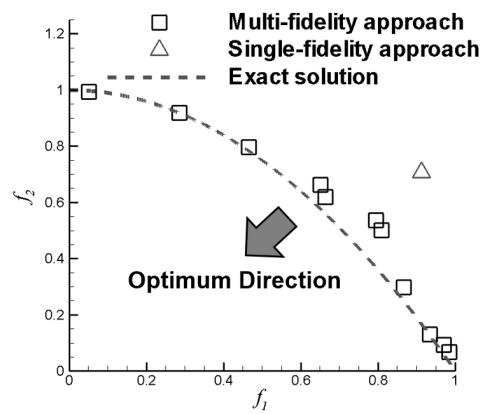


Figure 4.4: Non-dominated solution of two-objective optimization test problem.

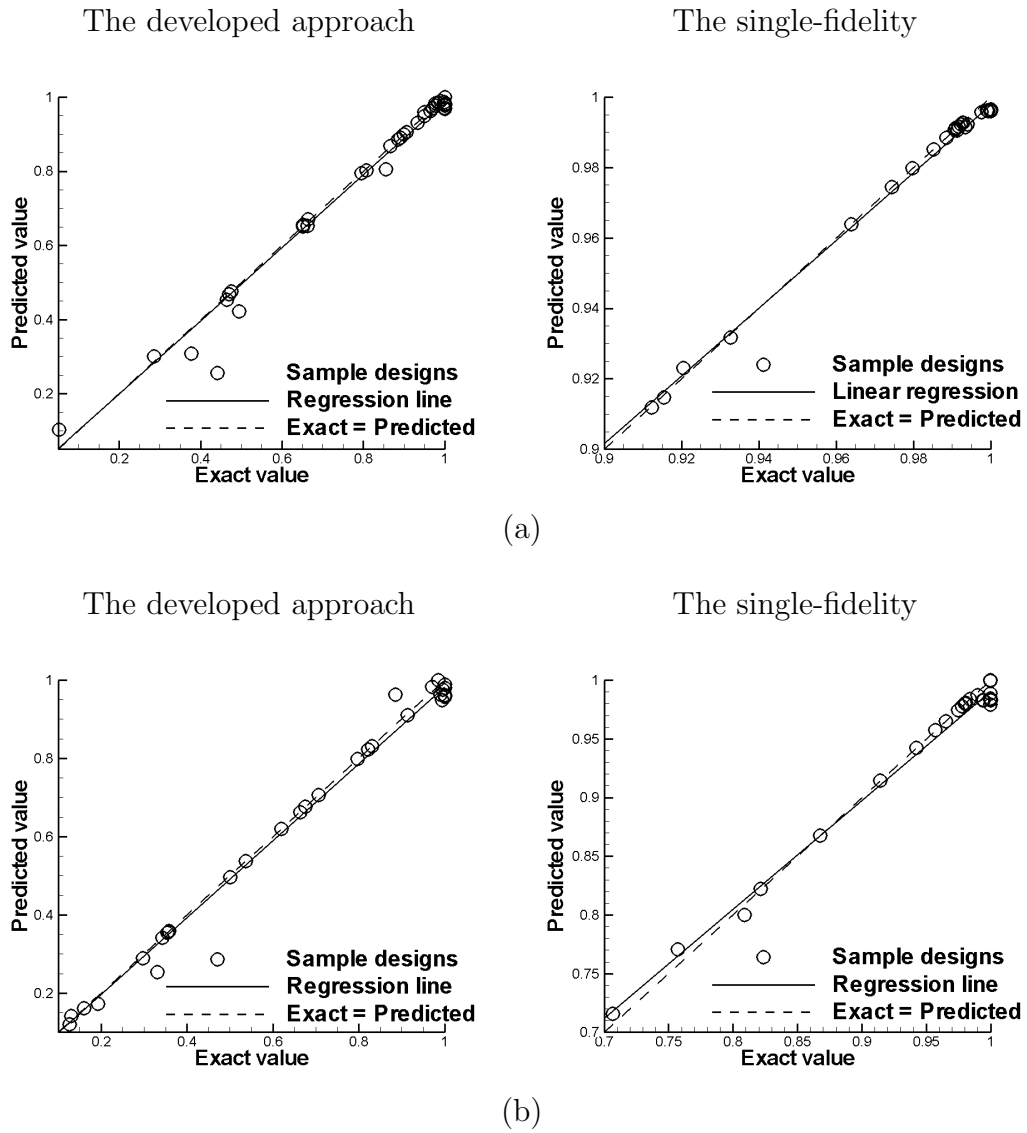


Figure 4.5: Cross-validation results: (a) result of f_1 , (b) result of f_2 .

To investigate the reason of superiority of the proposed multi-fidelity/multi-objective EGO, the cross-validation [24, 25] of f_1 and f_2 were compared, as shown in Figs. 4.5. It can be seen that the linear regression line nearly coincides with the predicted line in the case of the proposed multi-fidelity/multi-objective EGO. Thus, the multi-fidelity surrogate model achieves higher accuracy than the single-fidelity surrogate model. More specifically, the proposed multi-fidelity/multi-objective EGO achieves higher accuracy because the data set obtained by low-fidelity evaluation enables the surrogate model to predict the solution in the uncertainty region.

4.3.3 Three-objective Test Function Results

Further, all the samples acquired by the two methods (the proposed multi-fidelity/multi-objective EGO and the single-fidelity/multi-objective EGO) are compared as shown in Fig. 4.6. In addition, the non-dominated solutions of the two methods are compared in Fig. 4.7. According to these results, the proposed multi-fidelity/multi-objective EGO and the single-fidelity/multi-objective EGO have similar non-dominated solutions. However, the results of the multi-fidelity/multi-objective EGO are better than those of the single-fidelity/multi-objective EGO because some of the results of additional sampling by the single-fidelity/multi-objective EGO stall at local optimum points. The hypervolumes of the two methods are compared in Fig. 4.8. The hypervolume of the proposed multi-fidelity/multi-objective EGO gives better solutions than that of the single-fidelity/multi-objective EGO. These results indicate that the proposed multi-fidelity/multi-objective EGO has a higher convergence rate than the single-fidelity/multi-objective EGO. The solution of the proposed multi-fidelity/multi-objective EGO converges after 18 iterations with a larger hypervolume, whereas the solution of the single-fidelity/multi-objective EGO converges after 23 iterations.

The cross-validation results for f_1 , f_2 , and f_3 , are shown in Fig. 4.9. The results indicate that the multi-fidelity surrogate model can achieve higher accuracy than the single-fidelity surrogate model for f_1 and f_2 . Moreover, the results show that the non-dominated solution of the multi-fidelity/multi-objective EGO has a higher convergence rate because of the higher accuracy of the multi-fidelity surrogate model. With regard to f_3 , a comparison between the multi-fidelity

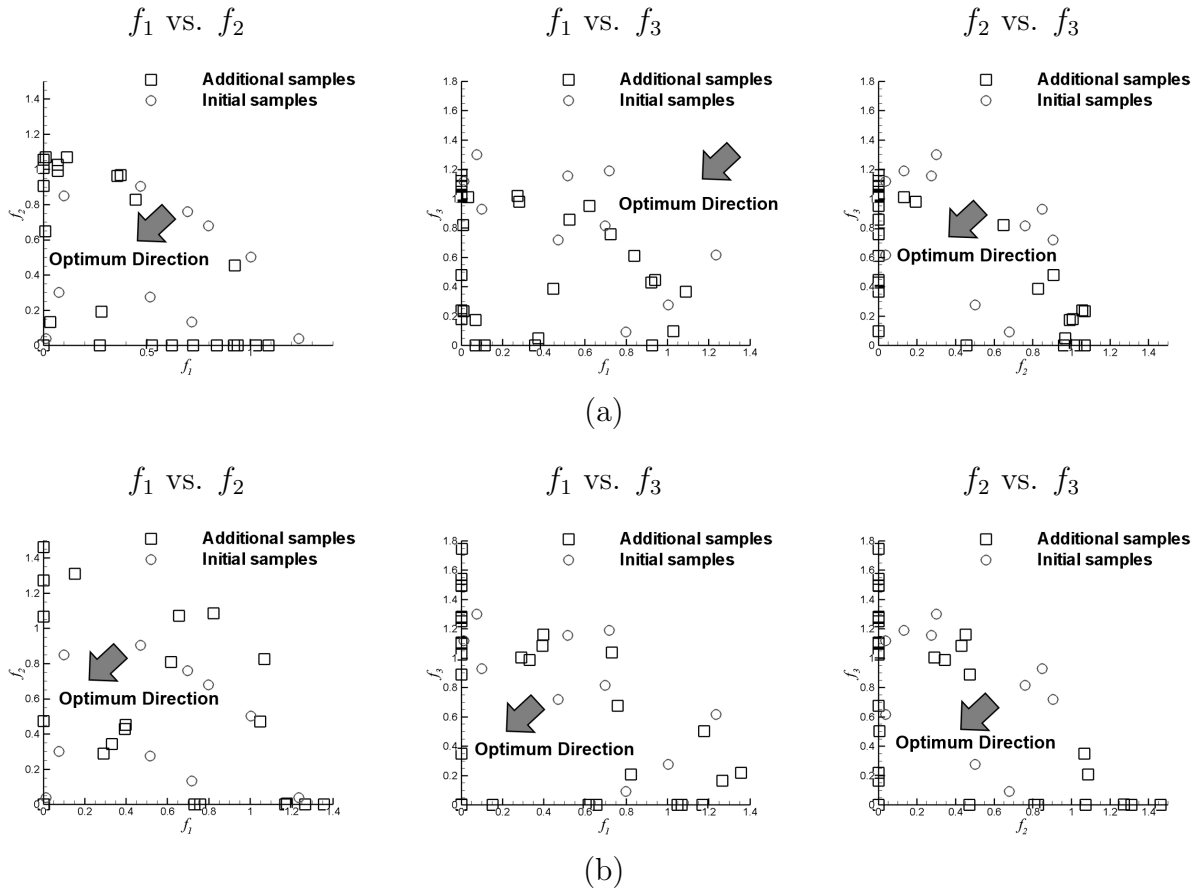


Figure 4.6: Initial sampling data and additional sampling data: (a) multi-fidelity approach, (b) single-fidelity approach.

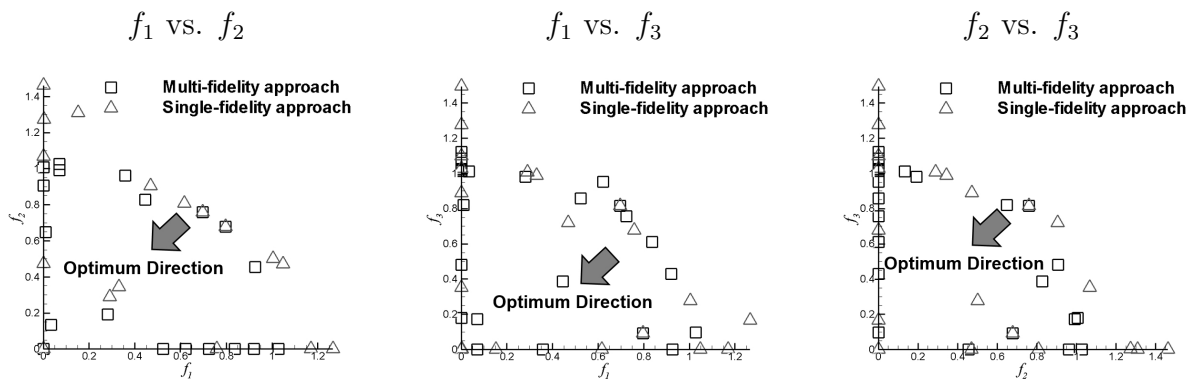


Figure 4.7: Comparison of non-dominated solutions of three-objective optimization test problem.

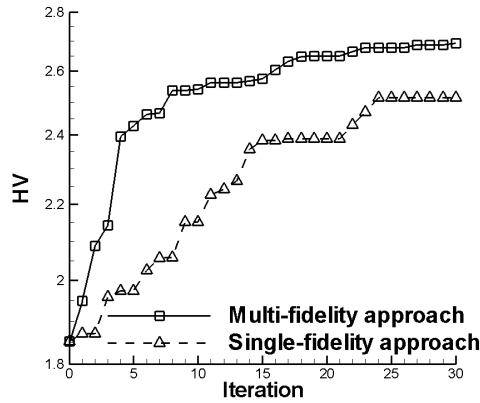


Figure 4.8: Hypervolume comparison of multi-fidelity approach and single-fidelity approach.

and single-fidelity surrogate models shows that the two methods have similar accuracy because f_3 has a simpler shape than f_1 and f_2 .

4.4 Airfoil Design Problem

The proposed multi-fidelity/multi-objective design method discussed in Section 3 was also investigated by solving two UAV airfoil design problems, which have the chord length 1 meter [1], as real-world design problems.

4.4.1 Formulation

Two-objective case

The first problem has two objectives: minimize the aerodynamic drag force (C_d) at cruise speed, which requires a target lift of 0.5, and maximize the airfoil thickness at 75% of the chord length (t_{75}), which can be obtained directly by the real function because it can be calculated rapidly. In this case, the airfoil thickness needs to be predicted by the surrogate model because the EGO process must find the additional sampling point based on the uncertainty of the model.

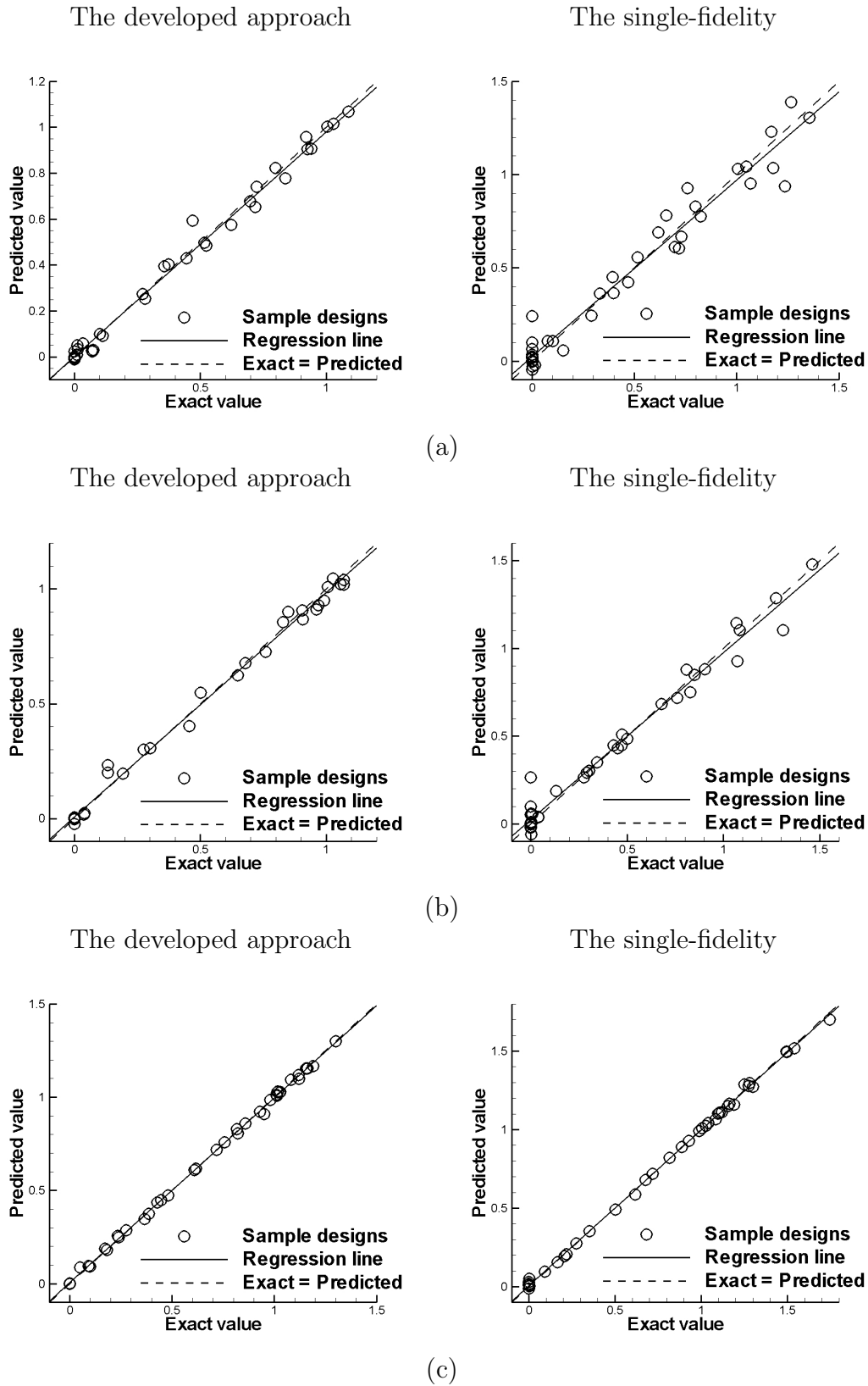


Figure 4.9: Cross-validation of f_3 : (a) multi-fidelity approach, (b) single-fidelity approach.

Thus, two surrogate models are constructed. The optimization problem can be expressed as

$$\begin{aligned} \text{Minimize: } & C_d \text{ at } Re = 4 \times 10^6, Ma = 0.3, C_l = 0.5 \\ \text{Maximize: } & t_{75} \end{aligned} \quad (4.4)$$

The number of initial samples for the high-fidelity/high-cost function is set to 10, and the number of low-fidelity/low-cost functions for the multi-fidelity surrogate model is 150. Further, the number of additional samples for this problem is set to 30. In this problem, the EHVI from (4.1) is modified to

$$EHVI = \int_{-\infty}^{C_{d,\max}} HVI[C_d, t_{75}] \times \phi_1(C_d) dC_d, \quad (4.5)$$

where $f_1(\mathbf{x})$ is C_d and $f_2(\mathbf{x})$ is t_{75} .

Three-objective case

The second problem has three objectives: minimize C_d at cruising speed, maximize t_{75} , and maximize the lift coefficient (C_l) in the landing condition at an angle of attack of 5.0° . In this problem, the hybrid surrogate model is used to predict C_d and C_l . Further, t_{75} can be directly obtained by the real function. The optimization problem is expressed as

$$\begin{aligned} \text{Minimize: } & C_d \text{ at } Re = 4 \times 10^6, Ma = 0.3, C_l = 0.5 \\ \text{Maximize: } & t_{75} \\ \text{Maximize: } & C_l \text{ at } Re = 2 \times 10^6, Ma = 0.15 \end{aligned} \quad (4.6)$$

The number of initial samples for the high-fidelity/high-cost function is set to 10, and the number of low-fidelity/low-cost functions for the multi-fidelity surrogate model is 150 (for C_d and C_l prediction only). Further the number of additional samples for this problem is set to 30. In this problem, the EHVI from (4.1) is modified to

$$EHVI = \int_{-\infty}^{C_{d,\max}} \int_{C_{l,\min}}^{\infty} HVI[C_d, t_{75}, C_l] \times \phi_1(C_d) \phi_2(C_l) dC_d dC_l. \quad (4.7)$$

4.4.2 Evaluation Methods

High-fidelity Evaluation using CFD as High-cost Function

The aerodynamic evaluation as a high-fidelity function was carried out using a Reynolds-averaged Navier-Stokes (RANS) solver [26]. The governing equation is expressed as

$$\frac{\partial}{\partial T} \int_{\Omega} \Psi dV + \oint_{\partial\Omega} Q \cdot n ds = 0, \quad (4.8)$$

Ψ is a vector that consists of conservative quantities and Q is the summation of conservative quantities entering and leaving the area. A lower-upper symmetric Gauss-Seidel (LU-SGS) implicit method [27] was employed for time integration, and a third-order-accurate upwind difference scheme with a monotone upstream-centered scheme for conservation laws (MUSCL) method [28] was employed for the flux evaluation. Further, the Baldwin-Lomax model [29] was used as a turbulent model. In addition, a structured grid was automatically created by an algebraic method for each design (200×61 structured grid for the RANS solver, as shown in Fig. 4.15). The size of the structured grid based on the boundary layer theory. The non-dimensional distance from the wall (y^+) is defined by the recommend value for the Baldwin-Lomax model [30]. The recommend value to simulation the pressure distributions is $y^+ \leq 5.0$. In this work, $y^+ = 4.0$ is used to defined the size of the structured grid.

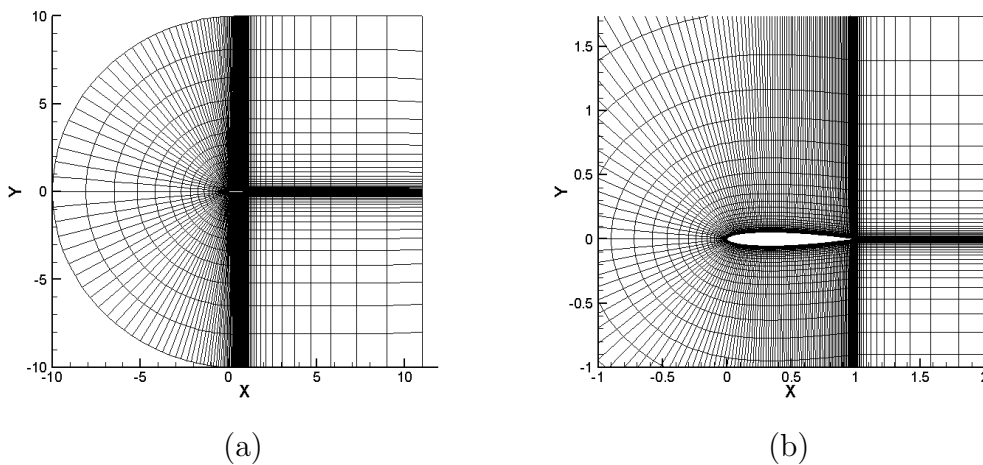


Figure 4.10: Computation structured grid: (a) full length, (b) grid around airfoil.

Low-fidelity Solver as High-cost Function

XFOIL [31] was employed as the computational flow solver. In XFOIL, the inviscid pressure distribution is modeled using a linear vortex strength distribution, while the viscous effects and the development of the laminar-turbulent boundary layer are modeled using integral boundary layer theory.

Airfoil Representation

In this study, the CST parameterization method [32] was used for airfoil shape parameterization. The theory of the CST has been represent in Chapter 2. In this study, N_1 was set to 0.5 and N_2 was set to 1.0. Further, third-degree Bernstein polynomials [33] were used to generate the airfoil shape for the lower side $b_1 - b_3$ and the upper side $b_4 - b_6$. The ranges of the design parameters are defined in Table 4.1.

Table 4.1: Design spaces for airfoil design problem.

Design parameter	Design range
$b_1(dv1)$	(-)0.18 – (-)0.01
$b_2(dv2)$	(-)0.15 – (-)0.05
$b_3(dv3)$	(-)0.18 – (-)0.02
$b_4(dv4)$	(-)0.10 – (-)0.18
$b_5(dv5)$	(-)0.05 – (-)0.15
$b_6(dv6)$	(-)0.05 – (-)0.15

4.5 Results

Two-objective Airfoil Shape Optimization Results

All the samples obtained by the two methods (the proposed multi-fidelity/multi-objective EGO and the single-fidelity/multi-objective EGO) are shown in Fig. 4.11. These results show that the proposed multi-fidelity/multi-objective EGO can achieve greater diversity in the solution

space than the single-fidelity/multi-objective EGO. The hypervolume of the proposed multi-fidelity/multi-objective EGO showed faster convergence (after 20 iterations) than that of the single-fidelity/multi-objective EGO (after 26 iterations). In addition, as shown in Fig. 4.12, the non-dominated solutions of the proposed multi-fidelity/multi-objective EGO included C_d ranging from 0.006 to 0.027 and t_{75} ranging from 0.034 to 0.064. On the other hand, the non-dominated solutions of the single-fidelity/multi-objective EGO included C_d ranging from 0.009 to 0.016 and t_{75} ranging from 0.047 to 0.064. The histories of the hypervolumes of the two methods are compared in Fig. 4.13. According to these results, the single-fidelity surrogate model could find only local optimum points, whereas the proposed multi-fidelity approach could find global optimum points.

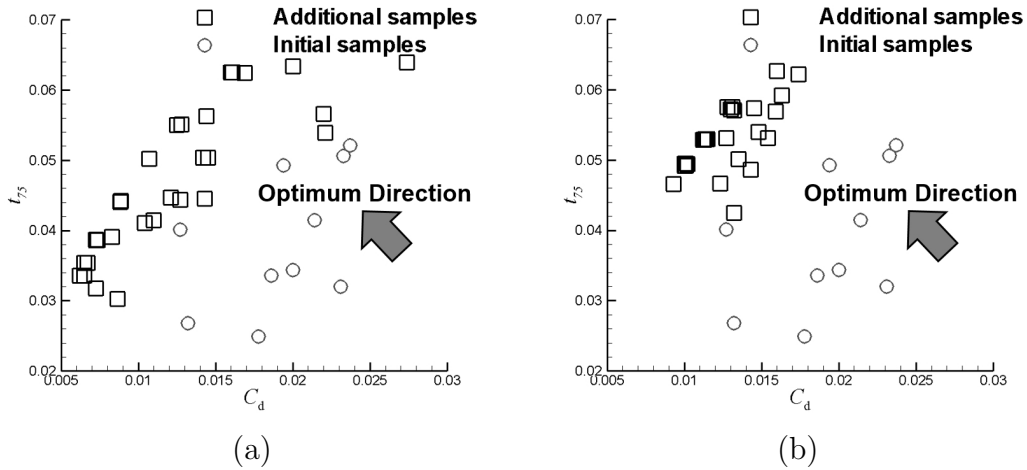


Figure 4.11: Initial sampling data and additional sampling data: (a) multi-fidelity approach, (b) single-fidelity approach.

The cross-validation results for C_d are shown in Fig. 4.14. It can be confirmed that the hybrid surrogate model achieves higher accuracy than the single-fidelity Kriging-based surrogate model. This is because the low-fidelity data enables the surrogate model to predict the data in the uncertainty region. Thus, the multi-fidelity/multi-objective EGO achieves faster solution converge because the multi-fidelity surrogate model achieves higher accuracy than the single-fidelity surrogate model. Because the proposed multi-fidelity surrogate model achieves higher accuracy, the optimization process based on it is more likely to obtain global optimum points.

The parallel coordinated plots (PCPs) obtained by the two methods are shown in Fig. 4.15.

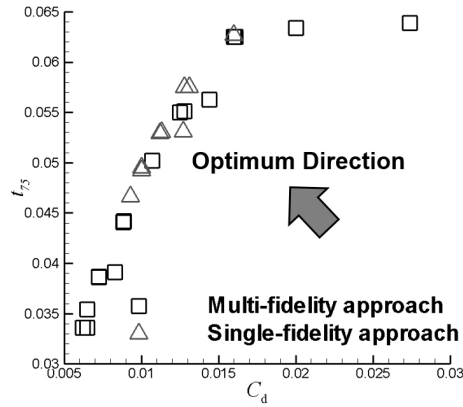


Figure 4.12: Non-dominated solution of two-objective airfoil shape optimization problem.

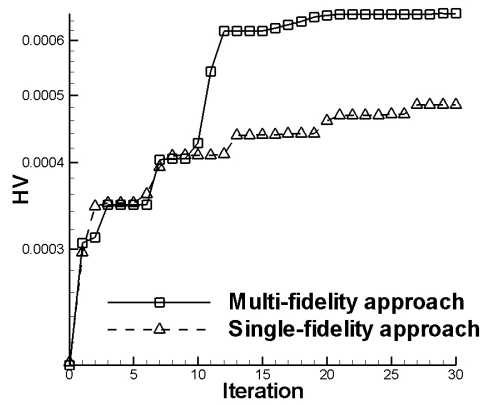


Figure 4.13: Hypervolume comparison of multi-fidelity approach and single-fidelity approach.

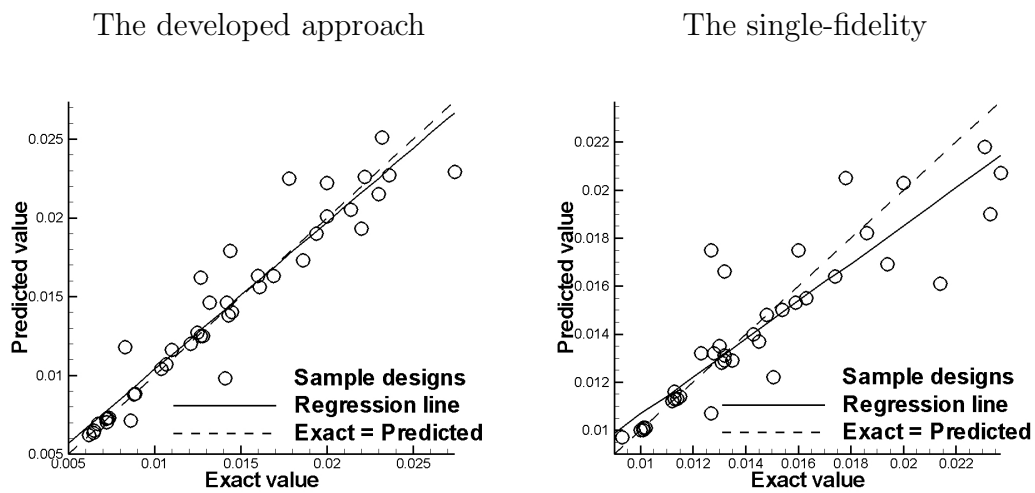


Figure 4.14: Cross validation of C_d .

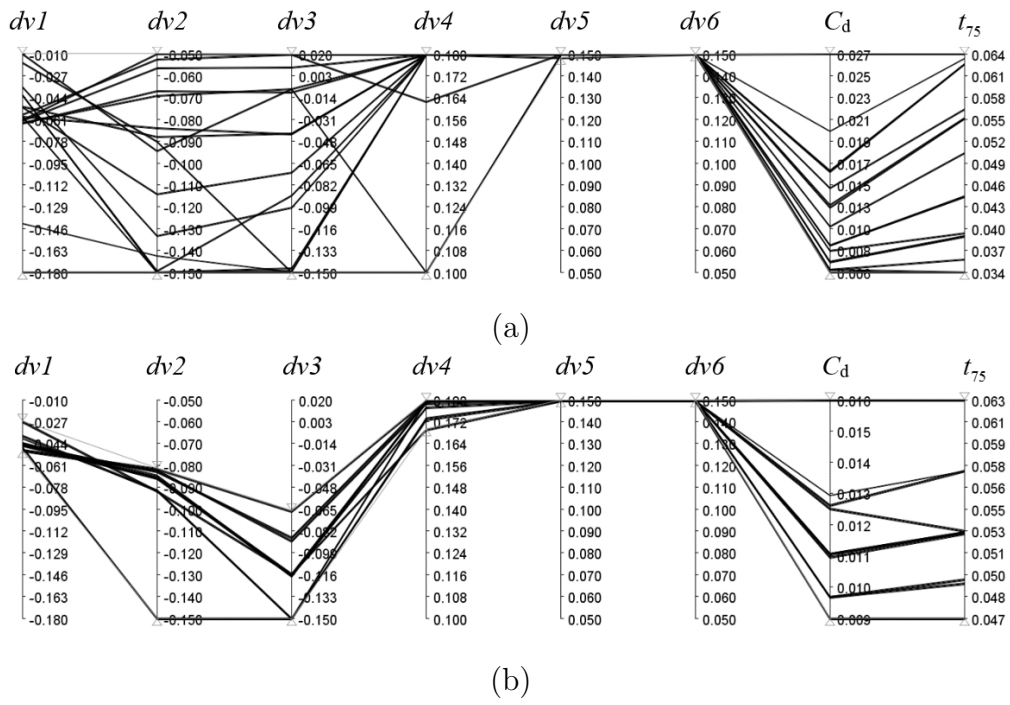


Figure 4.15: Parallel coordinated plots of non-dominated solutions: (a) multi-fidelity approach, (b) single-fidelity approach.

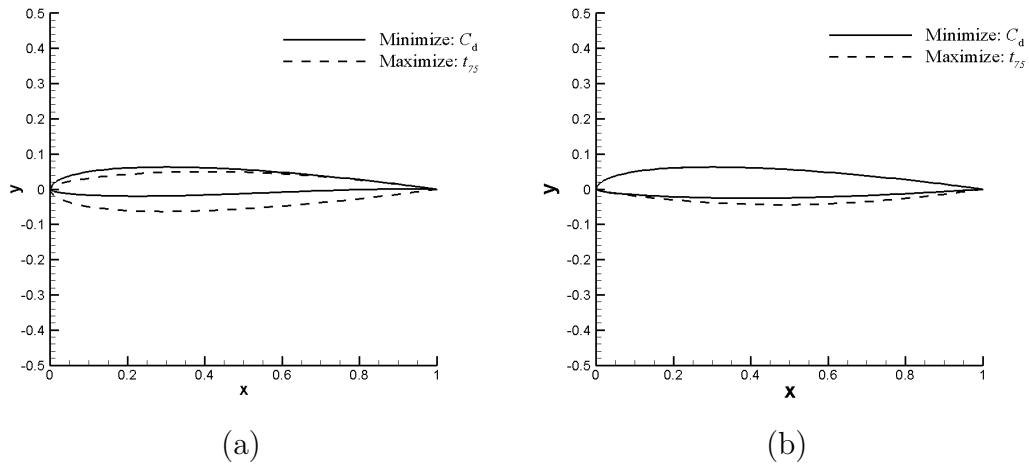


Figure 4.16: Comparison of design geometries: (a) multi-fidelity approach, (b) single-fidelity approach.

According to Fig. 4.15 (a), the PCP results show that the proposed multi-fidelity/multi-objective EGO can achieve greater diversity in design space than the single-fidelity/multi-objective EGO. The results indicate that the optimum design, i.e., the lowest C_d and highest t_{75} values, can be obtained when $dv4 - dv6$ have large values. Further, if $dv2$ and $dv3$ have large values, t_{75} has a low value; in this case, C_d also has a low value. The optimal shapes of the non-dominated solutions of the two methods that minimize C_d and maximize t_{75} are compared in Fig. 4.16. The optimal designs of the single-fidelity/multi-objective EGO have similar shapes because the algorithm converges early at these optimum points. On the other hand, the optimal designs of the proposed multi-fidelity/multi-objective EGO have different shapes for each objective.

Three-objective Airfoil Shape Optimization Results

All the samples obtained by the two methods (the proposed multi-fidelity/multi-objective EGO and the single-fidelity/multi-objective EGO) are compared in Fig. 4.17. In addition, the histories of the hypervolumes of the two methods are compared in Fig. 4.18, and the non-dominated solutions of the two methods are compared in Fig. 4.19. These results show that the proposed multi-fidelity/multi-objective EGO achieves greater diversity of the non-dominated solutions because its hypervolume is larger than that of the single-fidelity/multi-objective EGO. The non-dominated solutions of the proposed multi-fidelity/multi-objective EGO included C_d ranging from 0.007 to 0.022, t_{75} ranging from 0.034 to 0.065, and C_l ranging from 0.0938 to 1.054. On the other hand, the non-dominated solutions of the single-fidelity/multi-objective EGO included C_d ranging from 0.010 to 0.022, t_{75} ranging from 0.047 to 0.065, and C_l ranging from 0.0938 to 1.039. Thus, the proposed multi-fidelity/multi-objective EGO achieved greater diversity of the solutions than the single-fidelity/multi-objective EGO. The cross-validation results for C_d and C_l are shown in Fig. 4.20. It can be seen that the proposed hybrid surrogate model achieves higher accuracy than the single-fidelity Kriging-based surrogate model. Thus, the proposed multi-fidelity/multi-objective EGO can achieve greater diversity of the solutions because its surrogate model achieves higher accuracy.

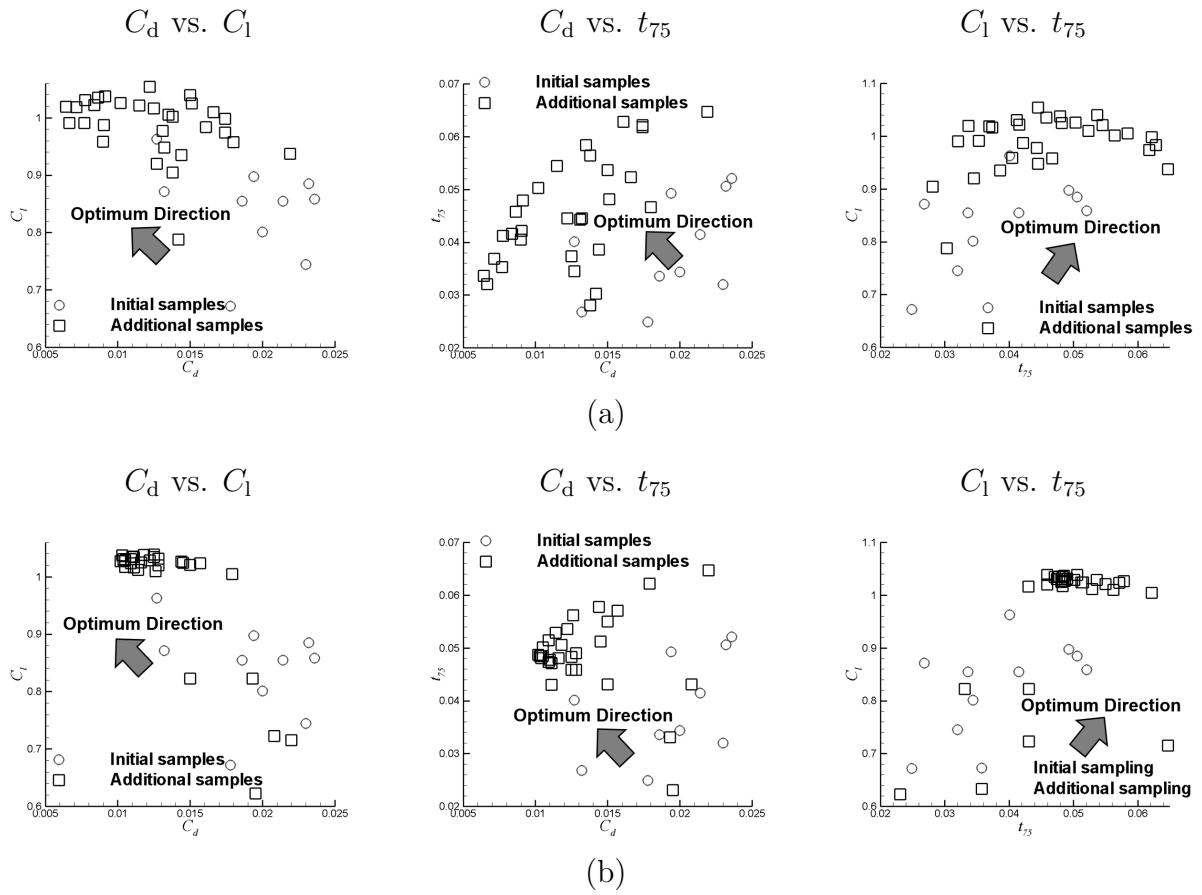


Figure 4.17: Initial sampling data and additional sampling data: (a) multi-fidelity approach, (b) single-fidelity approach.

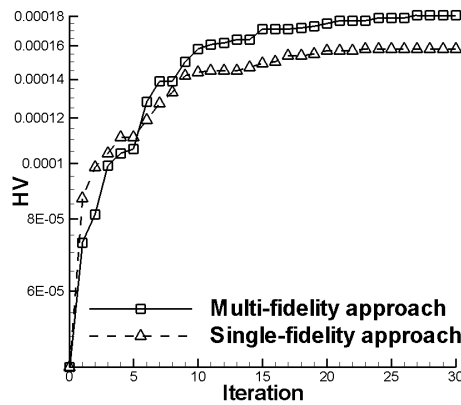


Figure 4.18: Hypervolume comparison of multi-fidelity approach and single-fidelity approach.

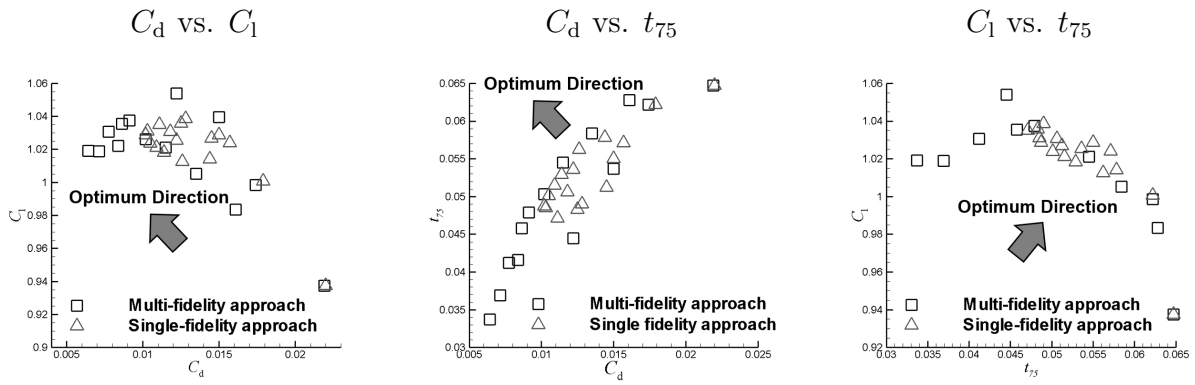


Figure 4.19: Comparison of non-dominated solutions of three-objective optimization test problem.

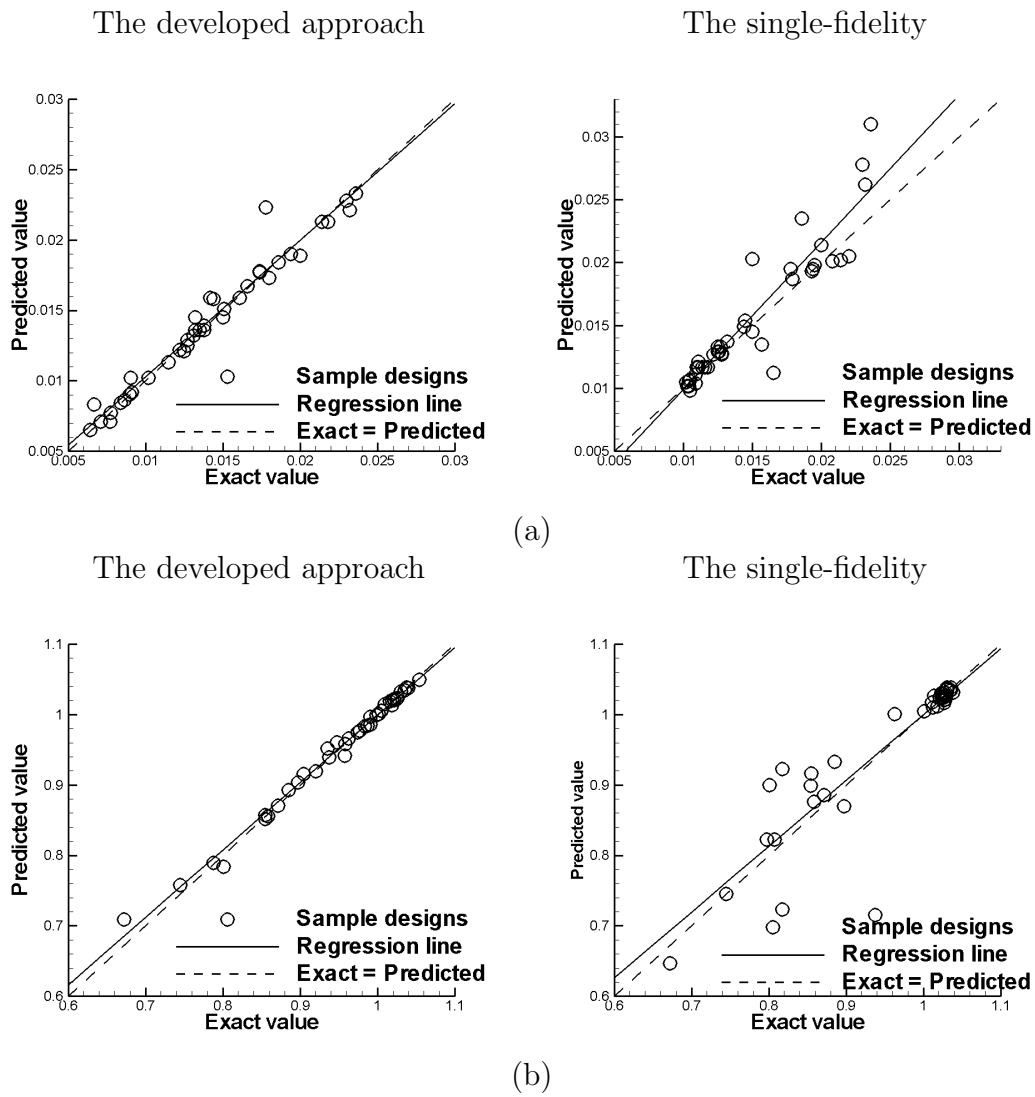


Figure 4.20: Cross-validation results: (a) results of C_d , (b) results of C_1 .

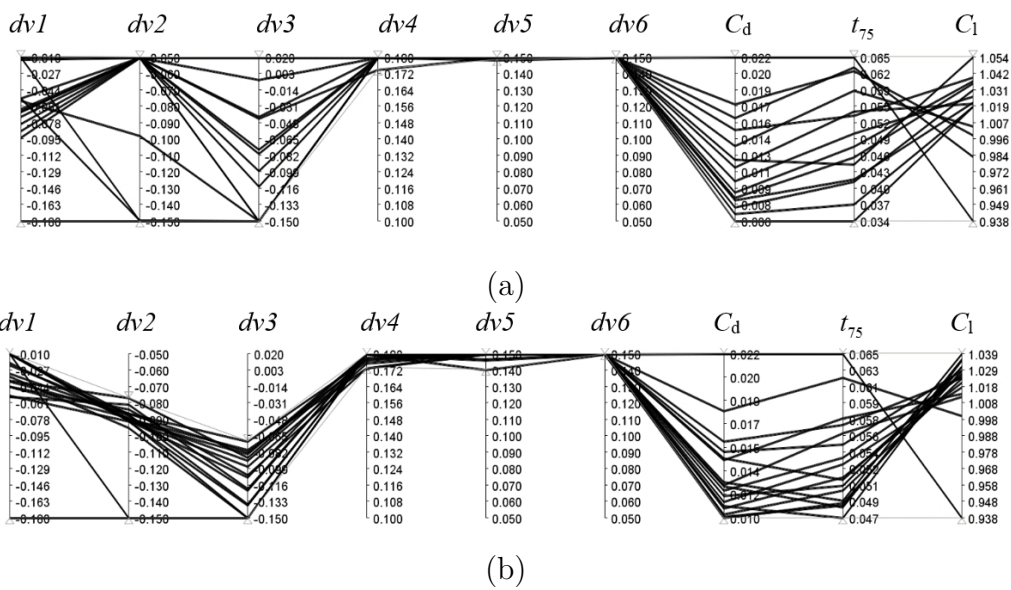


Figure 4.21: Parallel coordinated plots of non-dominated solutions: (a) multi-fidelity approach, (b) single-fidelity approach.

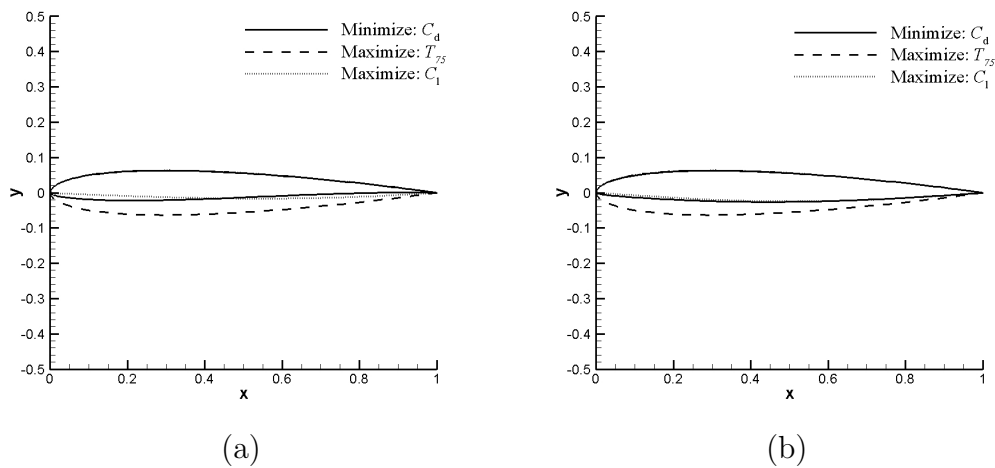


Figure 4.22: Comparison of design geometries: (a) multi-fidelity approach, (b) single-fidelity approach.

The design space visualizations based on the PCP results of the two methods are compared in Fig. 4.21. The PCP results show that the proposed multi-fidelity/multi-objective EGO achieves greater diversity in the design space than the single-fidelity/multi-objective EGO. Moreover, the results indicate that large values of $dv4 - dv6$ give low C_d , high t_{75} , and high C_1 values. If $dv1$ is large, C_d and C_1 will have high values. On the other hand, if $dv2$ and $dv3$ have large values, C_d , C_1 , and will have low values. Because the single-fidelity approach only performs local exploration in the design space, the non-dominated solutions of the single-fidelity/multi-objective EGO miss the global optimum and cannot maintain the diversity. The optimal shapes of the non-dominated solutions of the two methods that minimize C_d , maximize t_{75} , and maximize C_1 are compared in Fig. 4.22. The optimal designs of the single-fidelity/multi-objective EGO have similar shapes for minimize C_d and maximize C_1 because the algorithm converges early at these optimum points. On the other hand, the optimal designs of the proposed multi-fidelity/multi-objective EGO have different shapes for each objective.

4.6 Conclusions

In this chapter, a multi-fidelity/multi-objective EGO was proposed for efficient solutions of multi-objective optimization problems. The proposed method constructed a hybrid model based on an RBF that predicts a global model and an ordinary kriging method that predicts the local variance. EHVI was used as an index to find additional samples for the optimization process. For multi-fidelity optimization, the global model was constructed using a data set evaluated by a low-fidelity function, and the local variance was estimated using a data set evaluated by a high-fidelity function.

To examine the proposed multi-fidelity/multi-objective EGO, two-/three-objective test problems were solved and the results of the proposed multi-fidelity/multi-objective EGO were compared with those of the single-fidelity/multi-objective EGO. The results for the test functions showed that the proposed multi-fidelity/multi-objective EGO achieves faster convergence than the single-fidelity/multi-objective EGO. Moreover, the results showed that the proposed multi-

fidelity/multi-objective EGO has greater diversity of the non-dominated solutions than the single-fidelity/multi-objective EGO. In addition, the results showed that the proposed multi-fidelity/multi-objective EGO has fewer global errors. Thus, the proposed multi-fidelity/multi-objective EGO can be widely applied to real-world problems.

Further, the proposed multi-fidelity/multi-objective EGO was applied to an aerodynamic airfoil shape optimization problem with two objectives: minimize C_d at cruising speed and maximize the thickness around the trailing edge. To evaluate the aerodynamic performance, XFOIL was used to construct a low-fidelity/low-cost data set and a Navier-Stokes solver was used to construct a high-fidelity/high-cost data set. The results of the proposed multi-fidelity/multi-objective EGO were compared with those of the single-fidelity/multi-objective EGO. The optimization results showed that the proposed multi-fidelity/multi-objective EGO achieves greater diversity of the non-dominated solutions than the single-fidelity/multi-objective EGO. In addition, the cross-validation results showed that the proposed multi-fidelity/multi-objective EGO has fewer global errors. Finally, the proposed multi-fidelity/multi-objective EGO was applied to an aerodynamic airfoil shape optimization problem with three objectives: minimize C_d at cruising speed, maximize the thickness around the trailing edge, and maximize C_l in the landing condition. The results showed that the proposed multi-fidelity/multi-objective EGO achieves greater diversity of the non-dominated solutions than the single-fidelity/multi-objective EGO. In addition, the error between the exact value and the predicted value of the hybrid surrogate model was smaller than that of the single-fidelity model. These results suggest that the multi-fidelity/multi-objective EGO is suitable for real-world multi-objective design problems. In this study, we limited the optimization to two/three objectives for simple aerodynamic design problems. In the future, we expect that our algorithm will be used to solve more complicated design problems.

Bibliography

- [1] Wickramasinghe, Upali K., Robert Carrese, and Xiaodong Li. "Designing airfoils using a reference point based evolutionary many-objective particle swarm optimization algorithm." *IEEE Congress on Evolutionary Computation*. IEEE, 2010.
- [2] Ariyarit, Atthaphon, and Masahiro Kanazaki. "Multi-modal distribution crossover method based on two crossing segments bounded by selected parents applied to multi-objective design optimization." *Journal of Mechanical Science and Technology* 29.4 (2015): 1443-1448.
- [3] Choi, Seongim, Juan J. Alonso, and Ilan M. Kroo. "Two-level multifidelity design optimization studies for supersonic jets." *Journal of Aircraft* 46.3 (2009): 776-790.
- [4] Wu-fa, L. I. U., et al. "Airfoil Optimization Design by Panel Methods for Small Size Aerial Vehicle at Low Reynolds Number." *Proceedings of the 1st International Conference on Mechanical Engineering and Material Science*. Atlantis Press, 2012.
- [5] Jameson, Antony. "Optimum aerodynamic design using CFD and control theory." *AIAA paper* 1729 (1995): 124-131.
- [6] Choi, Seongim, et al. "Multifidelity design optimization of low-boom supersonic jets." *Journal of Aircraft* 45.1 (2008): 106-118.
- [7] Forrester, Alexander IJ, Andr as S obester, and Andy J. Keane. "Multi-fidelity optimization via surrogate modelling." *Proceedings of the royal society of london a: mathematical, physical and engineering sciences*. Vol. 463. No. 2088. The Royal Society, 2007.

- [8] Huang, Likeng, Zhenghong Gao, and Dehu Zhang. "Research on multi-fidelity aerodynamic optimization methods." *Chinese Journal of Aeronautics* 26.2 (2013): 279-286.
- [9] Rethore, Pierre-Elouan, et al. "TopFarm: Multi-fidelity optimization of offshore wind farm." *The Twenty-first International Offshore and Polar Engineering Conference*. International Society of Offshore and Polar Engineers, 2011.
- [10] Rethore, Pierre - Elouan, et al. "TOPFARM: Multi - fidelity optimization of wind farms." *Wind Energy* 17.12 (2014): 1797-1816.
- [11] Leon, Enric Roca, et al. "Multi-Fidelity Concurrent Aerodynamic Optimization of Rotor Blades in Hover and Forward Flight." *40th European Rotorcraft Forum*. 2014.
- [12] Leusink, Debbie, David Alfano, and Paola Cinnella. "Multi-fidelity optimization strategy for the industrial aerodynamic design of helicopter rotor blades." *Aerospace Science and Technology* 42 (2015): 136-147.
- [13] Jones, Donald R., Matthias Schonlau, and William J. Welch. "Efficient global optimization of expensive black-box functions." *Journal of Global Optimization* 13.4 (1998): 455-492.
- [14] Couckuyt, Ivo, Dirk Deschrijver, and Tom Dhaene. "Fast calculation of multiobjective probability of improvement and expected improvement criteria for Pareto optimization." *Journal of Global Optimization* 60.3 (2014): 575-594.
- [15] Hupkens, Iris, Michael Emmerich, and André Deutz. "Faster Computation of Expected Hypervolume Improvement." *arXiv preprint arXiv:1408.7114* (2014).
- [16] Orr, Mark JL. "Introduction to radial basis function networks." (1996).
- [17] Praveen, C., and R. Duvigneau. "Radial basis functions and kriging metamodels for aerodynamic optimization." *Rapp. Tech* 6151 (2007): 159.
- [18] Matheron, Georges. "Principles of geostatistics." *Economic Geology* 58.8 (1963): 1246-1266.

- [19] Bader, Johannes, and Eckart Zitzler. "HypE: An algorithm for fast hypervolume-based many-objective optimization." *Evolutionary Computation* 19.1 (2011): 45-76.
- [20] .Goldberg, David E., and John H. Holland. "Genetic algorithms and machine learning." *Machine Learning* 3.2 (1988): 95-99.
- [21] Eshelman, Larry J. "Real-Coded Genetic Algorithms and Interval-Schemata." *Foundations of Genetic Algorithms 2* (1993): 187-202.
- [22] Melanie, Mitchell. "An introduction to genetic algorithms." *Cambridge, Massachusetts London, England, fifth edition 3* (1999): 62-75.
- [23] Huband, Simon, et al. "A review of multiobjective test problems and a scalable test problem toolkit." *IEEE Transactions on Evolutionary Computation* 10.5 (2006): 477-506.
- [24] Liem, Rhea P., Charles A. Mader, and Joaquim RRA Martins. "Surrogate models and mixtures of experts in aerodynamic performance prediction for aircraft mission analysis." *Aerospace Science and Technology* 43 (2015): 126-151.
- [25] Meckesheimer, Martin, et al. "Computationally inexpensive metamodel assessment strategies." *AIAA journal* 40.10 (2002): 2053-2060.
- [26] Obayashi, Shigeru, and Guru P. Guruswamy. "Convergence acceleration of a Navier-Stokes solver for efficient static aeroelastic computations." *AIAA Journal* 33.6 (1995): 1134-1141.
- [27] Yoon, Seokkwan, and Antony Jameson. "Lower-upper symmetric-Gauss-Seidel method for the Euler and Navier-Stokes equations." *AIAA Journal* 26.9 (1988): 1025-1026.
- [28] Fujii, Kozo, and Shigeru Obayashi. "High-resolution upwind scheme for vortical-flow simulations." *Journal of Aircraft* 26.12 (1989): 1123-1129.
- [29] Baldwin, Barrett Stone, and Timothy J. Barth. *A one-equation turbulence transport model for high Reynolds number wall-bounded flows*. . National Aeronautics and Space Administration, Ames Research Center, 1990.

- [30] Nichols, Robert H. "Turbulence models and their application to complex flows." *University of Alabama at Birmingham, Revision 4* (2010): 89.
- [31] Drela, Mark. "XFOIL: An analysis and design system for low Reynolds number airfoils." *Low Reynolds Number Aerodynamics*. Springer Berlin Heidelberg, 1989. 1-12.
- [32] Kulfan, Brenda M. "Universal parametric geometry representation method." *Journal of Aircraft* 45.1 (2008): 142-158.
- [33] Lorentz, George G. *Bernstein polynomials*. American Mathematical Soc., 2012.

Chapter 5

Conclusion

5.1 Conclusions

The work in this thesis deals with the development of the high performance optimization tool for aeronautical design. The final target of this research is increase the efficiency of the aeronautical performance optimization via multi-fidelity approach of low-fidelity/low-cost evaluations and high-fidelity/high-cost evaluations. To achieve this target, the efficiency global optimization for multi-fidelity approach was developed.

This thesis started with reviews and development of genetic algorithm (GA) for low-fidelity evaluations. The GA with multi-modal crossover method (MMDX) was developed to increase the performance of the algorithm. This method used to solve a real-world airfoil design problem. Results suggested that the MMDX method provided superior solutions compared with the other crossover method, such as BLX and UNDX crossovers, because the MMDX method can maintain higher diversity because of its larger search space. These results imply the possibility of obtaining better solutions to real-world problems using the MMDX crossover method.

Next, multi-fidelity optimization technique by an efficient global optimization process using a hybrid surrogate model is investigated for solving real-world design problems. The proposed hybrid surrogate model - based EGO used a radial basis function to predict a global model,

and an ordinary Kriging-based EGO was used to predict a local variance. Four test functions are solved, and the results obtained by the proposed hybrid surrogate model - based EGO are compared with those obtained by the co-Kriging model - based EGO and ordinary Kriging-based EGO. The optimization results for the test functions show that the proposed hybrid surrogate model-based EGO achieved higher accuracy compared to the surrogate model, co-Kriging, and Kriging-based EGO methods for each test function. The proposed hybrid surrogate model - based EGO is also applied to aerodynamic optimization of a helicopter' s blade shape. Results by the proposed hybrid surrogate model - based EGO method are compared with those by the co-Kriging - based EGO and ordinary Kriging-based EGO. The results of the aerodynamic helicopter blade design problem also show that the proposed hybrid surrogate model - based EGO could design a better blade shape from the perspective of aerodynamic efficiency.

Finally, a multi-fidelity/multi-objective EGO was proposed for efficient solutions of multi-objective optimization problems. The proposed method constructed a hybrid model based on an RBF an ordinary Kriging method. EHVI was used as an index to find additional samples for the optimization process. To examine the proposed multi-fidelity/multi-objective EGO, two-/three-objective test problems were solved and the results of the proposed multi-fidelity/multi-objective EGO were compared with those of the single-fidelity/multi-objective EGO. The results showed that the proposed multi-fidelity/multi-objective EGO has fast convergence and has greater diversity of the non-dominated solution than the single-fidelity/multi-objective EGO. The proposed multi-fidelity/multi-objective EGO was applied to an aerodynamic airfoil shape optimization problem with two objectives and three objectives. The results still showed that the proposed multi-fidelity/multi-objective EGO has fast convergence and has greater diversity of the non-dominated solution than the single-fidelity/multi-objective EGO for the aerodynamic airfoil shape optimization problem. These results suggest that the multi-fidelity/multi-objective EGO is suitable for real-world multi-objective design problems.